

UNIVERSITY OF BELGRADE
FACULTY OF CIVIL ENGINEERING

Marija T. Nefovska-Danilović

DYNAMIC ANALYSIS OF
SOIL-STRUCTURE SYSTEM USING
SPECTRAL ELEMENT METHOD

Doctoral dissertation

Belgrade, December 2012

УНИВЕРЗИТЕТ У БЕОГРАДУ
ГРАЂЕВИНСКИ ФАКУЛТЕТ

Марија Т. Нефовска-Даниловић

**ДИНАМИЧКА АНАЛИЗА СИСТЕМА
ТЛО-КОНСТРУКЦИЈА ПРИМЕНОМ
СПЕКТРАЛНИХ ЕЛЕМЕНАТА**

Докторска дисертација

Београд, децембар 2012.

Ментор: Др Мира Петронијевић, ванредни професор,
Грађевински факултет, Универзитет у Београду

Чланови Комисије:

1. _____
2. _____
3. _____
4. _____
5. _____

Датум одбране:

DYNAMIC ANALYSIS OF SOIL-STRUCTURE SYSTEM USING SPECTRAL ELEMENT METHOD

Abstract

3D numerical model for dynamic response analysis of multi-storey frame structures including soil-structure interaction has been developed using the Spectral Element Method (SEM). The structure was modeled using the SEM, while the dynamic stiffness matrix of the soil – foundation interface was determined using the Integral Transform Method (ITM). The structure consists of one – dimensional elements: beams and columns, and two – dimensional elements: plates. The soil consists of horizontal layers over the bedrock or half space. The Projection method was used to develop the dynamic stiffness matrices for the transverse and in-plane vibration of plates with arbitrary boundary conditions. The method for coupling one-dimensional and two-dimensional spectral elements was developed, as well as the coupling of the spectral elements with the soil spring – dashpot elements. Using the proposed numerical model 3D frame structures founded on soil of variable stiffness and subjected to ground vibrations induced by traffic were analyzed.

Key words: dynamics of structures, spectral element method, integral transform method, soil-structure interaction, substructure approach, frequency domain, dynamic stiffness

Scientific field: Civil engineering

Specific scientific field: Theory of structures (Dynamic of structures)

UDK: 624.04.004.92(043.3)

ДИНАМИЧКА АНАЛИЗА СИСТЕМА ТЛО-КОНСТРУКЦИЈА ПРИМЕНОМ СПЕКТРАЛНИХ ЕЛЕМЕНАТА

Резиме

У овом раду приказан је 3Д нумерички модел за динамичку анализу вишеспратних рамовских конструкција узимајући у обзир садејство између тла и конструкције. За моделирање конструкције коришћен је Метод спектралних елемената, док је динамичка матрица крутости тла одређена применом Методе интегралних трансформација. Конструкција се састоји од једнодимензионалних елемената: греда и стубова, и дводимензионалних елемената: плоча. Тло се састоји од хоризонталних слојева изнад круте базе или полупростора. Матрице крутости плоча напрегнутих на савијање и у својој равни одређене су применом Методе пројекције. Развијен је поступак спрезања једнодимензионалних и дводимензионалних спектралних елемената, као и спрезање тако формираног модела са тлом. Примена формираног 3Д модела приказана је на анализи 3Д рамовских конструкција фундираних на тлу различите крутости, изложених дејству вибрација изазваних саобраћајним оптерећењем.

Кључне речи: динамика конструкција, метод спектралних елемената, метод интегралних трансформација, интеракција конструкција-тло, метода подструктура, фреквентни домен, динамичка крутост

Научна област: Грађевинарство

Ужа научна област: Теорија конструкција (Динамика конструкција)

УДК: 624.04.004.92(043.3)

Acknowledgements

First of all, I would like to express my deep gratitude to my mentor, Prof. Mira Petronijević for her selfless support, encouragement and for giving me scientific freedom during this work.

I would like to thank to Prof. Nawawi Chow for the support and valuable advises, especially at the beginning of my work. I would also like to thank to prof. Gerhard Muller, prof. Stanko Brčić and prof. Branislav Pujević for the revision of the thesis.

Thanks to my colleagues from the chair of Engineering mechanics and theory of structures for supporting me during the work on the thesis.

At the end, I want to thank to my parents who have always supported me and believed in me. Also, I would like to thank to my children and husband for being patient with me, especially at the final stages of writing the thesis.

The work on this thesis was supported by the Serbian Ministry of Science and Education – Project TR36046.

Contents

1.	Introduction	1
1.1	Outline of the thesis	3
2.	Spectral Element Method	4
2.1	Literature review	4
2.2	One-dimensional spectral elements	6
2.2.1	Spectral element for bars	6
2.2.2.	Spectral element for beams.....	8
2.2.3.	Spectral element for torsional bar.....	11
2.2.4.	Development of the dynamic stiffness matrix for 3D frame structures ...	12
2.2.5.	Dynamic response analysis.....	13
2.3	Two-dimensional spectral elements	18
2.3.1	Plate spectral element for transverse vibration.....	21
2.3.2	Plate spectral element for in-plane vibration.....	41
3.	Coupling of spectral elements	61
3.1	Dynamic stiffness matrix for plate element with edge beams	62
3.2.	Column supported plate element	65
3.3	Numerical examples	71
3.3.1.	Transverse free vibrations of completely free square plate with edge beams	71
3.3.2.	In-plane free vibrations of completely free square plate with edge beams ..	73
3.3.3	Free vibrations of column supported square plate.....	73
3.3.4	Transverse vibration of corner-supported square plate with edge beams	76
4.	Soil-structure interaction	77
4.1	Soil modeling.....	77
4.1.1	Equations of motion	77

4.1.2	Dynamic stiffness matrix of a single soil layer	79
4.1.3	Dynamic stiffness matrix for layered soil	82
4.2	Equations of motion of soil-structure system	83
4.3	Dynamic stiffness matrix for flexible foundations	84
4.4	Dynamic stiffness matrix for rigid foundations	84
4.5	Soil – structure coupling	86
5.	Applications.....	88
5.1	Effects of soil stiffness and foundation size on natural frequencies.....	90
5.2	Effects of soil stiffness on structural response	92
5.2.1	Input ground excitation.....	92
5.2.2	Dynamic response to traffic-induced ground vibration.....	100
6.	Conclusions and recommendations for further research	117
	Appendix	119
A.1.	Fourier Transformations	119
A.2.	Fourier series	119
	List of Figures.....	121
	References	124
	Биографија аутора	129
	Изјава о ауторству.....	130
	Изјава о истоветности штампане и електронске верзије докторског рада.....	131
	Изјава о коришћењу	132

1. Introduction

Conventional static and dynamic structural analyses are based on the assumption that the structure is fixed to the soil, and that there is no interaction between the soil and the structure. In general, the structure interacts with the surrounding soil, so it is necessary to account for soil-structure interaction (SSI), especially in dynamic load cases. Moreover, some dynamic loads like earthquakes, blast and traffic induced vibrations are applied to the soil region around the structure. Therefore, both the structure and the soil region have to be properly modeled. For structural modeling conventional Finite Element Method (FEM) is used. The structure is meshed in order to represent the geometry, boundary conditions, mass and applied loads. In order to model the soil region finite elements can also be used, but since the soil is an unbounded medium, an appropriate boundary has to be introduced. For static loading a fictitious boundary at a sufficient distance from the structure is used, so the obtained finite domain of the soil can be modeled similarly as the structure. For dynamic loading, the fictitious boundary reflects waves originating from the vibrating structure back into the discretized soil region, instead letting them propagate toward infinity. To overcome this, transmitting boundaries have been developed (Lysmer and Waas 1972), (Roesset and Ettouney 1977), (M. Petronijevic 1992).

Contemporary SSI analyses are based on the substructure approach, where the structure and soil have been analyzed separately and the dynamic analysis has been carried out in several steps. The FEM is usually used for structural modeling, while the soil region can be modeled using the FEM (M. Petronijevic 1992), BEM (Boundary Element Method) (Wolf 1993), TLM (Thin Layer Method) (Waas 1972), (Kausel, Roesset and Waas 1975) or ITM (Integral Transform Method), (Rastandi 2003), (Grundmann and Trommer 2001). In the TLM, the soil is vertically discretized using horizontal thin layers over the bedrock or half-space. Basic equations have been developed in the frequency domain, with exact expressions in the horizontal direction, while the accuracy in the vertical direction corresponds to the FEM, since linear variation of the displacements in the vertical direction is assumed. Based on the TLM, computer code SASSI 2000 in the frequency domain has been developed, (Laysmer et al. (1999)). It is based on the sub-structure approach. The structure is modeled using the FEM, while the

dynamic stiffness matrix of the soil has been obtained using the TLM. The BEM has been used by many researches in order to solve soil – structure interaction problems. It is a numerical technique based on boundary integral equation formulation of continuum mechanics problems. The key feature of the BEM is that the equations and unknowns of the problem are established only on the boundary, so only the boundary has to be discretized, which makes the BEM a very powerful numerical method for solving soil – structure interaction problems. The BEM formulation is based on the fundamental solution of the differential equation of motion for homogeneous, isotropic and linear – elastic media. In the ITM using a threefold Fourier transformation of horizontal space variables – x , y and time – t into the wave-number – frequency domain, basic partial equations of motion of the soil region have been transformed in a set of ordinary differential equations which can be solved analytically. This allows developing the dynamic stiffness matrix of a soil layer in the exact form. Consequently, the vertical discretization of the soil is influenced only by soil's material properties.

In the FEM the displacement field of each finite element is given as a polynomial function. The accuracy of the results depends on the size of finite elements used in the mesh, but the increase the number of finite elements takes greater computer time and effort to solve the problem. Generally, in dynamic analysis more finite elements are required than in the static analysis. The size of finite elements is also influenced by the highest frequency in the analysis. The higher the frequency is, the larger the number of finite elements is required in the analysis. According to Lysmer (1978) the size of the finite element needs to be 5 to 10 times as small as the wavelength of the highest frequency wave of interest. Alford et al. (1974) suggested the maximum size of finite element to be even 10 to 20 times smaller than the wavelength of the highest frequency.

As an alternative to the FEM in dynamic analysis, the Spectral Element Method (SEM) can be used to analyze a wide range of vibration problems (Doyle 1997), (Banerjee 1997), (Lee 2000), Lee et al.(2000). For one-dimensional elements, like beams and bars the displacement field of the spectral element is the exact solution of the partial differential equation of motion. Therefore, only one element can exactly represent the dynamic behavior of a structural member at any frequency. The shape functions and dynamic stiffness matrix of the spectral element are frequency dependent. Consequently, dynamic response analysis has to be carried out in the frequency domain.

For two-dimensional elements like plates it is not possible to obtain the exact solutions of the governing equations of motion that satisfy all boundary conditions, which are continuous functions of spatial variables. In order to find a solution of a problem, plate displacements are presented as infinite Fourier type series. For practical purposes, the series have to be truncated, which introduces an error. Consequently, the solutions are approximate and satisfy the prescribed degree of accuracy. Nevertheless, this is not a serious drawback, since the truncation point can be easily controlled by the user without re-meshing of the structure.

Application of spectral elements significantly reduces the number of the unknowns, increases the accuracy of the numerical results and decreases the computational time (Lee et al.(2000)). The precision of the SEM is one of its strongest points. As a consequence, arbitrarily and even infinitely large elements can be used without loss of accuracy, (Kulla 1997). In addition, the dynamic stiffness of the soil-foundation system, which is frequency dependent, can be easily and more efficiently incorporated in the spectral element model, Petronijevic et al. (2008), Nefovska-Danilovic et al. (2011), Radišić et al. (2012). The combination of continuous mass distribution, simple assemblage procedure (as in FEM) and the efficient Fast Fourier Transform (FFT) algorithms makes the SEM a powerful tool for solving wave propagation problems in structures.

1.1 Outline of the thesis

This thesis presents the application of the SEM in the dynamic response analysis of soil-structure system. The structure consists of one-dimensional elements: beams and columns and two-dimensional elements: plates. The substructure method has been applied, where the structure was modeled using the SEM, while the dynamic stiffness matrix of the soil-foundation interface was obtained using the ITM.

After the Introduction section, Section 2 introduces the Spectral Element Method. At the beginning the brief literature review of the application of one-dimensional and two-dimensional spectral elements is given. Afterwards, dynamic stiffness matrices for one-dimensional elements have been presented. The Projection method proposed by Kevorkian and Pascal (2001) and Casimir et al. (2005) as well as Gorman's superposition method (Gorman 1978), has been used in order to develop the dynamic

stiffness matrix for plate spectral element with arbitrary boundary conditions for both transverse and in-plane vibration. The developed dynamic stiffness matrices have been verified through several numerical examples.

Coupling of one-dimensional and two-dimensional spectral elements is presented in Section 3. The dynamic stiffness matrix of plate spectral element coupled with symmetrically distributed edge beams has been presented. Afterwards, the column - plate coupling has been developed. Verification of the proposed couplings has been carried out through several numerical examples using the FEM software SAP2000 (1996).

Section 4 starts with basic equations for the soil region. Using the spectral representation of the displacement field and Helmholtz's decomposition, equations of motion in the transformed wave number – frequency domain have been presented as well as the dynamic stiffness matrix of horizontally layered soil. Equations of motion for the soil – structure system have been developed in the frequency domain using the substructure approach. The dynamic stiffness matrix of surface rigid foundation is calculated from the corresponding stiffness matrix for flexible foundation, using kinematic transformation. At the end, the coupling between the structure modeled using the SEM, and the soil has been presented.

In Section 5 the developed numerical model has been applied in order to analyze the dynamic response of several 3D frame structures subjected to traffic-induced ground vibration including SSI.

The conclusions of the presented work and the ideas for the future research are given in Section 6.

2. Spectral Element Method

2.1 Literature review

As mentioned in the previous section, the SEM is based on the spectral representation of the displacement field and on the exact solution of the governing differential equations of motion defined in the frequency domain. First research in this area has been directed toward the development of the dynamic stiffness matrix and its application to the frequency response and free vibration analysis of one-dimensional elements. Kolousek

was the first one who developed the dynamic stiffness matrix of an Euler-Bernoulli beam in 1941, according to Banerjee and Williams (1992). In the past four decades numerous investigations have been carried out in order to develop the dynamic stiffness matrices for wide range of one-dimensional elements: Timoshenko beams (Wang et al. (1971), Banerjee and Williams(1992), Rafezy and Howson(2006)), beams on elastic foundation (Williams and Kennedy(1987)) and sandwich beams (Howson and Zare (2005)).

Doyle applied the SEM to wave propagation in structures. In his book (Doyle 1997) he investigated different types of elements: beams, bars, plates and cylindrical shells and applied the FFT and inverse FFT algorithm to transform the dynamic response from the frequency to time domain and vice versa. In addition, he developed the spectral super element which connects the SEM with the FEM. Various types of dynamic response analyses using the SEM have been analyzed by Lee et al.: continuum modeling of truss-type structures(Lee and Lee 1996), vibration analysis of one-dimensional structures using the spectral transfer matrix method (Lee 2000), analysis of elastic-piezoelectric two-layer beams (Lee and Kim 2000). The SEM can be easily coupled with the soil using the substructure method. The application of SEM in the SSI of 2D frame structures was done by Petronijevic et al. (2008) and Nefovska-Danilovic et al. (2011).

Vibration of two-edge plate assemblies have been analyzed by many researchers using the SEM. Anderson et al. developed the dynamic stiffness matrix of two-edge plate element, which incorporated in the computer program VIPASA for exact buckling and vibration analysis of plate assemblies such as stiffened panels, open and box section members (Anderson et al. (1983)). Danial et al. (1996) developed the dynamic stiffness matrix for two-edge infinite plates for both transverse and in-plane vibrations of folded plate structures. Bercin and Langley(1996) and Bercin (1997) employed the dynamic stiffness method to calculate free vibration characteristics of various simply supported, stiffened and directly coupled rectangular plate assemblies. Boscolo and Banerjee (2011)–a investigated the in-plane free vibration behavior of plates using the Dynamic Stiffness Method - DSM. They developed the dynamic stiffness matrix of plate element with two opposite edges simply supported and arbitrary boundary conditions assigned to another two edges.

Lee et al. investigated transverse vibrations of Levy-type plates subjected to distributed dynamic loads, ((Lee and Lee 1999), Lee et al. (2000)). Kulla (1997) was the first who developed high precision continuous element for transverse vibration analysis of plates with arbitrary boundary conditions and applied it to dynamic response analysis of plate assembly subjected to harmonic line load. Casimir et al. (2005) built the dynamic stiffness matrix of two-dimensional Kirchoff's plate element with free edges using Gorman's superposition method. Boscolo and Banerjee (2011) – b developed the dynamic stiffness matrix of plate using first order shear deformation theory. The dynamic stiffness matrix of plate undergoing in-plane vibration has been developed in this thesis, as well as the coupling of one-dimensional and two dimensional spectral elements.

2.2 One-dimensional spectral elements

In this section the dynamic stiffness matrix for one-dimensional elements: bars and beams, is presented. The dynamic stiffness matrix is formed in the frequency domain, using the exact solution of wave equations. It allows describing the inertia of the distributed mass exactly.

2.2.1 Spectral element for bars

A bar element with nodal displacements and corresponding forces is given in Figure 1. A bar element assumes only longitudinal wave motion. The equation of motion for a bar element can be obtained from the balance of forces, including the inertial force:

$$(N + dN) - N - \rho A i i dx = 0, \quad (1)$$

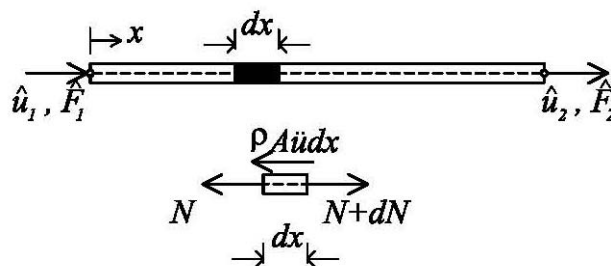


Figure 1. A bar spectral element

where A , ρ , $u = u(x, t)$ are, respectively, cross-sectional area, mass density and displacement in x direction of bar element. Assuming the linear elastic material behavior and constant cross section of bar element, the stress-strain relation is given as:

$$\sigma = \frac{N}{A} = E\varepsilon = E \frac{\partial u}{\partial x}, \quad (2)$$

where E is Young's modulus. According to expressions (1) and (2) the equation of motion of bar element is given as:

$$EA \frac{\partial^2 u}{\partial x^2} = \rho A \frac{\partial^2 u}{\partial t^2}. \quad (3)$$

Introducing spectral representation of the displacement $u(x, t)$ as:

$$u(x, t) = \sum_n \hat{u}(x, \omega_n) e^{i\omega_n t}, \quad (4)$$

where ω_n is angular frequency and $\hat{u}(x, \omega_n)$ is the amplitude of the n^{th} harmonic, the Fourier transform of Eq. (4) can be expressed as:

$$\frac{\partial^2 \hat{u}}{\partial x^2} + k_n^2 \hat{u} = 0, \quad n=1, 2, \dots, N \quad (5)$$

where $k_n = \omega_n \sqrt{\frac{\rho A}{EA}} = \frac{\omega_n}{c_p}$ is the wave number and $c_p = \sqrt{\frac{E}{\rho}}$ is the velocity of the

longitudinal - P waves. Eq. (5) represents the system of N independent ordinary differential equations. In the following, the subscript n will be omitted, but it will be understood that Eq. (5) has to be solved for each frequency. The general solution of differential Eq. (5) is given as:

$$\hat{u}(x, \omega) = C_1 e^{-ikx} + C_2 e^{ikx}. \quad (6)$$

Constants C_1 and C_2 are obtained from the boundary conditions:

$$\hat{u}(0) = \hat{u}_1, \quad \hat{u}(L) = \hat{u}_2. \quad (7)$$

The above relation can be written in matrix form as:

$$\hat{\mathbf{q}} = \mathbf{DC}, \quad (8)$$

where $\hat{\mathbf{q}}^T = [\hat{u}_1 \quad \hat{u}_2]$ is the vector of nodal displacements, $\mathbf{C}^T = [C_1 \quad C_2]$ is the constant vector and

$$\mathbf{D} = \begin{bmatrix} 1 & 1 \\ e^{-ikL} & e^{ikL} \end{bmatrix}. \quad (9)$$

Vector of nodal forces of bar element $\hat{\mathbf{Q}}^T = [\hat{F}_1 \quad \hat{F}_2] = \left[-EA \frac{\partial \hat{u}(0)}{\partial x} \quad EA \frac{\partial \hat{u}(L)}{\partial x} \right]$ can be expressed in the matrix form as:

$$\hat{\mathbf{Q}} = \mathbf{F} \mathbf{C}, \quad (10)$$

where

$$\mathbf{F} = ikEA \begin{bmatrix} 1 & -1 \\ -e^{-ikL} & e^{ikL} \end{bmatrix}. \quad (11)$$

Eliminating the constant vector \mathbf{C} from Eq. (8) and (10) gives:

$$\hat{\mathbf{Q}} = \mathbf{F} \mathbf{D}^{-1} \hat{\mathbf{q}} = \mathbf{K}_D^a \hat{\mathbf{q}}, \quad (12)$$

where \mathbf{K}_D^a is frequency dependent dynamic stiffness matrix of bar element:

$$\mathbf{K}_D^a = \frac{EA}{L} \frac{ikL}{1 - e^{-i2kL}} \begin{bmatrix} 1 + e^{-i2kL} & -2e^{-ikL} \\ -2e^{-ikL} & 1 + e^{-i2kL} \end{bmatrix}. \quad (13)$$

Generally, the dynamic stiffness matrix of bar element is complex, but in case when there is no damping, it becomes real.

2.2.2. Spectral element for beams

The dynamic stiffness matrix of a beam element for flexural motion, can be derived in a similar way as for the bar element. An Euler-Bernoulli beam element with nodal displacements and corresponding forces is given in Figure 2. The beam element has two equilibrium equations, obtained neglecting the rotational inertia:

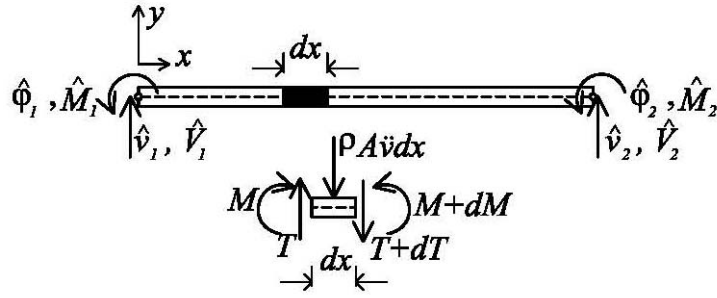


Figure 2. A beam spectral element

$$\begin{aligned} \frac{\partial T}{\partial x} + \rho A \frac{\partial^2 v}{\partial t^2} &= 0 \\ \frac{\partial M}{\partial x} &= T \end{aligned} \quad (14)$$

where $v = v(x, t)$ is the transverse displacement of beam element. According to the Euler-Bernoulli theory, the axial strain in x direction is:

$$\varepsilon = \frac{\partial u}{\partial x} = -y \frac{\partial^2 v}{\partial x^2}. \quad (15)$$

Assuming linear elastic behavior of beam element, the corresponding stress and resultant bending moment are given as:

$$\begin{aligned} \sigma &= E\varepsilon = -yE \frac{\partial^2 v}{\partial x^2} \\ M &= \int_A -\sigma y dA = EI \frac{\partial^2 v}{\partial x^2} \end{aligned} \quad (16)$$

where $I = \int_A y^2 dA$ is the second moment of inertia. Substituting Eq. (16) into Eq. (14), the differential equation of motion of beam element is obtained:

$$EI \frac{\partial^4 v}{\partial x^4} + \rho A \frac{\partial^2 v}{\partial t^2} = 0. \quad (17)$$

Introducing spectral representation of displacement $v(x, t)$ as

$$v(x, t) = \sum \hat{v}(x, \omega) e^{i\omega t}, \quad (18)$$

where ω is the angular frequency, the Fourier transform of Eq. (17) can be expressed as

$$\frac{\partial^4 \hat{v}}{\partial x^4} - k^4 \hat{v} = 0, \quad (19)$$

where $k = \sqrt{\omega \sqrt{\frac{\rho A}{EI}}}$ is the wave number. The general solution of differential Eq. (19) is

$$\hat{v}(x, \omega) = C_1 e^{-ikx} + C_2 e^{ikx} + C_3 e^{-kx} + C_4 e^{kx}. \quad (20)$$

C_1, C_2, C_3 and C_4 are constants, which can be obtained from the boundary conditions at the beam's ends:

$$\hat{v}(0) = \hat{v}_1, \quad \hat{\phi}(0) = \left(\frac{d\hat{v}}{dx} \right)_0 = \hat{\phi}_1, \quad \hat{v}(L) = \hat{v}_2, \quad \hat{\phi}(L) = \left(\frac{d\hat{v}}{dx} \right)_L = \hat{\phi}_2. \quad (21)$$

The above relation can be written in the matrix form as:

$$\hat{\mathbf{q}} = \mathbf{D}\mathbf{C}, \quad (22)$$

where $\hat{\mathbf{q}}^T = [\hat{v}_1 \quad \hat{\phi}_1 \quad \hat{v}_2 \quad \hat{\phi}_2]$ is the vector of nodal displacements,

$\mathbf{C}^T = [C_1 \quad C_2 \quad C_3 \quad C_4]$ is the vector of integration constants and

$$\mathbf{D} = \begin{bmatrix} 1 & 1 & 1 & 1 \\ -ik & ik & -k & k \\ e^{-ikL} & e^{ikL} & e^{-kL} & e^{kL} \\ -ike^{-ikL} & ike^{ikL} & -ke^{-kL} & ke^{kL} \end{bmatrix}. \quad (23)$$

Vector of nodal forces of beam element can be expressed as:

$$\hat{\mathbf{Q}} = \mathbf{F}\mathbf{C}, \quad (24)$$

where

$$\mathbf{F} = EI \begin{bmatrix} ik^3 & -ik^3 & -k^3 & k^3 \\ k^2 & k^2 & -k^2 & -k^2 \\ -ik^3 e^{-ikL} & ik^3 e^{ikL} & k^3 e^{-kL} & -k^3 e^{kL} \\ -k^2 e^{-ikL} & -k^2 e^{ikL} & k^2 e^{-kL} & k^2 e^{kL} \end{bmatrix}. \quad (25)$$

Eliminating the constant vector \mathbf{C} from Eq. (22) and (24) gives:

$$\hat{\mathbf{Q}} = \mathbf{F}\mathbf{D}^{-1}\hat{\mathbf{q}} = \mathbf{K}_D^b\hat{\mathbf{q}}. \quad (26)$$

$\mathbf{K}_D^b = \mathbf{F}\mathbf{D}^{-1}$ is frequency dependent dynamic stiffness matrix of beam element:

$$\mathbf{K}_D^b = \begin{bmatrix} k_{11} & k_{12} & k_{13} & k_{14} \\ & k_{22} & k_{23} & k_{24} \\ \text{symm} & & k_{33} & k_{34} \\ & & & k_{44} \end{bmatrix}, \quad (27)$$

where

$$\begin{aligned} k_{11} = k_{33} &= \frac{(1+i)k^3(-i-e_2^2+e_1^2(1+ie_2^2))}{\Delta} \\ k_{22} = k_{44} &= \frac{(1+i)k(-1+ie_2^2+e_1^2(i+e_2^2))}{\Delta} \\ k_{12} = -k_{34} &= \frac{ik^2(e_1^2-1)(e_2^2-1)}{\Delta} \\ k_{13} &= \frac{2k^3(ie_2-ie_1^2e_2+e_1(e_2^2-1))}{\Delta} \\ k_{14} = -k_{23} &= \frac{2k^2(e_2+e_1^2e_2-e_1(e_2^2+1))}{\Delta} \\ \Delta &= 1-4e_1e_2+e_1^2(1+e_2^2), \quad e_1 = e^{ikL}, \quad e_2 = e^{kL}. \end{aligned} \quad (28)$$

2.2.3. Spectral element for torsional bar

Figure 3 shows nodal moments and rotations for a torsional bar element. The equation of motion is obtained from the balance of forces including the inertial force and using the well-known moment-rotation relation:

$$\left. \begin{aligned} \frac{\partial M_t}{\partial x} &= \rho J \ddot{\varphi}_x \\ M_t &= GJ \frac{\partial \varphi_x}{\partial x} \end{aligned} \right\} \Rightarrow \frac{\partial^2 \varphi_x}{\partial x^2} = \rho J \frac{\partial^2 \varphi_x}{\partial t^2}, \quad (29)$$

where G and J are respectively, the shear modulus and torsional inertia moment for the element cross-section. Introducing the spectral representation of the rotation:

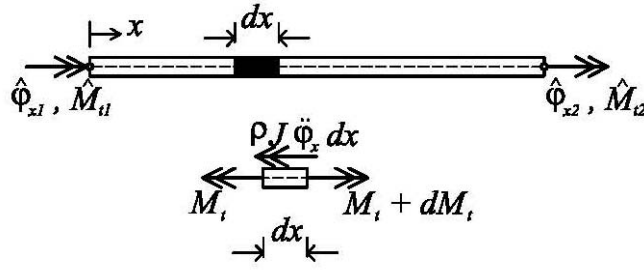


Figure 3. Torsional bar element

$$\varphi_x(x, t) = \sum \hat{\varphi}_x(x, \omega) e^{i\omega t}, \quad (30)$$

the Fourier transform of Eq. (30) can be expressed as:

$$\frac{d^2 \hat{\varphi}_x}{dx^2} + k^2 \hat{\varphi}_x = 0 \quad (31)$$

where $k = \omega \sqrt{\frac{\rho J}{GJ}} = \frac{\omega}{c_s}$ is the wave number and $c_s = \sqrt{\frac{G}{\rho}}$ is the velocity of the shear - S

waves. It can be seen that equations of motion for longitudinal and torsional waves in bar element have the same form. Consequently, the dynamic stiffness matrix for torsional bar has the same form as the corresponding dynamic stiffness matrix of bar element:

$$\hat{\mathbf{Q}} = \mathbf{K}_D^t \hat{\mathbf{q}}$$

$$\hat{\mathbf{q}} = \begin{bmatrix} \hat{\varphi}_{x1} \\ \hat{\varphi}_{x2} \end{bmatrix} \quad \hat{\mathbf{Q}} = \begin{bmatrix} \hat{M}_{t1} \\ \hat{M}_{t2} \end{bmatrix} \quad \mathbf{K}_D^t = \frac{GJ}{L} \frac{ikL}{1 - e^{-i2kL}} \begin{bmatrix} 1 + e^{-i2kL} & -2e^{-ikL} \\ -2e^{-ikL} & 1 + e^{-i2kL} \end{bmatrix}. \quad (32)$$

2.2.4. Development of the dynamic stiffness matrix for 3D frame structures

In order to analyze 3D frame structures using the SEM, the frequency dependent dynamic stiffness matrix is formed by the assemblage of the dynamic stiffness matrices for bar and beam elements at a specific frequency. It comprises axial loading, torsion and bending about each of the two principal axes. 3D frame element with nodal displacements and corresponding nodal forces is presented in Figure 4. The dynamic stiffness matrix is obtained by superimposing the dynamic stiffness matrices for axial loading - a , bending - b and torsion - t , developed in the previous subsections:

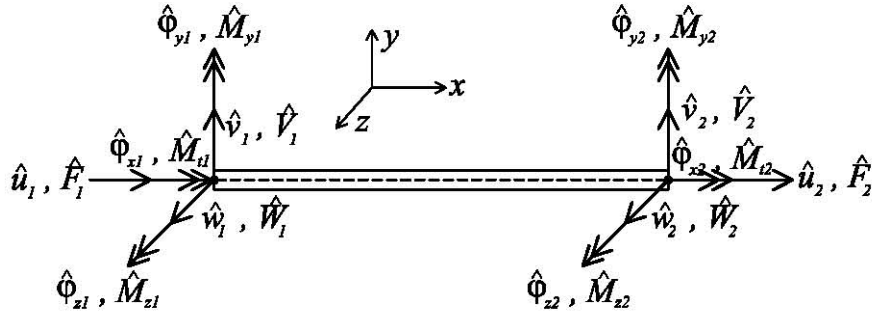


Figure 4. 3D frame element

$$\begin{bmatrix} \hat{F}_1 \\ \hat{V}_1 \\ \hat{W}_1 \\ \hat{M}_{x_1} \\ \hat{M}_{y_1} \\ \hat{M}_{z_1} \\ \hat{F}_2 \\ \hat{V}_2 \\ \hat{W}_2 \\ \hat{M}_{x_2} \\ \hat{M}_{y_2} \\ \hat{M}_{z_2} \end{bmatrix} = \begin{bmatrix} k_{11}^a & 0 & 0 & 0 & 0 & 0 & k_{12}^a & 0 & 0 & 0 & 0 & 0 \\ & k_{11}^b & 0 & 0 & 0 & k_{12}^b & 0 & k_{13}^b & 0 & 0 & 0 & k_{14}^b \\ & & k_{11}^b & 0 & -k_{12}^b & 0 & 0 & 0 & k_{13}^b & 0 & -k_{14}^b & 0 \\ & & & k_{11}^t & 0 & 0 & 0 & 0 & 0 & k_{12}^t & 0 & 0 \\ & & & & k_{22}^b & 0 & 0 & 0 & -k_{23}^b & 0 & k_{24}^b & 0 \\ & & & & & k_{22}^b & 0 & k_{23}^b & 0 & 0 & 0 & k_{24}^b \\ & & & & & & k_{22}^a & 0 & 0 & 0 & 0 & 0 \\ & & & & & & & k_{33}^b & 0 & 0 & 0 & k_{34}^b \\ & & & & & & & & k_{33}^b & 0 & -k_{34}^b & 0 \\ & & & & & & & & & k_{22}^t & 0 & 0 \\ & & & & & & & & & & k_{44}^b & 0 \\ & & & & & & & & & & & k_{44}^b \end{bmatrix} \begin{bmatrix} \hat{u}_1 \\ \hat{v}_1 \\ \hat{w}_1 \\ \hat{\phi}_{x_1} \\ \hat{\phi}_{y_1} \\ \hat{\phi}_{z_1} \\ \hat{u}_2 \\ \hat{v}_2 \\ \hat{w}_2 \\ \hat{\phi}_{x_2} \\ \hat{\phi}_{y_2} \\ \hat{\phi}_{z_2} \end{bmatrix} \quad (33)$$

The dynamic stiffness matrix of frame structure is obtained using the well known transformation and assembling techniques of the FEM, (Bathe and Wilson 1976).

2.2.5. Dynamic response analysis

The fundamental equation of frame structure in the frequency domain is:

$$\hat{\mathbf{F}} = \mathbf{K}_D \hat{\mathbf{u}}, \quad (34)$$

where $\hat{\mathbf{F}}$ and $\hat{\mathbf{u}}$ are the nodal force and displacement vectors in the frequency domain, respectively and \mathbf{K}_D is the structural dynamic stiffness matrix. In order to account for damping in the structure, a hysteretic damping model is adopted, where the Young's modulus E is replaced with the complex value:

$$E_c = E(1 + 2i\zeta), \quad (35)$$

where ζ is the damping ratio.

Decomposing the dynamic stiffness matrix with respect to the unknown (n) and the prescribed (p) degrees of freedom, Eq. (34) can be written in the following form:

$$\begin{bmatrix} \mathbf{K}_{D_{nn}} & \mathbf{K}_{D_{np}} \\ \mathbf{K}_{D_{pn}} & \mathbf{K}_{D_{pp}} \end{bmatrix} \begin{bmatrix} \hat{\mathbf{u}}_n \\ \hat{\mathbf{u}}_p \end{bmatrix} = \begin{bmatrix} \hat{\mathbf{F}}_n \\ \hat{\mathbf{F}}_p \end{bmatrix}, \quad (36)$$

Eq. (36) is a system of linear algebraic equations with complex coefficients. Unknown displacements in the frequency domain can be calculated from the Eq. (36) as:

$$\hat{\mathbf{u}}_n = \mathbf{K}_{D_{nn}}^{-1} \left(\hat{\mathbf{F}}_n - \mathbf{K}_{D_{np}} \hat{\mathbf{u}}_p \right). \quad (37)$$

Using the inverse Fourier transformation, the dynamic response in the time domain can be obtained. Transformation from time to frequency domain and vice versa is defined with the Fourier transform pair of an arbitrary function x :

$$\hat{x}(\omega) = \int_{-\infty}^{+\infty} x(t) e^{-i\omega t} dt, \quad x(t) = \frac{1}{2\pi} \int_{-\infty}^{+\infty} \hat{x}(\omega) e^{i\omega t} d\omega. \quad (38)$$

Integrals in Eq. (38) are solved numerically, using Discrete Fourier Transformation (DFT) or Fast Fourier Transformation (FFT), (Bracewell 2000). The discrete Fourier transform pair is defined as:

$$\begin{aligned} \hat{x}(\omega_m) &= \Delta t \sum_{n=0}^{N-1} x(t_n) e^{-2\pi i \frac{nm}{N}} \quad m = 0, 1, 2, \dots, N-1 \\ x(t_n) &= \frac{\Delta \omega}{2\pi} \sum_{m=0}^{N-1} \hat{x}(\omega_m) e^{2\pi i \frac{nm}{N}} \quad n = 0, 1, 2, \dots, N-1 \end{aligned}, \quad (39)$$

where $t_n = n\Delta t$, $\omega_m = m\Delta\omega$, N is the number of points in the transformation, Δt and $\Delta\omega$ are respectively the time and frequency increments. Application of FFT algorithms efficiently transforms the dynamic response from one domain to another.

Natural frequencies and mode shapes of frame structure can be obtained from Eq. (36) setting the force vector to zero:

$$\mathbf{K}_{D_{nn}} \hat{\mathbf{u}}_n = 0 \quad (40)$$

Zeros of the determinant of the dynamic stiffness matrix $\mathbf{K}_{D_{nn}}$ define the natural frequencies of the frame structure. In order to avoid numerical difficulties, instead of plotting the determinant $\det|\mathbf{K}_{D_{nn}}|$, the natural frequencies are defined as maxima of the following expression, (Doyle 1997):

$$\log\left(\frac{1}{\det|\mathbf{K}_{D_{nn}}(\omega)|}\right). \quad (41)$$

The mode shapes are computed using Eq. (40) and setting one of the nodal displacements to an arbitrary value.

1.1.1.1 Numerical examples

➤ Dynamic response of a cantilever beam

As the first illustrative example, let's consider an Euler-Bernoulli beam fixed at one end, as described in Figure 5. The beam is subjected to rectangular impulse force given in Figure 6. The duration of the impulse is 0.1 seconds.

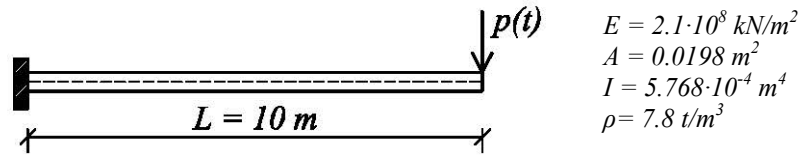


Figure 5. Layout of beam geometry

Natural frequencies calculated using the SEM and FEM - for different number of finite elements are presented in Table 1. For the FEM modeling, SAP2000 software has been used, (SAP2000 1996). The mass of the structure has been lumped in the structural nodes. Unlike the FEM, the SEM provides infinite number of modes using only one spectral element. As the number of finite elements increase, the natural frequencies obtained by the FEM converge to those obtained by the SEM. Time history and corresponding response spectrum of beam displacement using the SEM are given in Figure 7. Vibration response has been calculated for different number of points (NFFT) in the FFT. Due to the discretization of the input and response functions in both time and frequency domain, these functions are periodic.

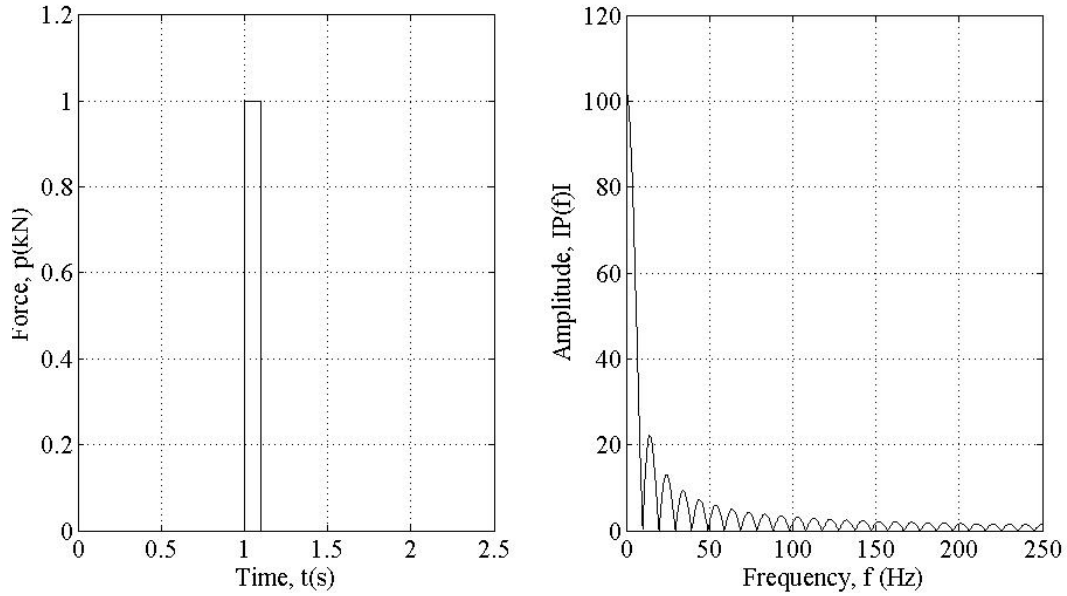


Figure 6. Time history and spectrum of input force

Consequently, choosing a sufficiently large number of points in the FFT, errors due to the periodicity assumption can be minimized, as it was shown in Figure 7. Figure 8 shows the comparison between the time histories and frequency responses of a beam using the SEM and FEM. As the number of finite elements increase, the FEM provides more accurate response.

Table 1. Natural frequencies of cantilever beam obtained using SEM and FEM

Mode No.	f_{SEM} (Hz)	f_{FEM} (Hz) - SAP2000				
		$n=1$	$n=2$	$n=4$	$n=8$	$n=16$
1	4.96	3.45	4.45	4.82	4.92	4.95
2	31.1		22.9	28.3	30.3	30.9
3	87			75	83.6	86.1
4	170.4			130.7	161.1	168
5	281.7				261.3	276.5
6	420.8				379	411.3
7	587.7				498.9	571.7

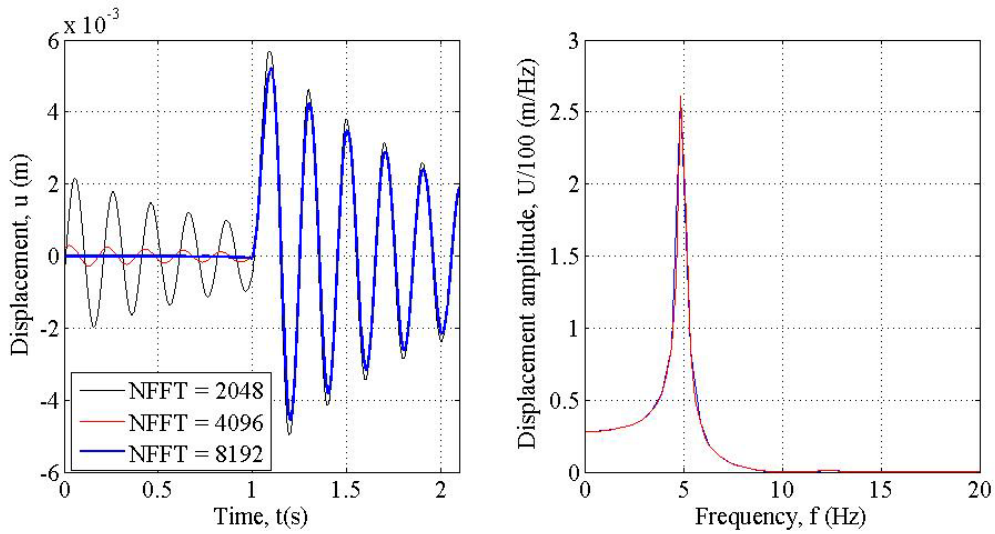


Figure 7. Time history and frequency response spectrum of cantilever beam obtained using SEM

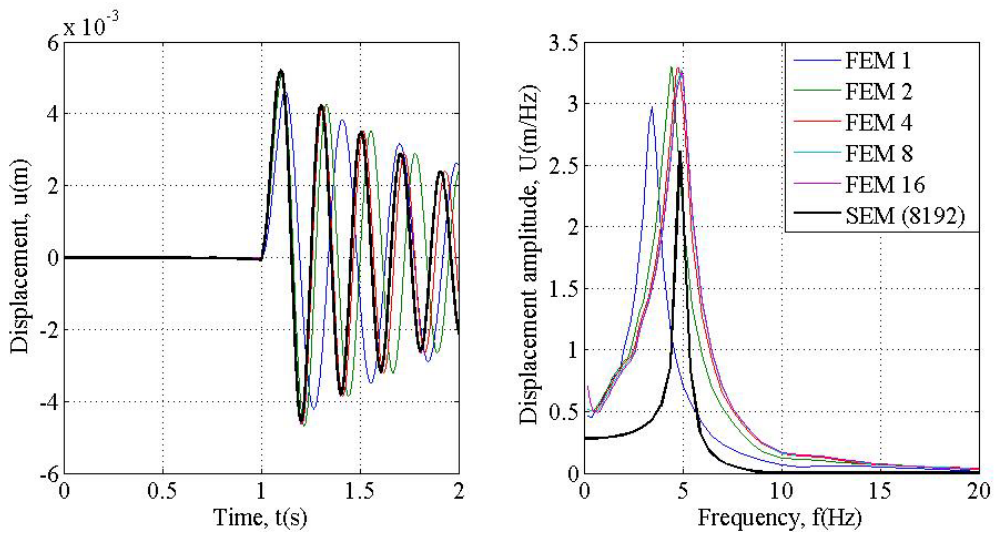


Figure 8. Comparison of vibration responses obtained using SEM and FEM

➤ Free vibration analysis of 3D frame

A simple 3D frame structure is presented in Figure 9. All members have the same geometrical and material properties. Free vibration analysis has been carried out using the SEM and FEM. The number of finite elements per member - n in the FEM analysis has been varied from 1 to 8. The results are presented in Table 2. The FEM model created in SAP 2000 did not include the torsional inertia in the analysis. Good agreement is achieved especially for lower vibration modes.

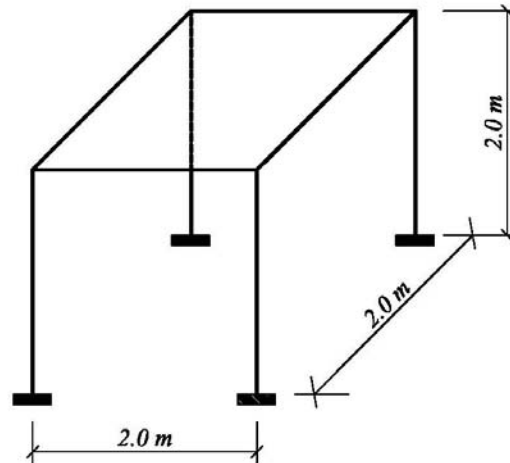


Figure 9. Layout and geometry of 3D frame structure

Table 2. Natural frequencies of 3D frame structure

Mode No.	f_{SEM} (Hz)	f_{FEM} (Hz) - SAP2000			
		$n=1$	$n=2$	$n=4$	$n=8$
1	29.6	28.1	29.6	29.8	29.9
2	37.7	31.1	36.3	37.7	38
3	65.1	55.7	64.9	65.6	65.7
4	120.7	225	122.4	123.1	123
5	135	227.1	138.8	138.5	137.9
6	147	229.8	147.9	150.7	150.8
7	151	319.2	151.4	153.4	153.1
8	201	320.4	191.8	204.1	204.8
9	222.6		209.1	224.2	225.0
10	236.3		215.6	237.4	238.5
11	242		216.1	242.7	244.5

2.3 Two-dimensional spectral elements

In this section the development of the dynamic stiffness matrices of the completely free rectangular plates undergoing transverse and in-plane vibrations will be developed. The basic idea is to describe the plate displacements in the form of infinite series, which has to be truncated for practical purposes. The Projection method proposed by Kevorkian and Pascal, (2001) and Casimir et al. (2005) and Gorman's superposition method (Gorman 1978) has been used in order to develop the dynamic stiffness matrices.

Depending on an elastodynamic theory, general form of the equation of motion of the two-dimensional domain V in the frequency domain without the presence of external distributed load can be given as:

$$L(\mathbf{u}) + \rho h \omega^2 \mathbf{u} = 0, \quad (42)$$

where $\mathbf{u} = \mathbf{u}(x, y)$ is the displacement vector, ρ is the mass density, h is the plate thickness, ω is the circular frequency, and L is the differential operator. The number p of components of the displacement vector depends on the elastodynamic plate theory, i.e. whether transverse or in-plane vibrations are analyzed. As said in the previous sections, for two-dimensional elements like plates there is no exact solution of the governing equations of motion that satisfies arbitrary boundary conditions. In order to find a solution of a problem, p components u_i of plate displacement vector \mathbf{u} are presented as infinite series:

$$u_i(x, y) = \sum_{m=1}^{\infty} C_m f_m(x, y), \quad i = 1, \dots, p, \quad (43)$$

where C_m are integration constants, which can be obtained from the boundary conditions and $f_m(x, y)$ are base functions that satisfy the homogeneous Eq. (42). For practical purposes, the infinite series representation has to be truncated to a point M , i.e. the displacement field is represented in the following form:

$$u_i(x, y) \approx \sum_{m=1}^M C_m f_m(x, y). \quad (44)$$

The functions $f_m(x, y)$ are chosen so that they give a good approximation of the general solution of the Eq. (42) for small number of M . Eq. (44) can be written in the matrix form as:

$$\mathbf{u}(x, y) \approx \mathbf{\Phi}(x, y) \mathbf{C}, \quad (45)$$

where \mathbf{C} is the vector of integration constants and $\mathbf{\Phi}(x, y)$ is matrix which contains functions $f_m(x, y)$. The force vector $\mathbf{f}(x, y)$ is function of derivatives of the displacement functions and can be expressed as:

$$\mathbf{f}(x, y) \approx \mathbf{G}(x, y) \mathbf{C}, \quad (46)$$

where the elements of matrix $\mathbf{G}(x, y)$ are the derivatives of the components of the matrix $\mathbf{\Phi}(x, y)$.

Boundary conditions

If $B(s)$ is the function which defines the boundary of the two-dimensional domain V and s is the curvilinear abscissa, the displacements along the boundary $\mathbf{q}(s)$ can be written as:

$$\mathbf{q}(s) \approx \mathbf{\Phi}(B(s))\mathbf{C} = \mathbf{\Phi}_b(s)\mathbf{C}. \quad (47)$$

From Eq. (46) the force vector along the boundary - $\mathbf{Q}(s)$ is given as:

$$\mathbf{Q}(s) \approx \mathbf{G}(B(s))\mathbf{C} = \mathbf{G}_b(s)\mathbf{C}. \quad (48)$$

The displacements $\mathbf{q}(s)$ and forces $\mathbf{Q}(s)$ along the boundary are continuous functions of spatial variable s . Therefore it is not possible to define the relation between the displacement and force vectors on the boundary, as in case of one – dimensional elements. The spatial dependence can be avoided by so-called Projection method (Kevorkian and Pascal 2001), which is based on the projection of the displacements and forces on the boundary onto a set of functions $h(s)$:

$$\begin{aligned} \tilde{q}_i(s) &\approx \sum_{m=1}^M \langle q_i, h_m \rangle h_m(s), \quad i = 1, \dots, p \\ \tilde{Q}_i(s) &\approx \sum_{m=1}^M \langle Q_i, h_m \rangle h_m(s), \quad i = 1, \dots, p \end{aligned}, \quad (49)$$

The projections of the functions are defined as the scalar product:

$$\langle f, g \rangle = \int_{B(s)} f(s)g(s)ds. \quad (50)$$

If the functions $h(s)$ are trigonometric, then this method is equivalent to the Fourier series development of the displacement and force functions along the boundary. Now, the $p \times M$ projections of the displacements and forces along the boundary B are collected into vectors:

$$\begin{aligned} \tilde{\mathbf{q}} &= [\langle q_i, h_m \rangle] \\ \tilde{\mathbf{Q}} &= [\langle Q_i, h_m \rangle] \end{aligned}, \quad i = 1, \dots, p \quad m = 1, \dots, M \quad (51)$$

Dynamic stiffness matrix

Using Eq. (47), (48) and (51) the following relations are obtained between the displacement and force projections and integration constants:

$$\begin{aligned}\tilde{q}_{(i-1)M+m} &= \langle q_i, h_m \rangle = \langle \Phi_{b_{ij}} C_j, h_m \rangle = \langle \Phi_{b_{ij}}, h_m \rangle C_j \\ \tilde{Q}_{(i-1)M+m} &= \langle Q_i, h_m \rangle = \langle G_{b_{ij}} C_j, h_m \rangle = \langle G_{b_{ij}}, h_m \rangle C_j\end{aligned}\quad (52)$$

or in matrix form:

$$\begin{aligned}\tilde{\mathbf{q}} &= \tilde{\mathbf{D}}\mathbf{C} \\ \tilde{\mathbf{Q}} &= \tilde{\mathbf{F}}\mathbf{C}\end{aligned}\quad (53)$$

where

$$\begin{aligned}D_{(i-1)M+m,j} &= \langle \Phi_{b_{ij}}, h_m \rangle \\ F_{(i-1)M+m,j} &= \langle G_{b_{ij}}, h_m \rangle\end{aligned}\quad (54)$$

Eliminating the vector of unknown constants \mathbf{C} from the expressions in Eq. (53), the following relation is obtained:

$$\tilde{\mathbf{Q}} = \tilde{\mathbf{F}}\tilde{\mathbf{D}}^{-1}\tilde{\mathbf{q}} = \tilde{\mathbf{K}}_D\tilde{\mathbf{q}}. \quad (55)$$

$\tilde{\mathbf{K}}_D = \tilde{\mathbf{F}}\tilde{\mathbf{D}}^{-1}$ is the dynamic stiffness matrix of two-dimensional domain. Eqs. (53) and (55) have the same form as the corresponding expressions for one-dimensional spectral elements. The only difference is in the displacement and force vectors $\tilde{\mathbf{q}}$ and $\tilde{\mathbf{Q}}$, which contain the projections of the plate displacements and forces along the boundary.

In the following sections the dynamic stiffness matrix for transverse and in-plane vibration of rectangular plates with completely free boundaries will be developed using the aforementioned theory.

2.3.1 Plate spectral element for transverse vibration

2.3.1.1 Equation of motion

A rectangular plate of thickness h and dimensions $2a \times 2b$ is shown in Figure 10. The plate spectral element is based on Kirchhoff's plate theory, which is the equivalent of Euler-Bernoulli beam theory. It is based on the assumptions that the plate is incompressible in the transverse - z direction and that the transverse shear deformation

is negligible, i.e. $\varepsilon_z = 0$ and $\gamma_{xz} = \gamma_{yz} = 0$. According to these assumptions, the displacements of the plate are:

$$u(x, y, z) = -z \frac{\partial w(x, y)}{\partial x}, \quad v(x, y, z) = -z \frac{\partial w(x, y)}{\partial y}, \quad w(x, y, z) = w(x, y), \quad (56)$$

where $w(x, y)$ is the transverse displacement of the plate mid-surface. The corresponding normal and shear strains are:

$$\varepsilon_x = \frac{\partial u}{\partial x} = -z \frac{\partial^2 w}{\partial x^2}, \quad \varepsilon_y = \frac{\partial v}{\partial y} = -z \frac{\partial^2 w}{\partial y^2}, \quad \gamma_{xy} = \frac{\partial u}{\partial y} + \frac{\partial v}{\partial x} = -2z \frac{\partial^2 w}{\partial x \partial y}. \quad (57)$$

Using Eq. (57) and the Hooke's law for plain stress the following stress – displacement relations are obtained:

$$\begin{aligned} \sigma_x &= -z \frac{E}{1-\nu^2} \left(\frac{\partial^2 w}{\partial x^2} + \nu \frac{\partial^2 w}{\partial y^2} \right) \\ \sigma_y &= -z \frac{E}{1-\nu^2} \left(\frac{\partial^2 w}{\partial y^2} + \nu \frac{\partial^2 w}{\partial x^2} \right). \\ \tau_{xy} &= -z \frac{E}{1+\nu} \frac{\partial^2 w}{\partial x \partial y} \end{aligned} \quad (58)$$

Internal forces of the plate defined in Figure 10 are resultant forces of the corresponding stresses acting on the edge faces:

$$\begin{aligned} M_x &= - \int_{-h/2}^{h/2} \sigma_x z dz = D \left(\frac{\partial^2 w}{\partial x^2} + \nu \frac{\partial^2 w}{\partial y^2} \right) \\ M_y &= - \int_{-h/2}^{h/2} \sigma_y z dz = D \left(\frac{\partial^2 w}{\partial y^2} + \nu \frac{\partial^2 w}{\partial x^2} \right), \\ M_{xy} &= - \int_{-h/2}^{h/2} \tau_{xy} z dz = D(1-\nu) \frac{\partial^2 w}{\partial x \partial y} \end{aligned} \quad (59)$$

where $D = \frac{Eh^3}{12(1-\nu^2)}$ is flexural stiffness of the plate. The shear forces cannot be obtained integrating the corresponding shear stresses, since the stresses do not have a relationship to the corresponding deformations γ_{xz} and γ_{yz} , which are equal zero. The shear forces are obtained from the equilibrium equations of the infinitesimal element of

the plate, presented in Figure 11. According to Figure 11 the following equilibrium equations are derived:

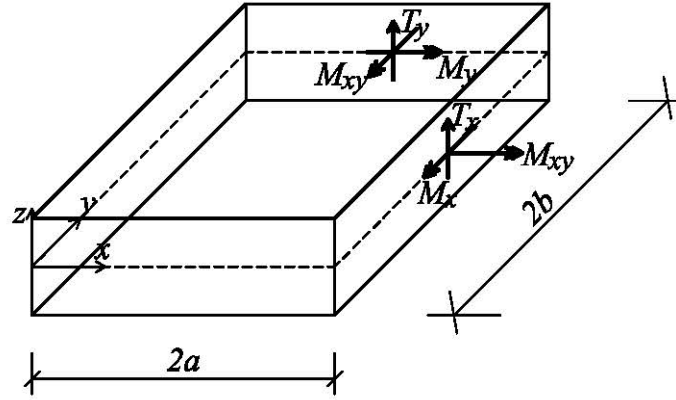


Figure 10. Internal forces of plate element undergoing transverse vibration

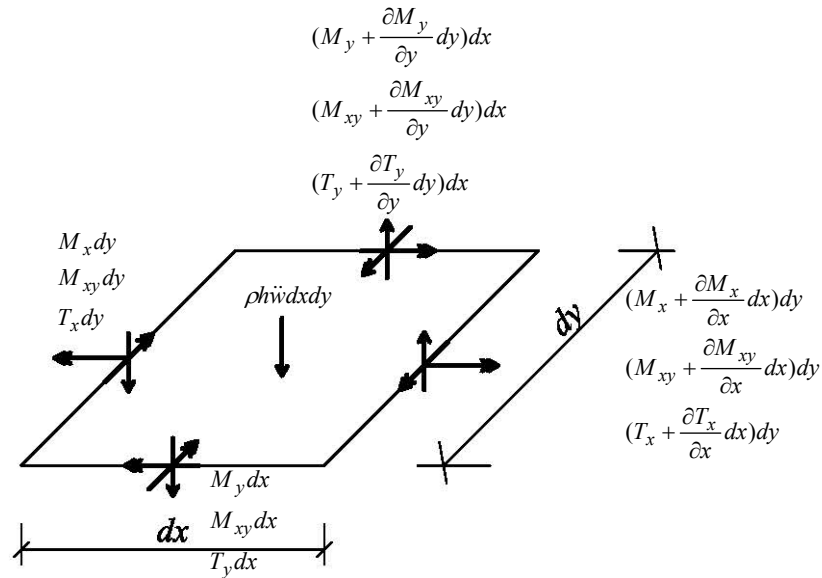


Figure 11. Infinitesimal element of plate

$$\begin{aligned}
 \frac{\partial M_x}{\partial x} + \frac{\partial M_{xy}}{\partial y} + T_x &= 0 \\
 \frac{\partial M_{xy}}{\partial x} + \frac{\partial M_y}{\partial y} + T_y &= 0 \quad . \\
 \frac{\partial T_x}{\partial x} + \frac{\partial T_y}{\partial y} - \rho h \frac{\partial^2 w}{\partial t^2} &= 0
 \end{aligned} \tag{60}$$

Substituting Eq. (59) into Eq. (60)-(a) and (60)-(b), and then into Eq. (60)-(c), the equation of motion of plate undergoing transverse vibration is obtained:

$$\Delta\Delta w + \frac{\rho h}{D} \frac{\partial^2 w}{\partial t^2} = 0, \quad (61)$$

where $\Delta\Delta$ is Laplace operator: $\frac{\partial^4}{\partial x^4} + 2\frac{\partial^4}{\partial x^2 \partial y^2} + \frac{\partial^4}{\partial y^4}$.

Introducing spectral representation of the transverse displacement $w(x, y, t)$ as:

$$w(x, y, t) = \sum w(x, y, \omega) e^{i\omega t}, \quad (62)$$

the Fourier transform of Eq.(61) can be expressed as:

$$\Delta\Delta \hat{w} - \frac{\rho h}{D} \omega^2 \hat{w} = 0. \quad (63)$$

2.3.1.2 General solution

According to Gorman's superposition method (Gorman 1978), the transverse displacement of rectangular plate is split into four contributions: symmetric-symmetric (SS), antisymmetric-antisymmetric (AA), symmetric-antisymmetric (SA) and antisymmetric-symmetric (AS):

$$\hat{w}(x, y) = \hat{w}_{SS}(x, y) + \hat{w}_{AA}(x, y) + \hat{w}_{SA}(x, y) + \hat{w}_{AS}(x, y). \quad (64)$$

The first letter in the subscripts in Eq. (64) designates the type of symmetry about y -axis and the second about x -axis. This method allows one to analyze only one quarter of the rectangular plate. Each of the above contributions $\hat{w}_{ab}(x, y)$ ($a, b = S, A$) are expressed according to Eq. (44). The displacement vector has only one component, the transverse displacement w , i.e. $p = 1$.

➤ Symmetric-symmetric contribution (SS)

In order to satisfy double symmetry condition, the transverse displacement is defined as:

$$\hat{w}_{SS}(x, y) = \sum_{m=0}^M {}^1W_{SS_m}(y) \cos \frac{m\pi x}{a} + \sum_{m=0}^M {}^2W_{SS_m}(x) \cos \frac{m\pi y}{b}, \quad (65)$$

where ${}^1W_{SS_m}(y)$ and ${}^2W_{SS_m}(x)$ are even functions. They are obtained substituting Eq. (65) into the equation of motion (63), and omitting the odd contributions of the solution:

$$\begin{aligned} {}^1W_{SS_m}(y) &= C_m \cosh \beta_{1_m} y + D_m \cos \beta_{2_m} y \\ {}^2W_{SS_m}(x) &= A_m \cosh \alpha_{1_m} x + B_m \cos \alpha_{2_m} x \end{aligned} \quad (66)$$

In the above equations A_m , B_m , C_m and D_m are integration constants and

$$\begin{aligned} \beta_{1_m}^2 &= \omega \sqrt{\frac{\rho h}{D}} + k_{a_m}^2, & \beta_{2_m}^2 &= \omega \sqrt{\frac{\rho h}{D}} - k_{a_m}^2, & k_{a_m} &= \frac{m\pi}{a} \\ \alpha_{1_m}^2 &= \omega \sqrt{\frac{\rho h}{D}} + k_{b_m}^2, & \alpha_{2_m}^2 &= \omega \sqrt{\frac{\rho h}{D}} - k_{b_m}^2, & k_{b_m} &= \frac{m\pi}{b} \end{aligned} \quad (67)$$

Now, the transverse displacement for double symmetry case can be written according to Eq. (44) in the following form:

$$\begin{aligned} \hat{w}_{SS}(x, y) &= \sum_{m=0}^M \left(A_m f_{1_m}(x, y) + B_m f_{2_m}(x, y) \right) + \\ &+ \sum_{m=0}^M \left(C_m f_{3_m}(x, y) + D_m f_{4_m}(x, y) \right) \end{aligned} \quad (68)$$

where

$$\begin{aligned} f_{1_m}(x, y) &= \cosh \alpha_{1_m} x \cos \frac{m\pi y}{b} \\ f_{2_m}(x, y) &= \cos \alpha_{2_m} x \cos \frac{m\pi y}{b} \\ f_{3_m}(x, y) &= \cosh \beta_{1_m} y \cos \frac{m\pi x}{a} \\ f_{4_m}(x, y) &= \cos \beta_{2_m} y \cos \frac{m\pi x}{a} \end{aligned} \quad (69)$$

The solutions for AA, SA and AS contributions are obtained similarly. The expressions of these contributions are the following:

➤ Antisymmetric-antisymmetric contribution (AA)

$$\hat{w}_{AA}(x, y) = \sum_{m=1}^M {}^1W_{AA_m}(y) \sin \frac{(2m-1)\pi x}{2a} + \sum_{m=1}^M {}^2W_{AA_m}(x) \sin \frac{(2m-1)\pi y}{2b}, \quad (70)$$

$$\begin{aligned} {}^1W_{AA_m}(y) &= C_m \sinh \beta_{1_m} y + D_m \sin \beta_{2_m} y \\ {}^2W_{AA_m}(x) &= A_m \sinh \alpha_{1_m} x + B_m \sin \alpha_{2_m} x \end{aligned} \quad (71)$$

$$\begin{aligned}
 f_{1_m}(x, y) &= \sinh \alpha_{1_m} x \sin \frac{(2m-1)\pi y}{2b} \\
 f_{2_m}(x, y) &= \sin \alpha_{2_m} x \sin \frac{(2m-1)\pi y}{2b} \\
 f_{3_m}(x, y) &= \sinh \beta_{1_m} y \sin \frac{(2m-1)\pi x}{2a} \\
 f_{4_m}(x, y) &= \sin \beta_{2_m} y \sin \frac{(2m-1)\pi x}{2a}
 \end{aligned} \tag{72}$$

β_{i_m} and α_{i_m} are given by the Eq. (67), while $k_{a_m} = \frac{(2m-1)\pi}{2a}$, $k_{b_m} = \frac{(2m-1)\pi}{2b}$.

➤ Symmetric-antisymmetric contribution (SA)

$$\hat{w}_{SA}(x, y) = \sum_{m=0}^M {}^1W_{SA_m}(y) \cos \frac{m\pi x}{a} + \sum_{m=1}^M {}^2W_{SA_m}(x) \sin \frac{(2m-1)\pi y}{2b}. \tag{73}$$

$$\begin{aligned}
 {}^1W_{SA_m}(y) &= C_m \sinh \beta_{1_m} y + D_m \sin \beta_{2_m} y \\
 {}^2W_{SA_m}(x) &= A_m \cosh \alpha_{1_m} x + B_m \cos \alpha_{2_m} x
 \end{aligned} \tag{74}$$

$$\begin{aligned}
 f_{1_m}(x, y) &= \cosh \alpha_{1_m} x \sin \frac{(2m-1)\pi y}{2b} \\
 f_{2_m}(x, y) &= \cos \alpha_{2_m} x \sin \frac{(2m-1)\pi y}{2b} \\
 f_{3_m}(x, y) &= \sinh \beta_{1_m} y \cos \frac{m\pi x}{a} \\
 f_{4_m}(x, y) &= \sin \beta_{2_m} y \cos \frac{m\pi x}{a}
 \end{aligned} \tag{75}$$

β_{i_m} and α_{i_m} are given by the Eq. (67), while $k_{a_m} = \frac{m\pi}{a}$, $k_{b_m} = \frac{(2m-1)\pi}{2b}$.

➤ Antisymmetric-symmetric contribution (AS)

$$\hat{w}_{AS}(x, y) = \sum_{m=1}^M {}^1W_{AS_m}(y) \sin \frac{(2m-1)\pi x}{2a} + \sum_{m=0}^M {}^2W_{AS_m}(x) \cos \frac{m\pi y}{b}. \tag{76}$$

$$\begin{aligned}
 {}^1W_{AS_m}(y) &= C_m \cosh \beta_{1_m} y + D_m \cos \beta_{2_m} y \\
 {}^2W_{AS_m}(x) &= A_m \sinh \alpha_{1_m} x + B_m \sin \alpha_{2_m} x
 \end{aligned} \tag{77}$$

$$\begin{aligned}
 f_{1_m}(x, y) &= \sinh \alpha_{1_m} x \cos \frac{m\pi y}{b} \\
 f_{2_m}(x, y) &= \sin \alpha_{2_m} x \cos \frac{m\pi y}{b} \\
 f_{3_m}(x, y) &= \cosh \beta_{1_m} y \sin \frac{(2m-1)\pi x}{2a} \\
 f_{4_m}(x, y) &= \cos \beta_{2_m} y \sin \frac{(2m-1)\pi x}{2a}
 \end{aligned} \tag{78}$$

β_{i_m} and α_{i_m} are given by the Eq. (67), while $k_{a_m} = \frac{(2m-1)\pi}{2a}$, $k_{b_m} = \frac{m\pi}{b}$.

2.3.1.3 Development of the dynamic stiffness matrix

The development of the dynamic stiffness matrix will be shown on the example of the double symmetry contribution of the displacement field, using the general procedure described previously and considering only one quarter of the plate. The geometry of plate element is given in Figure 12.

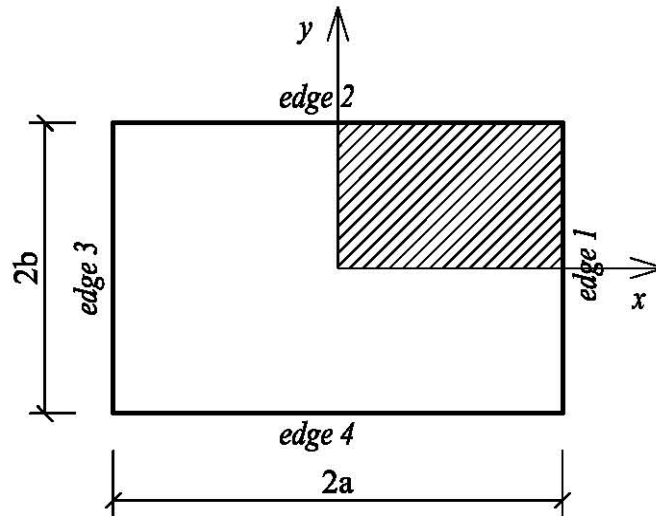


Figure 12. Geometry of the rectangular plate element

The displacement and force vectors, for each circular frequency ω , along the boundary $x = a$ and $y = b$ of the quarter segment of the rectangular plate, are defined as:

$$\begin{aligned}
 \mathbf{q}_{SS}^T &= \left[\hat{w}_{SS}(a, y) \quad -\frac{\partial \hat{w}_{SS}}{\partial x}(a, y) \quad \hat{w}_{SS}(x, b) \quad \frac{\partial \hat{w}_{SS}}{\partial y}(x, b) \right] \\
 \mathbf{Q}_{SS}^T &= \left[\hat{T}_{x_{SS}}(a, y) \quad -\hat{M}_{x_{SS}}(a, y) \quad \hat{T}_{y_{SS}}(x, b) \quad \hat{M}_{y_{SS}}(x, b) \right]
 \end{aligned} \tag{79}$$

where

$$\begin{aligned}\hat{T}_x(x, y) &= \hat{T}_x + \frac{\partial M_{xy}}{\partial y} = -D \left(\frac{\partial^3 \hat{w}}{\partial x^3} + (2-\nu) \frac{\partial^3 \hat{w}}{\partial x \partial y^2} \right) \\ \hat{T}_y(x, y) &= \hat{T}_y + \frac{\partial M_{xy}}{\partial x} = -D \left(\frac{\partial^3 \hat{w}}{\partial y^3} + (2-\nu) \frac{\partial^3 \hat{w}}{\partial x^2 \partial y} \right)\end{aligned}\quad (80)$$

are Kirchoff shear forces, while bending moments are defined by Eq. (59).

Projections $\tilde{\mathbf{q}}_{SS}$ and $\tilde{\mathbf{Q}}_{SS}$ of the vectors \mathbf{q}_{SS} and \mathbf{Q}_{SS} have been obtained using the following set of projection functions:

$$h_{n_{SS}}(x) = \cos \frac{n\pi x}{a}, \quad h_{n_{SS}}(y) = \cos \frac{n\pi y}{b}, \quad n = 0, 1, \dots, M. \quad (81)$$

According to Eq. (51) the projections of the vectors \mathbf{q}_{SS} and \mathbf{Q}_{SS} are given in the following form:

$$\begin{aligned}\tilde{\mathbf{q}}_{SS} &= \frac{2}{L_s} \int \mathbf{H}_{SS} \mathbf{q}_{SS} ds = \frac{2}{L_s} \int \mathbf{H}_{SS} \mathbf{\Phi}_b \mathbf{C} ds = \tilde{\mathbf{D}}_{SS} \mathbf{C} \\ \tilde{\mathbf{Q}}_{SS} &= \frac{2}{L_s} \int \mathbf{H}_{SS} \mathbf{Q}_{SS} ds = \frac{2}{L_s} \int \mathbf{H}_{SS} \mathbf{G}_b \mathbf{C} ds = \tilde{\mathbf{F}}_{SS} \mathbf{C}\end{aligned}\quad (82)$$

where:

$$\begin{aligned}\tilde{\mathbf{D}}_{SS} &= \frac{2}{L_s} \int \mathbf{H}_{SS} \mathbf{\Phi}_b ds \\ \tilde{\mathbf{F}}_{SS} &= \frac{2}{L_s} \int \mathbf{H}_{SS} \mathbf{G}_b ds\end{aligned}\quad (83)$$

$$\mathbf{C}^T = [A_o \quad B_o \quad C_o \quad D_o \quad \dots \quad A_m \quad B_m \quad C_m \quad D_m \quad \dots \quad A_M \quad B_M \quad C_M \quad D_M]$$

$$\begin{aligned}\tilde{\mathbf{q}}_{SS}^T &= [\tilde{\mathbf{q}}_{SS_o} \quad \tilde{\mathbf{q}}_{SS_1} \quad \dots \quad \tilde{\mathbf{q}}_{SS_m} \quad \dots \quad \tilde{\mathbf{q}}_{SS_M}]_{1 \times (4M+4)} \\ \tilde{\mathbf{q}}_{SS_m}^T &= \begin{bmatrix} {}^x w_{SS_m} & \left(\frac{\partial w}{\partial x} \right)_{SS_m} & {}^y w_{SS_m} & \left(\frac{\partial w}{\partial y} \right)_{SS_m} \end{bmatrix} \\ \tilde{\mathbf{Q}}_{SS}^T &= [\tilde{\mathbf{Q}}_{SS_o} \quad \tilde{\mathbf{Q}}_{SS_1} \quad \dots \quad \tilde{\mathbf{Q}}_{SS_m} \quad \dots \quad \tilde{\mathbf{Q}}_{SS_M}] \\ \tilde{\mathbf{Q}}_{SS_m}^T &= \begin{bmatrix} {}^x \bar{T}_{x_{SSm}} & {}^x M_{x_{SSm}} & {}^y \bar{T}_{y_{SSm}} & {}^y M_{y_{SSm}} \end{bmatrix}\end{aligned}\quad (84)$$

$$\mathbf{H}_{SS} = \begin{bmatrix} \mathbf{H}_o \\ \mathbf{H}_1 \\ \vdots \\ \mathbf{H}_n \\ \vdots \\ \mathbf{H}_M \end{bmatrix}_{(4M+4) \times 4}, \quad \mathbf{H}_n = \begin{bmatrix} h_{nSS}(y) & 0 & 0 & 0 \\ 0 & h_{nSS}(y) & 0 & 0 \\ 0 & 0 & h_{nSS}(x) & 0 \\ 0 & 0 & 0 & h_{nSS}(x) \end{bmatrix}, \quad \mathbf{H}_o = \frac{1}{2} \begin{bmatrix} 1 & 0 & 0 & 0 \\ 0 & 1 & 0 & 0 \\ 0 & 0 & 1 & 0 \\ 0 & 0 & 0 & 1 \end{bmatrix} \quad (85)$$

$$\mathbf{\Phi}_b^T = \begin{bmatrix} \Phi_{bo} \\ \Phi_{b1} \\ \vdots \\ \Phi_{bm} \\ \vdots \\ \Phi_{bM} \end{bmatrix}_{(4M+4) \times 4}, \quad \Phi_{bm} = \begin{bmatrix} f_{1_m}(a,y) & f_{2_m}(a,y) & f_{3_m}(a,y) & f_{4_m}(a,y) \\ \frac{\partial f_{1_m}(a,y)}{\partial x} & \frac{\partial f_{2_m}(a,y)}{\partial x} & \frac{\partial f_{3_m}(a,y)}{\partial x} & \frac{\partial f_{4_m}(a,y)}{\partial x} \\ f_{1_m}(x,b) & f_{2_m}(x,b) & f_{3_m}(x,b) & f_{4_m}(x,b) \\ \frac{\partial f_{1_m}(x,b)}{\partial y} & \frac{\partial f_{2_m}(x,b)}{\partial y} & \frac{\partial f_{3_m}(x,b)}{\partial y} & \frac{\partial f_{4_m}(x,b)}{\partial y} \end{bmatrix} \quad (86)$$

$$\mathbf{G}_b = \left[\mathbf{G}_{b_o} \quad \mathbf{G}_{b_1} \quad \dots \quad \mathbf{G}_{b_m} \quad \dots \quad \mathbf{G}_{b_M} \right]_{4 \times (4M+4)}$$

$$\mathbf{G}_{b_m} = -D \begin{bmatrix} \frac{\partial^3 f_1(a,y) + v^* \frac{\partial^3 f_1(a,y)}{\partial x \partial y^2}}{\partial x^3} & \frac{\partial^3 f_2(a,y) + v^* \frac{\partial^3 f_2(a,y)}{\partial x \partial y^2}}{\partial x^3} & \frac{\partial^3 f_3(a,y) + v^* \frac{\partial^3 f_3(a,y)}{\partial x \partial y^2}}{\partial x^3} & \frac{\partial^3 f_4(a,y) + v^* \frac{\partial^3 f_4(a,y)}{\partial x \partial y^2}}{\partial x^3} \\ \frac{\partial^2 f_1(a,y) - v \frac{\partial^2 f_1(a,y)}{\partial y^2}}{\partial x^2} & \frac{\partial^2 f_2(a,y) - v \frac{\partial^2 f_2(a,y)}{\partial y^2}}{\partial x^2} & \frac{\partial^2 f_3(a,y) - v \frac{\partial^2 f_3(a,y)}{\partial y^2}}{\partial x^2} & \frac{\partial^2 f_4(a,y) - v \frac{\partial^2 f_4(a,y)}{\partial y^2}}{\partial x^2} \\ \frac{\partial^3 f_1(x,b) + v^* \frac{\partial^3 f_1(x,b)}{\partial x^2 \partial y}}{\partial y^3} & \frac{\partial^3 f_2(x,b) + v^* \frac{\partial^3 f_2(x,b)}{\partial x^2 \partial y}}{\partial y^3} & \frac{\partial^3 f_3(x,b) + v^* \frac{\partial^3 f_3(x,b)}{\partial x^2 \partial y}}{\partial y^3} & \frac{\partial^3 f_4(x,b) + v^* \frac{\partial^3 f_4(x,b)}{\partial x^2 \partial y}}{\partial y^3} \\ \frac{\partial^2 f_1(x,b) + v \frac{\partial^2 f_1(x,b)}{\partial x^2}}{\partial y^2} & \frac{\partial^2 f_2(x,b) + v \frac{\partial^2 f_2(x,b)}{\partial x^2}}{\partial y^2} & \frac{\partial^2 f_3(x,b) + v \frac{\partial^2 f_3(x,b)}{\partial x^2}}{\partial y^2} & \frac{\partial^2 f_4(x,b) + v \frac{\partial^2 f_4(x,b)}{\partial x^2}}{\partial y^2} \end{bmatrix} \quad (87)$$

$$v^* = 2 - v$$

$$L = \begin{cases} 2b, & \text{for } x = a \\ 2a, & \text{for } y = b \end{cases} \quad ds = \begin{cases} dy, & \text{for } x = a \\ dx, & \text{for } y = b \end{cases} \quad (88)$$

The superscripts x and y in Eq. (84) refer to the plate boundaries $x = a$ and $y = b$, respectively.

Using simple mathematical operations, the elements of the matrices $\tilde{\mathbf{D}}_{SS}$ and $\tilde{\mathbf{F}}_{SS}$ have been calculated from Eq. (83)-(a). The dynamic stiffness matrix for the double symmetry contribution is obtained as:

$$\tilde{\mathbf{K}}_{D_{SS}}(\omega) = \tilde{\mathbf{F}}_{SS} \tilde{\mathbf{D}}_{SS}^{-1} \quad (89)$$

The size of the dynamic stiffness matrix is $4(M+1)$.

The dynamic stiffness matrices of other three contributions: $\tilde{\mathbf{K}}_{\mathbf{D}_{SA}}(\omega)$, $\tilde{\mathbf{K}}_{\mathbf{D}_{AS}}(\omega)$ and $\tilde{\mathbf{K}}_{\mathbf{D}_{AA}}(\omega)$ are obtained likewise, using the corresponding base functions $f_{i_m}(x, y)$ and projection functions $h_n(x)$ and $h_n(y)$:

$$\begin{aligned} h_{n_{SA}}(x) &= \cos \frac{n\pi x}{a}, & h_{n_{SA}}(y) &= \sin \frac{(2n-1)\pi y}{2b} \\ h_{n_{AS}}(x) &= \sin \frac{(2n-1)\pi x}{2a}, & h_{n_{AS}}(y) &= \cos \frac{n\pi y}{b}, & n = 0, 1, \dots, M. & \quad (90) \\ h_{n_{AA}}(x) &= \sin \frac{(2n-1)\pi x}{2a}, & h_{n_{AA}}(y) &= \sin \frac{(2n-1)\pi y}{2b} \end{aligned}$$

The size of the matrices $\tilde{\mathbf{K}}_{\mathbf{D}_{SA}}$ and $\tilde{\mathbf{K}}_{\mathbf{D}_{AS}}$ are $4M+2$, while the size of matrix $\tilde{\mathbf{K}}_{\mathbf{D}_{AA}}$ is $4M$, since $m=0$ term is omitted in the antisymmetric contribution. M is the number of terms in the general solution.

Dynamic stiffness matrix of completely free rectangular plate

The dynamic stiffness matrix of completely free rectangular plate is obtained superimposing the dynamic stiffness matrices of each symmetry contribution, which will be described in the following. The displacement components along each edge are expressed using the Projection method.

The transverse displacements and rotations along the plate edges 1, 2, 3 and 4 are given as:

$$\begin{aligned}
 \hat{w}(a, y) &= {}^1w_{S_o} + \sum_{m=1}^M {}^1w_{S_m} \cos \frac{m\pi y}{b} + \sum_{m=1}^M {}^1w_{A_m} \sin \frac{(2m-1)\pi y}{2b} \\
 \hat{w}(x, b) &= {}^2w_{S_o} + \sum_{m=1}^M {}^2w_{S_m} \cos \frac{m\pi x}{a} + \sum_{m=1}^M {}^2w_{A_m} \sin \frac{(2m-1)\pi x}{2a} \\
 \hat{w}(-a, y) &= {}^3w_{S_o} + \sum_{m=1}^M {}^3w_{S_m} \cos \frac{m\pi y}{b} + \sum_{m=1}^M {}^3w_{A_m} \sin \frac{(2m-1)\pi y}{2b} \\
 \hat{w}(x, -b) &= {}^4w_{S_o} + \sum_{m=1}^M {}^4w_{S_m} \cos \frac{m\pi x}{a} + \sum_{m=1}^M {}^4w_{A_m} \sin \frac{(2m-1)\pi x}{2a} \\
 -\frac{\partial \hat{w}(a, y)}{\partial x} &= {}^1w'_{S_o} + \sum_{m=1}^M {}^1w'_{S_m} \cos \frac{m\pi y}{b} + \sum_{m=1}^M {}^1w'_{A_m} \sin \frac{(2m-1)\pi y}{2b} \\
 \frac{\partial \hat{w}(x, b)}{\partial y} &= {}^2w'_{S_o} + \sum_{m=1}^M {}^2w'_{S_m} \cos \frac{m\pi x}{a} + \sum_{m=1}^M {}^2w'_{A_m} \sin \frac{(2m-1)\pi x}{2a} \\
 -\frac{\partial \hat{w}(-a, y)}{\partial x} &= {}^3w'_{S_o} + \sum_{m=1}^M {}^3w'_{S_m} \cos \frac{m\pi y}{b} + \sum_{m=1}^M {}^3w'_{A_m} \sin \frac{(2m-1)\pi y}{2b} \\
 \frac{\partial \hat{w}(x, -b)}{\partial y} &= {}^4w'_{S_o} + \sum_{m=1}^M {}^4w'_{S_m} \cos \frac{m\pi x}{a} + \sum_{m=1}^M {}^4w'_{A_m} \sin \frac{(2m-1)\pi x}{2a}
 \end{aligned} \tag{91}$$

Terms ${}^i w_{S_m}$, ${}^i w_{A_m}$, ${}^i w'_{S_m}$ and ${}^i w'_{A_m}$, ($i = 1, 2, 3, 4$) are the projections of the displacements along the plate edges, which are collected into the sub - vector $\tilde{\mathbf{q}}_m$ ($m = 0, 1, 2, \dots, M$), i.e. into the vector $\tilde{\mathbf{q}}$:

$$\begin{aligned}
 \tilde{\mathbf{q}}_m^T &= \left[{}^1w_{S_m} \quad {}^1w_{A_m} \quad {}^1\left(\frac{\partial w}{\partial x}\right)_{S_m} \quad {}^1\left(\frac{\partial w}{\partial x}\right)_{A_m} \quad \dots \quad {}^4w_{S_m} \quad {}^4w_{A_m} \quad {}^4\left(\frac{\partial w}{\partial y}\right)_{S_m} \quad {}^4\left(\frac{\partial w}{\partial y}\right)_{A_m} \right]_{1 \times 16} \\
 \tilde{\mathbf{q}}_0^T &= \left[{}^1w_{S_o} \quad {}^1\left(\frac{\partial w}{\partial x}\right)_{S_o} \quad \dots \quad {}^4w_{S_o} \quad {}^4\left(\frac{\partial w}{\partial y}\right)_{S_o} \right]_{1 \times 8} \\
 \tilde{\mathbf{q}}^T &= [\tilde{\mathbf{q}}_0 \quad \tilde{\mathbf{q}}_1 \quad \dots \quad \tilde{\mathbf{q}}_m \quad \dots \quad \tilde{\mathbf{q}}_M]_{1 \times (16M+8)}
 \end{aligned} \tag{92}$$

From Eq. (84)-(b) the transverse displacements and rotations of the double symmetry contribution are given as

$$\begin{aligned}
 \hat{w}_{SS}(a, y) &= {}^x w_{SS_0} + \sum_{m=1}^M {}^x w_{SS_m} \cos \frac{m\pi y}{b} \\
 -\frac{\partial \hat{w}_{SS}(a, y)}{\partial x} &= {}^x w'_{SS_0} + \sum_{m=1}^M {}^x w'_{SS_m} \cos \frac{m\pi y}{b} \\
 \hat{w}_{SS}(x, b) &= {}^y w_{SS_0} + \sum_{m=1}^M {}^y w_{SS_m} \cos \frac{m\pi x}{a} \\
 \frac{\partial \hat{w}_{SS}(x, b)}{\partial y} &= {}^y w'_{SS_0} + \sum_{m=1}^M {}^y w'_{SS_m} \cos \frac{m\pi x}{a}
 \end{aligned} \tag{93}$$

The projections of these displacements and rotations are collected into vector $\tilde{\mathbf{q}}_{SS}$:

$$\begin{aligned}
 \tilde{\mathbf{q}}_{SS}^T &= \left[\tilde{\mathbf{q}}_{SS_0} \quad \cdots \quad \tilde{\mathbf{q}}_{SS_m} \quad \tilde{\mathbf{q}}_{SS_M} \right]_{1 \times (4M+4)} \\
 \tilde{\mathbf{q}}_{SS_m}^T &= \left[{}^x w_{SS_m} \quad {}^x w'_{SS_m} \quad {}^y w_{SS_m} \quad {}^y w'_{SS_m} \right]
 \end{aligned} \tag{94}$$

The vectors $\tilde{\mathbf{q}}_{SA}$, $\tilde{\mathbf{q}}_{AS}$, $\tilde{\mathbf{q}}_{AA}$ of SA, AS and AA contributions can be expressed likewise.

They are collected into vector $\tilde{\mathbf{q}}_0$:

$$\tilde{\mathbf{q}}_0^T = \left[\tilde{\mathbf{q}}_{SS} \quad \tilde{\mathbf{q}}_{SA} \quad \tilde{\mathbf{q}}_{AS} \quad \tilde{\mathbf{q}}_{AA} \right]_{1 \times (16M+8)} \tag{95}$$

For example, the displacements along the edge $y = b$ can be written as:

$$\begin{aligned}
 \hat{w}(x, b) &= \hat{w}_{SS}(x, b) + \hat{w}_{SA}(x, b) + \hat{w}_{AS}(x, b) + \hat{w}_{AA}(x, b) \\
 \hat{w}(x, -b) &= \hat{w}_{SS}(x, -b) + \hat{w}_{SA}(x, -b) + \hat{w}_{AS}(x, -b) + \hat{w}_{AA}(x, -b) \\
 \hat{w}(-x, b) &= \hat{w}_{SS}(-x, b) + \hat{w}_{SA}(-x, b) + \hat{w}_{AS}(-x, b) + \hat{w}_{AA}(-x, b) \\
 \hat{w}(-x, -b) &= \hat{w}_{SS}(-x, -b) + \hat{w}_{SA}(-x, -b) + \hat{w}_{AS}(-x, -b) + \hat{w}_{AA}(-x, -b)
 \end{aligned} \tag{96}$$

Since

$$\begin{aligned}
 \hat{w}_{SA}(x, b) &= -\hat{w}_{SA}(x, -b) & \hat{w}_{SA}(-x, b) &= -\hat{w}_{SA}(-x, -b) \\
 \hat{w}_{AS}(x, b) &= -\hat{w}_{AS}(-x, b) & \hat{w}_{AS}(x, -b) &= -\hat{w}_{AS}(-x, -b), \\
 \hat{w}_{AA}(x, b) &= -\hat{w}_{AA}(x, -b) & \hat{w}_{AA}(-x, b) &= -\hat{w}_{AA}(-x, -b)
 \end{aligned} \tag{97}$$

the fully symmetric transverse displacement is given by:

$$\hat{w}_{SS}(x, b) = \frac{1}{4} \left(\hat{w}(x, b) + \hat{w}(x, -b) + \hat{w}(-x, b) + \hat{w}(-x, -b) \right). \tag{98}$$

For other displacement and rotation components similar expressions can be obtained:

$$\begin{aligned}\hat{w}_{SS}(a, y) &= \frac{1}{4}(\hat{w}(a, y) + \hat{w}(a, -y) + \hat{w}(-a, y) + \hat{w}(-a, -y)) \\ \frac{\partial \hat{w}_{SS}(a, y)}{\partial x} &= \frac{1}{4} \left(\frac{\partial \hat{w}(a, y)}{\partial x} - \frac{\partial \hat{w}(-a, y)}{\partial x} + \frac{\partial \hat{w}(a, -y)}{\partial x} - \frac{\partial \hat{w}(-a, -y)}{\partial x} \right) \\ \frac{\partial \hat{w}_{SS}(x, b)}{\partial y} &= \frac{1}{4} \left(\frac{\partial \hat{w}(x, b)}{\partial y} + \frac{\partial \hat{w}(-x, b)}{\partial y} - \frac{\partial \hat{w}(x, -b)}{\partial y} - \frac{\partial \hat{w}(-x, -b)}{\partial y} \right)\end{aligned}\quad (99)$$

From Eqs. (91), (93), (98) and (99) the following expressions are obtained:

$$\begin{aligned}{}^x w_{SS_m} &= \frac{1}{2}({}^1 w_{S_m} + {}^3 w_{S_m}) \\ {}^x w'_{SS_m} &= \frac{1}{2} \left(\left(\frac{\partial w}{\partial x} \right)_{S_m} - \left(\frac{\partial w}{\partial x} \right)_{S_m} \right) \\ {}^y w_{SS_m} &= \frac{1}{2}({}^2 w_{S_m} + {}^4 w_{S_m}) \\ {}^y w'_{SS_m} &= \frac{1}{2} \left(\left(\frac{\partial w}{\partial y} \right)_{S_m} - \left(\frac{\partial w}{\partial y} \right)_{S_m} \right)\end{aligned}, m = 0, 1, \dots, M. \quad (100)$$

Eq. (100) can be written in the matrix form as:

$$\tilde{\mathbf{q}}_{SS_m} = \frac{1}{2} \mathbf{t}_{SS} \tilde{\mathbf{q}}_m, m = 0, 1, \dots, M, \quad (101)$$

where

$$\mathbf{t}_{SS} = \begin{bmatrix} 1 & 0 & 0 & 0 & 0 & 0 & 0 & 0 & 1 & 0 & 0 & 0 & 0 & 0 & 0 \\ 0 & 0 & 1 & 0 & 0 & 0 & 0 & 0 & 0 & 0 & -1 & 0 & 0 & 0 & 0 \\ 0 & 0 & 0 & 0 & 1 & 0 & 0 & 0 & 0 & 0 & 0 & 0 & 1 & 0 & 0 \\ 0 & 0 & 0 & 0 & 0 & 0 & 1 & 0 & 0 & 0 & 0 & 0 & 0 & 0 & -1 \end{bmatrix}. \quad (102)$$

Now, the relation between the vectors $\tilde{\mathbf{q}}_{SS}$ and $\tilde{\mathbf{q}}_0$ is given as:

$$\tilde{\mathbf{q}}_{SS} = \frac{1}{2} \mathbf{T}_{SS} \tilde{\mathbf{q}}, \quad (103)$$

where

$$\mathbf{T}_{SS} = \begin{bmatrix} \mathbf{t}_{SS} & & & & \\ & \ddots & & & \\ & & \mathbf{t}_{SS} & & \\ & & & \ddots & \\ & & & & \mathbf{t}_{SS} \end{bmatrix}_{(4M+4) \times (16M+8)} \quad (104)$$

The above procedure is carried out for vectors $\tilde{\mathbf{q}}_{SA}$, $\tilde{\mathbf{q}}_{AS}$ and $\tilde{\mathbf{q}}_{AA}$, and the following relations are obtained:

$$\begin{aligned} \tilde{\mathbf{q}}_{SA} &= \frac{1}{2} \mathbf{T}_{SA} \tilde{\mathbf{q}} \\ \tilde{\mathbf{q}}_{AS} &= \frac{1}{2} \mathbf{T}_{AS} \tilde{\mathbf{q}} \\ \tilde{\mathbf{q}}_{AA} &= \frac{1}{2} \mathbf{T}_{AA} \tilde{\mathbf{q}} \end{aligned} \quad (105)$$

From Eq. (103)-(105) the relation between vectors $\tilde{\mathbf{q}}_o$ and $\tilde{\mathbf{q}}$ is given as:

$$\tilde{\mathbf{q}}_o = \frac{1}{2} \mathbf{T} \tilde{\mathbf{q}}, \quad (106)$$

where \mathbf{T} is transformation matrix :

$$\mathbf{T} = \begin{bmatrix} \mathbf{T}_{SS} \\ \mathbf{T}_{SA} \\ \mathbf{T}_{AS} \\ \mathbf{T}_{AA} \end{bmatrix}_{(16M+8) \times (16M+8)} \quad (107)$$

Similarly, the reverse procedure is carried out for the force components. For example, the Kirchhoff's shear force on edge 1 is given by:

$$\hat{T}_x(a, y) = \hat{T}_{x_{SS}}(a, y) + \hat{T}_{x_{SA}}(a, y) + \hat{T}_{x_{AS}}(a, y) + \hat{T}_{x_{AA}}(a, y), \quad (108)$$

where

$$\begin{aligned}
 \hat{T}_x(a, y) &= {}^1\bar{T}_{x_o} + \sum_{m=1}^M {}^1\bar{T}_{x_{S_m}} \cos \frac{m\pi y}{b} + \sum_{m=1}^M {}^1\bar{T}_{x_{A_m}} \sin \frac{(2m-1)\pi y}{2b} \\
 \hat{T}_{x_{SS}}(a, y) &= {}^x\bar{T}_{x_{SS_o}} + \sum_{m=1}^M \bar{T}_{x_{SS_m}} \cos \frac{m\pi y}{b} \\
 \hat{T}_{x_{SA}}(a, y) &= \sum_{m=1}^M {}^x\bar{T}_{x_{SA_m}} \sin \frac{(2m-1)\pi y}{2b} \\
 \hat{T}_{x_{AS}}(a, y) &= {}^x\bar{T}_{x_{AS_o}} + \sum_{m=1}^M {}^x\bar{T}_{x_{AS_m}} \cos \frac{m\pi y}{b} \\
 \hat{T}_{x_{AA}}(a, y) &= \sum_{m=1}^M {}^x\bar{T}_{x_{AA_m}} \sin \frac{(2m-1)\pi y}{2b}
 \end{aligned} \tag{109}$$

Substituting Eq. (109) into (108) the following expressions are obtained:

$$\begin{aligned}
 {}^1\hat{T}_{x_{S_m}} &= {}^x\hat{T}_{x_{SS_m}} + {}^x\hat{T}_{x_{AS_m}} \\
 {}^1\hat{T}_{x_{A_m}} &= {}^x\hat{T}_{x_{AA_m}} + {}^x\hat{T}_{x_{SA_m}}
 \end{aligned} \tag{110}$$

Similar expressions can be obtained for other forces along the plate boundary:

$$\begin{aligned}
 {}^1M_{x_{S_m}} &= {}^xM_{x_{SS_m}} + {}^xM_{x_{AS_m}} \\
 {}^1M_{x_{A_m}} &= {}^xM_{x_{AA_m}} + {}^xM_{x_{SA_m}} \\
 {}^2\hat{T}_{y_{S_m}} &= {}^y\hat{T}_{y_{SS_m}} + {}^y\hat{T}_{y_{AS_m}} & {}^2M_{y_{S_m}} &= {}^yM_{x_{SS_m}} + {}^yM_{x_{AS_m}} \\
 {}^2\hat{T}_{y_{A_m}} &= {}^y\hat{T}_{y_{AA_m}} + {}^y\hat{T}_{y_{SA_m}} & {}^2M_{y_{A_m}} &= {}^yM_{x_{AA_m}} + {}^yM_{x_{SA_m}} \\
 {}^3\hat{T}_{x_{S_m}} &= -{}^x\hat{T}_{x_{SS_m}} + {}^x\hat{T}_{x_{AS_m}} & {}^3M_{x_{S_m}} &= -{}^xM_{x_{SS_m}} + {}^xM_{x_{AS_m}} \\
 {}^3\hat{T}_{x_{A_m}} &= {}^x\hat{T}_{x_{AA_m}} - {}^x\hat{T}_{x_{SA_m}} & {}^3M_{x_{A_m}} &= {}^xM_{x_{AA_m}} - {}^xM_{x_{SA_m}} \\
 {}^4\hat{T}_{y_{S_m}} &= -{}^y\hat{T}_{y_{SS_m}} - {}^y\hat{T}_{y_{AS_m}} & {}^4M_{y_{S_m}} &= -{}^yM_{x_{SS_m}} - {}^yM_{x_{AS_m}} \\
 {}^4\hat{T}_{y_{A_m}} &= {}^y\hat{T}_{y_{AA_m}} + {}^y\hat{T}_{y_{SA_m}} & {}^4M_{y_{A_m}} &= {}^yM_{x_{AA_m}} + {}^yM_{x_{SA_m}}
 \end{aligned} \tag{111}$$

These relations can be written in the matrix form as:

$$\tilde{\mathbf{Q}} = \mathbf{T}^T \tilde{\mathbf{Q}}_0, \tag{112}$$

where

$$\begin{aligned}
 \tilde{\mathbf{Q}}_o^T &= [\tilde{\mathbf{Q}}_{SS} \quad \tilde{\mathbf{Q}}_{SA} \quad \tilde{\mathbf{Q}}_{AS} \quad \tilde{\mathbf{Q}}_{AA}], \\
 \tilde{\mathbf{Q}}^T &= [\tilde{\mathbf{Q}}_o \quad \tilde{\mathbf{Q}}_1 \quad \dots \quad \tilde{\mathbf{Q}}_m \quad \dots \quad \tilde{\mathbf{Q}}_M], \\
 \tilde{\mathbf{Q}}_m^T &= [{}^1\bar{T}_{xS_m} \quad {}^1\bar{T}_{xA_m} \quad {}^1M_{xS_m} \quad {}^1M_{xA_m} \quad \dots \quad {}^4\bar{T}_{yS_m} \quad {}^4\bar{T}_{yA_m} \quad {}^4M_{yS_m} \quad {}^4M_{yA_m}]
 \end{aligned} \tag{113}$$

and \mathbf{T} is the transformation matrix defined by Eq. (107). According to the relation between the vectors $\tilde{\mathbf{Q}}_o$ and $\tilde{\mathbf{q}}_o$:

$$\tilde{\mathbf{Q}}_o = \tilde{\mathbf{K}}_o \tilde{\mathbf{q}}_o = \begin{bmatrix} \tilde{\mathbf{K}}_{SS} & 0 & 0 & 0 \\ 0 & \tilde{\mathbf{K}}_{SA} & 0 & 0 \\ 0 & 0 & \tilde{\mathbf{K}}_{AS} & 0 \\ 0 & 0 & 0 & \tilde{\mathbf{K}}_{AA} \end{bmatrix} \tilde{\mathbf{q}}_o, \tag{114}$$

and Eqs. (106) and (112), the dynamic stiffness matrix of the completely free rectangular plate element is given by:

$$\tilde{\mathbf{K}}_D = \frac{1}{2} \mathbf{T}^T \tilde{\mathbf{K}}_o \mathbf{T}. \tag{115}$$

The size of the dynamic stiffness matrix is $16M+8$. In order to make it square, the number of terms in the general solution defined by Eq. (64) has to be the same as the number of projection functions.

The described method allows the vibration analysis of rectangular plate and plate assemblies with arbitrary boundary conditions. For that purpose a computer code using Matlab (2011) has been developed employing the same assemblage procedure like in the FEM. In contrast to the FEM, the discretization of plate assemblies is eliminated, which significantly improves the solution accuracy and reduces computational time. In the following examples the efficiency of the SEM in free vibration analysis of rectangular plates undergoing transverse vibration will be presented.

2.3.1.4 Numerical examples

➤ Free vibration analysis of simply supported square plate

Convergence and validation of the dynamic stiffness matrix developed in the previous section are demonstrated on the example of a simply supported square plate having dimensions $2a=4$ m, $h = 0.15$ m, $E = 30$ GPa, $\rho = 2.5$ kN/m³, $\nu = 0.15$. The results obtained

from the SEM are compared to those obtained by the finite element software SAP2000 and to the exact solution of the free vibration analysis obtained using Navier solution (Leissa 1973). In order to check the convergence of the proposed method, the natural frequencies of the plate have been calculated for various values of M . The results are given in Table 3, while the first six mode shapes are presented in Figure 13. It can be seen that natural frequencies of the first three modes calculated using the SEM agree well with the exact values. For higher frequencies, larger number of terms in the general solution – M is necessary. For $M = 3$ the error is less than 1%, while for $M = 5$ the results are practically the same. The natural frequencies of the plate obtained using SAP 2000 for different number of finite elements, are presented in Table 4.

Table 3. Natural frequencies of simply supported square plate using SEM

<i>Mode No.</i>	<i>f (Hz)</i>				<i>Exact solution</i>
	<i>M=1</i>	<i>M=2</i>	<i>M=3</i>	<i>M=5</i>	
1	29.1	29.6	29.7	29.7	29.8
2*	73.4	74.1	74.3	74.4	74.5
3	116.6	118.4	118.8	119.1	119.2
4*	138.2	148.9	148.9	148.8	148.9
5*	148.9	191.8	192.9	193.4	193.6
6*	179.5	252.5	252.9	253.1	253.2
7	220.3	262.5	266.5	267.6	268.1
8*	247.8	295.7	296.3	297.9	297.9
9*	266.6	364.3	370.2	371.8	372.3
10*	297.1	379.1	386.3	387.3	387.3
11*	313.4	387.0			
12	361.4				

Table 4. Natural frequencies (in Hz) of simply supported square plate using FEM

<i>Mode No.</i>	<i>Number of FE</i>				<i>Exact solution</i>
	<i>5x5</i>	<i>10x10</i>	<i>20x20</i>	<i>30x30</i>	
1	28.9	29.6	29.7	29.8	29.8
2*	70.9	73.6	74.2	74.4	74.5
3	105.6	115.7	118.3	118.8	119.2
4*	139.0	146.9	148.4	148.7	148.9
5*	162.4	185.8	191.6	192.7	193.6
6*	202.0	249.2	252.3	252.8	253.2
7	219.4	250.7	263.7	266.1	268.1
8*	229.3	283.7	294.3	296.3	297.9
9*	249.7	341.5	364.5	368.8	372.3
10*	277.1	379.2	385.7	386.6	387.3

* Double frequency due to symmetry

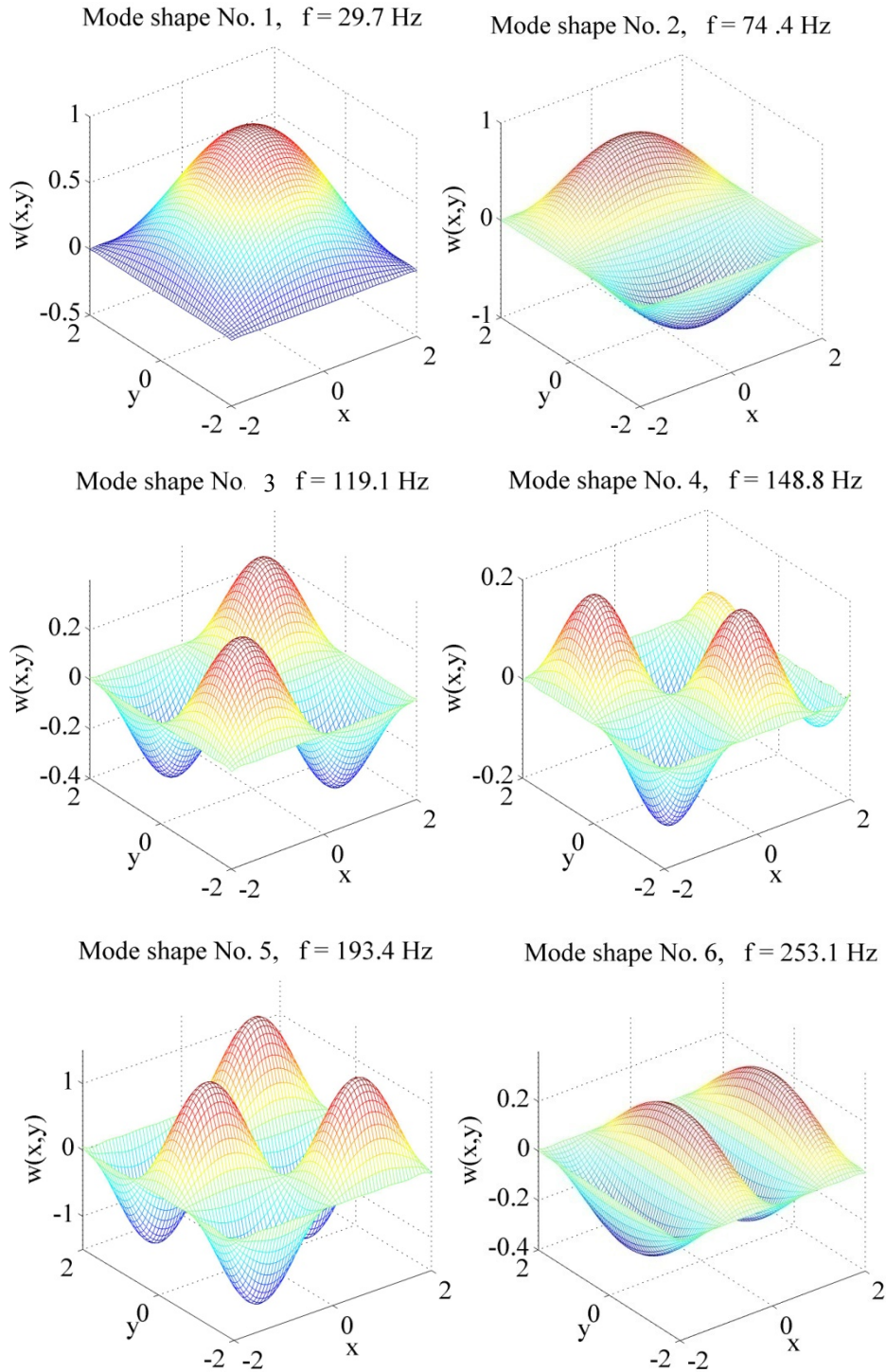


Figure 13. Mode shapes of simply supported square plate

By comparing the different mesh sizes of the FE model the results converge to the natural frequencies obtained using the SEM, as the number of finite elements (FE) increase. The coarsest mesh (5x5 elements) gives considerably different natural frequencies and mode shapes, especially for higher modes. Using finer FE meshes the error is considerably smaller. In order to obtain acceptably accurate results using the FEM, the mesh of 20x20=400 elements, i.e. 441 nodes should be used. On the other hand, using the SEM with only one spectral element and three terms in the general solution ($M = 3$) accurate values of the first 10 natural frequencies have been calculated.

➤ Free vibration analysis of completely free square plate

The natural frequencies of the completely free square plate having the same dimensions and properties as in the previous example have been calculated for various values of M . The results are given in Table 5. In this case an excellent accuracy has been achieved even for $M = 1$. It can be seen that the agreement between the columns in Table 5 is almost total. The first six mode shapes of the plate are presented in Figure 14.

Table 5. Natural frequencies of completely free square plate

<i>Mode No.</i>	<i>f (Hz)</i>				<i>FEM (SAP2000) 30x30</i>
	<i>M=1</i>	<i>M=2</i>	<i>M=3</i>	<i>M=5</i>	
1	22.2	22.2	22.2	22.2	22.2
2	31.9	31.8	31.9	31.9	31.7
3	35.4	35.4	35.4	35.4	35.2
4*	55.9	55.9	55.9	55.9	55.6
5*	92.9	92.9	92.9	92.9	92.3
6	101.8	101.7	101.7	101.7	101.2
7	111.3	111.3	111.3	111.3	110.4
8	117.2	117.2	117.2	117.2	116.4
9*	166.7	166.6	166.6	166.6	165.2
10	180.4	180.2	180.2	180.2	178.7
11	184.1	184.0	184.0	184.0	182.5

* Double frequency due to symmetry

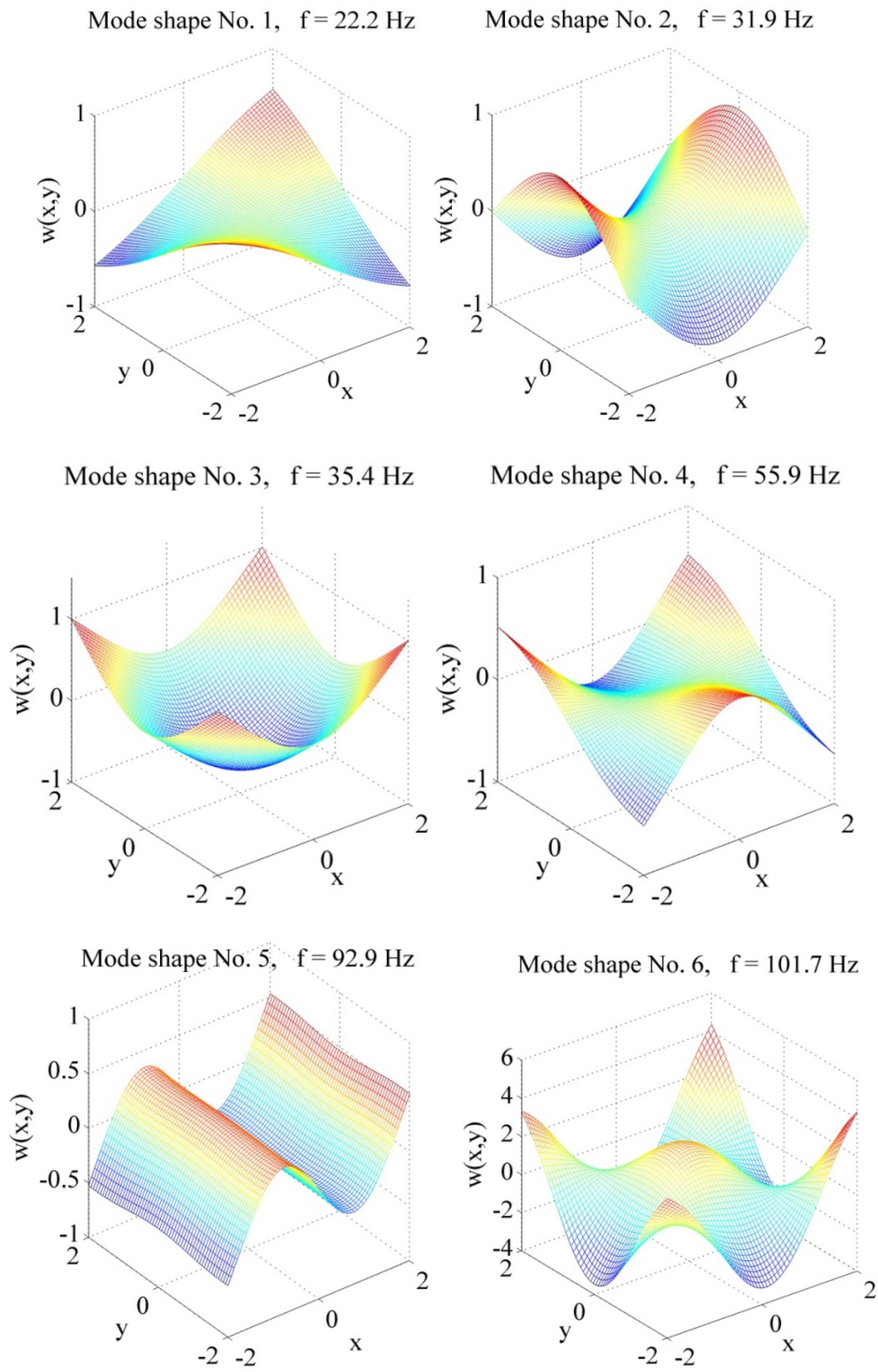


Figure 14. Mode shapes of completely free square plate

2.3.2 Plate spectral element for in-plane vibration

2.3.2.1 Equation of motion

A rectangular plate of thickness h and dimensions $2a \times 2b$ with in-plane internal forces is shown in Figure 15.

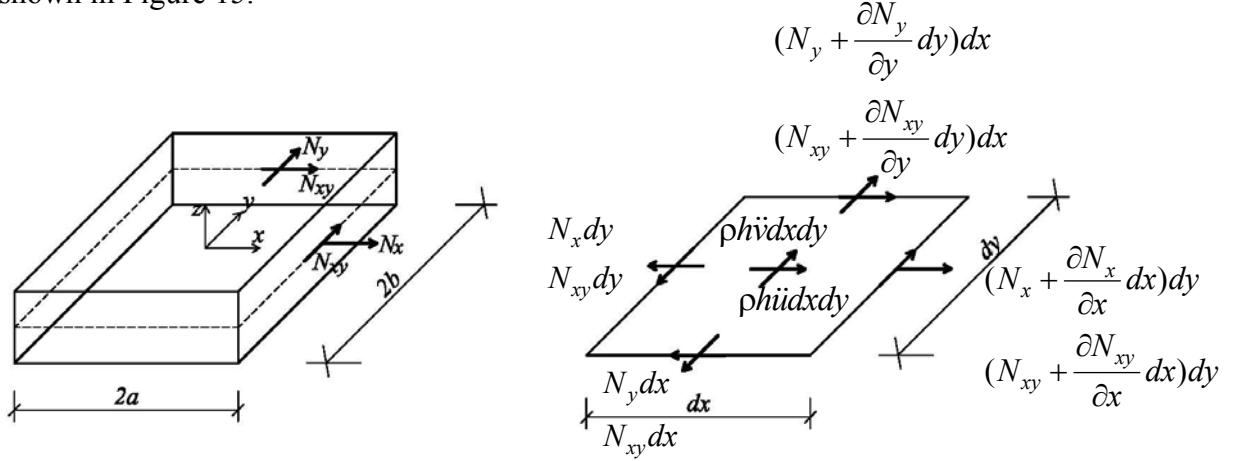


Figure 15. Internal forces of plate element undergoing in-plane vibration

Internal forces of the plate defined in Figure 15 are resultant forces of the corresponding stresses, which are uniformly distributed along the plate thickness:

$$\begin{aligned}
 N_x &= \int_{-h/2}^{h/2} \sigma_x dz = \sigma_x h \\
 N_y &= \int_{-h/2}^{h/2} \sigma_y dz = \sigma_y h \\
 N_{xy} &= \int_{-h/2}^{h/2} \tau_{xy} dz = \tau_{xy} h
 \end{aligned} \tag{116}$$

Using the Hooke's law for plain stress and strain-displacement relations:

$$\varepsilon_x = \frac{\partial u}{\partial x}, \quad \varepsilon_y = \frac{\partial v}{\partial y}, \quad \gamma_{xy} = \frac{\partial u}{\partial y} + \frac{\partial v}{\partial x}, \tag{117}$$

Eqs. (116) become:

$$\begin{aligned}
 N_x &= D \left(\frac{\partial u}{\partial x} + \nu \frac{\partial v}{\partial y} \right) \\
 N_y &= D \left(\frac{\partial v}{\partial y} + \nu \frac{\partial u}{\partial x} \right), \\
 N_{xy} &= Da_1 \left(\frac{\partial u}{\partial y} + \frac{\partial v}{\partial x} \right)
 \end{aligned} \tag{118}$$

where $u(x, y, t)$ and $v(x, y, t)$ are plate in-plane displacements in x and y direction respectively, $D = \frac{Eh}{1-\nu^2}$ is plate in-plane stiffness and $a_1 = \frac{1-\nu}{2}$. According to Figure 15 the following equilibrium equations are derived:

$$\begin{aligned} \frac{\partial N_x}{\partial x} + \frac{\partial N_{xy}}{\partial y} + \frac{\rho h}{D} \frac{\partial^2 u}{\partial t^2} &= 0 \\ \frac{\partial N_{xy}}{\partial x} + \frac{\partial N_y}{\partial y} + \frac{\rho h}{D} \frac{\partial^2 v}{\partial t^2} &= 0 \end{aligned} \quad (119)$$

According to Eq. (118) and (119) equations of motion of plate undergoing in-plane vibrations are:

$$\begin{aligned} \frac{\partial^2 u}{\partial x^2} + a_1 \frac{\partial^2 u}{\partial y^2} + a_2 \frac{\partial^2 v}{\partial x \partial y} - \frac{\rho h}{D} \frac{\partial^2 u}{\partial t^2} &= 0 \\ \frac{\partial^2 v}{\partial y^2} + a_1 \frac{\partial^2 v}{\partial x^2} + a_2 \frac{\partial^2 u}{\partial x \partial y} - \frac{\rho h}{D} \frac{\partial^2 v}{\partial t^2} &= 0 \end{aligned} \quad (120)$$

where ρ is mass density and $a_2 = \frac{1+\nu}{2}$. Introducing spectral representation of the displacements $u(x, y, t)$ and $v(x, y, t)$ as:

$$\begin{aligned} u(x, y, t) &= \sum \hat{u}(x, y, \omega) e^{i\omega t} \\ v(x, y, t) &= \sum \hat{v}(x, y, \omega) e^{i\omega t} \end{aligned} \quad (121)$$

the Fourier transform of Eq. (120) can be expressed as:

$$\begin{aligned} \frac{\partial^2 \hat{u}}{\partial x^2} + a_1 \frac{\partial^2 \hat{u}}{\partial y^2} + a_2 \frac{\partial^2 \hat{v}}{\partial x \partial y} + \frac{\omega^2}{c_p^2} \hat{u} &= 0 \\ \frac{\partial^2 \hat{v}}{\partial y^2} + a_1 \frac{\partial^2 \hat{v}}{\partial x^2} + a_2 \frac{\partial^2 \hat{u}}{\partial x \partial y} + \frac{\omega^2}{c_p^2} \hat{v} &= 0 \end{aligned} \quad (122)$$

where $c_p = \sqrt{\frac{E}{\rho(1-\nu^2)}}$ represents the longitudinal wave velocity.

2.3.2.2 General solution

Likewise the transverse vibration, using Gorman's superposition method (Gorman 2004), the in-plane displacements of rectangular plate are split into four contributions,

symmetric-symmetric (SS), antisymmetric-antisymmetric (AA), symmetric-antisymmetric (SA) and antisymmetric-symmetric (AS):

$$\begin{aligned}\hat{u}(x, y) &= \hat{u}_{SS}(x, y) + \hat{u}_{AA}(x, y) + \hat{u}_{SA}(x, y) + \hat{u}_{AS}(x, y) \\ \hat{v}(x, y) &= \hat{v}_{SS}(x, y) + \hat{v}_{AA}(x, y) + \hat{v}_{SA}(x, y) + \hat{v}_{AS}(x, y)\end{aligned}\quad (123)$$

According to Gorman, vibration mode is symmetric about an axis if displacement normal to this axis has a symmetric distribution about it, while it is antisymmetric about an axis if displacement normal to this axis has an antisymmetric distribution about it. Each of the above contributions is expressed according to Eq. (44), where two displacement components in x - y plane exist, i.e. $p = 2$.

➤ Symmetric-symmetric contribution (SS)

In order to satisfy the defined double symmetry condition, the in-plane plate displacements are defined as:

$$\begin{aligned}\hat{u}_{SS}(x, y) &= \sum_{m=1}^M {}^1U_{SSm}(y) \cos \frac{(2m-1)\pi x}{2a} + \sum_{m=1}^M {}^2U_{SSm}(x) \sin \frac{(2m-1)\pi y}{2b} \\ \hat{v}_{SS}(x, y) &= \sum_{m=1}^M {}^1V_{SSm}(y) \sin \frac{(2m-1)\pi x}{2a} + \sum_{m=1}^M {}^2V_{SSm}(x) \cos \frac{(2m-1)\pi y}{2b}\end{aligned}\quad (124)$$

where ${}^2U_{SSm}$ and ${}^1V_{SSm}$ are even functions, and ${}^1U_{SSm}$ and ${}^2V_{SSm}$ are odd functions.

Substituting Eq. (124) into Eq. (122), the following system of equations is obtained:

$$\begin{aligned}a_1 {}^1U''_{SSm} + c_{m_1} {}^1U_{SSm} + a_2 k_{a_m} {}^1V'_{SSm} &= 0 \\ {}^1V''_{SSm} + c_{m_2} {}^1V_{SSm} - a_2 k_{a_m} {}^1U'_{SSm} &= 0\end{aligned}\quad (125)$$

$$\begin{aligned}{}^2U''_{SSm} + c_{n_1} {}^2U_{SSm} - a_2 k_{b_m} {}^2V'_{SSm} &= 0 \\ a_1 {}^2V''_{SSm} + c_{n_2} {}^2V_{SSm} + a_2 k_{b_m} {}^2U'_{SSm} &= 0\end{aligned}\quad (126)$$

where

$$\begin{aligned}k_{a_m} &= \frac{(2m-1)\pi}{2a}, \quad k_{b_m} = \frac{(2m-1)\pi}{2b}, \\ c_{m_1} &= \frac{\omega^2}{c_p^2} - k_{a_m}^2 = k_p^2 - k_{a_m}^2, \quad c_{m_2} = k_p^2 - a_1 k_{a_m}^2, \\ c_{n_1} &= k_p^2 - a_1 k_{b_m}^2, \quad c_{n_2} = k_p^2 - k_{b_m}^2.\end{aligned}\quad (127)$$

Without going into details, system of equations (125) and (126) can be transformed into:

$$\begin{aligned} {}^1V_{SSm}^{IV} + b_1 {}^1V_{SSm}'' + c_1 {}^1V_{SSm} &= 0 \\ {}^2U_{SSm}^{IV} + b_2 {}^2U_{SSm}'' + c_2 {}^2U_{SSm} &= 0 \end{aligned} \quad (128)$$

where

$$\begin{aligned} b_1 &= c_{m_2} + \frac{c_{m_1}}{a_1} + \frac{a_2^2 k_{a_m}^2}{a_1}, \quad b_2 = c_{n_2} + \frac{c_{n_1}}{a_1} + \frac{a_2^2 k_{b_m}^2}{a_1}, \\ c_1 &= \frac{c_{m_1} c_{m_2}}{a_1}, \quad c_2 = \frac{c_{n_1} c_{n_2}}{a_1} \end{aligned} \quad (129)$$

Solutions of Eq. (128), omitting the odd parts, are given as:

$$\begin{aligned} {}^1V_{SSm} &= C_m \cos \beta_{1_m} y + D_m \cos \gamma_{1_m} y \\ {}^2U_{SSm} &= A_m \cos \beta_{2_m} x + B_m \cos \gamma_{2_m} x \end{aligned} \quad (130)$$

where β_{1_m} , γ_{1_m} , β_{2_m} , and γ_{2_m} are roots of the characteristic equations of Eq. (128) and A_m , B_m , C_m , and D_m are integration constants. Using Eqs. (125) and (126) the following expressions for functions ${}^1U_{SSm}$ and ${}^2V_{SSm}$ are obtained:

$$\begin{aligned} {}^1U_{SSm} &= C_m \alpha_{2_m} \sin \beta_{1_m} y + D_m \alpha_{4_m} \sin \gamma_{1_m} y \\ {}^2V_{SSm} &= A_m \alpha_{1_m} \sin \beta_{2_m} x + B_m \alpha_{3_m} \sin \gamma_{2_m} x \end{aligned} \quad (131)$$

where

$$\begin{aligned} \alpha_{1_m} &= \frac{1}{c_{m_1}} \left(a_2 k_{a_m} + \frac{a_1 c_{m_2}}{a_2 k_{a_m}} \right) \beta_{1_m} - \frac{a_1}{a_2 k_{a_m} c_{m_1}} \beta_{1_m}^3 \\ \alpha_{2_m} &= \frac{1}{c_{n_2}} \left(a_2 k_{b_m} + \frac{a_1 c_{n_1}}{a_2 k_{b_m}} \right) \beta_{2_m} - \frac{a_1}{a_2 k_{b_m} c_{n_2}} \beta_{2_m}^3 \\ \alpha_{3_m} &= \frac{1}{c_{n_2}} \left(a_2 k_{b_m} + \frac{a_1 c_{n_1}}{a_2 k_{b_m}} \right) \gamma_{2_m} - \frac{a_1}{a_2 k_{b_m} c_{n_2}} \gamma_{2_m}^3 \\ \alpha_{4_m} &= \frac{1}{c_{m_1}} \left(a_2 k_{a_m} + \frac{a_1 c_{m_2}}{a_2 k_{a_m}} \right) \gamma_{1_m} - \frac{a_1}{a_2 k_{a_m} c_{m_1}} \gamma_{1_m}^3 \end{aligned} \quad (132)$$

Now, the in-plane displacements for double symmetry case can be written according to Eq. (44) in the following form:

$$\begin{aligned}\hat{u}_{SS}(x, y) &= \sum_{m=1}^M \left(A_m f_{11_m}(x, y) + B_m f_{12_m}(x, y) \right) + \sum_{m=1}^M \left(C_m f_{13_m}(x, y) + D_m f_{14_m}(x, y) \right) \\ \hat{v}_{SS}(x, y) &= \sum_{m=1}^M \left(A_m f_{21_m}(x, y) + B_m f_{22_m}(x, y) \right) + \sum_{m=1}^M \left(C_m f_{23_m}(x, y) + D_m f_{24_m}(x, y) \right)\end{aligned}, \quad (133)$$

where

$$\begin{aligned}f_{11_m}(x, y) &= \cos \beta_{2_m} x \sin \frac{(2m-1)\pi y}{2b}, & f_{21_m}(x, y) &= \alpha_{1_m} \sin \beta_{2_m} x \cos \frac{(2m-1)\pi y}{2b} \\ f_{12_m}(x, y) &= \cos \gamma_{2_m} x \sin \frac{(2m-1)\pi y}{2b}, & f_{22_m}(x, y) &= \alpha_{3_m} \sin \gamma_{2_m} x \cos \frac{(2m-1)\pi y}{2b} \\ f_{13_m}(x, y) &= \alpha_{2_m} \sin \beta_{1_m} y \cos \frac{(2m-1)\pi x}{2a}, & f_{23_m}(x, y) &= \cos \beta_{1_m} y \sin \frac{(2m-1)\pi x}{2a} \\ f_{14_m}(x, y) &= \alpha_{4_m} \sin \gamma_{1_m} y \cos \frac{(2m-1)\pi x}{2a}, & f_{24_m}(x, y) &= \cos \gamma_{1_m} y \sin \frac{(2m-1)\pi x}{2a}\end{aligned} \quad (134)$$

➤ Antisymmetric-antisymmetric contribution (AA)

In order to satisfy this type of contribution, the in-plane displacements are defined as:

$$\begin{aligned}\hat{u}_{AA}(x, y) &= \sum_{m=0}^M {}^1U_{AAm}(y) \sin \frac{m\pi x}{a} + \sum_{m=0}^M {}^2U_{AAm}(x) \cos \frac{m\pi y}{b} \\ \hat{v}_{AA}(x, y) &= \sum_{m=0}^M {}^1V_{AAm}(y) \cos \frac{m\pi x}{a} + \sum_{m=0}^M {}^2V_{AAm}(x) \sin \frac{m\pi y}{b}\end{aligned}, \quad (135)$$

where ${}^2U_{AAm}$ and ${}^1V_{AAm}$ are odd functions, while ${}^1U_{AAm}$ and ${}^2V_{AAm}$ are even functions. They can be developed in analogous way as in the case of symmetric-symmetric contribution, and are given in the following form:

$$\begin{aligned}{}^1V_{AAm} &= C_m \sin \beta_{1_m} y + D_m \sin \gamma_{1_m} y \\ {}^2U_{AAm} &= A_m \sin \beta_{2_m} x + B_m \sin \gamma_{2_m} x \\ {}^1U_{AAm} &= -C_m \alpha_{2_m} \cos \beta_{1_m} y - D_m \alpha_{4_m} \cos \gamma_{1_m} y \\ {}^2V_{AAm} &= -A_m \alpha_{1_m} \cos \beta_{2_m} x - B_m \alpha_{3_m} \cos \gamma_{2_m} x\end{aligned}, \quad (137)$$

where $A_m, B_m, C_m,$ and D_m are integration constants and

$$\begin{aligned}
 \alpha_{1_m} &= -\frac{1}{c_{n_2}} \left(a_2 k_{b_m} + \frac{a_1 c_{n_1}}{a_2 k_{b_m}} \right) \beta_{2_m} + \frac{a_1}{a_2 k_{b_m} c_{n_2}} \beta_{2_m}^3 \\
 \alpha_{2_m} &= -\frac{1}{c_{m_1}} \left(a_2 k_{a_m} + \frac{a_1 c_{m_2}}{a_2 k_{a_m}} \right) \beta_{1_m} + \frac{a_1}{a_2 k_{a_m} c_{m_1}} \beta_{1_m}^3 \\
 \alpha_{3_m} &= -\frac{1}{c_{n_2}} \left(a_2 k_{b_m} + \frac{a_1 c_{n_1}}{a_2 k_{b_m}} \right) \gamma_{2_m} + \frac{a_1}{a_2 k_{b_m} c_{n_2}} \gamma_{2_m}^3 \\
 \alpha_{4_m} &= -\frac{1}{c_{m_1}} \left(a_2 k_{a_m} + \frac{a_1 c_{m_2}}{a_2 k_{a_m}} \right) \gamma_{1_m} + \frac{a_1}{a_2 k_{a_m} c_{m_1}} \gamma_{1_m}^3
 \end{aligned} \tag{138}$$

$$\begin{aligned}
 f_{11_m}(x, y) &= \sin \beta_{2_m} x \cos \frac{m\pi y}{b}, f_{21_m}(x, y) = -\alpha_{1_m} \cos \beta_{2_m} x \sin \frac{m\pi y}{b} \\
 f_{12_m}(x, y) &= \sin \gamma_{2_m} x \cos \frac{m\pi y}{b}, f_{22_m}(x, y) = -\alpha_{3_m} \cos \gamma_{2_m} x \sin \frac{m\pi y}{b} \\
 f_{13_m}(x, y) &= -\alpha_{2_m} \cos \beta_{1_m} y \sin \frac{m\pi x}{a}, f_{23_m}(x, y) = \sin \beta_{1_m} y \cos \frac{m\pi x}{a} \\
 f_{14_m}(x, y) &= -\alpha_{4_m} \cos \gamma_{1_m} y \sin \frac{m\pi x}{a}, f_{24_m}(x, y) = \sin \gamma_{1_m} y \cos \frac{m\pi x}{a}
 \end{aligned} \tag{139}$$

Eq. (136) and (137) are valid for $m > 0$. For $m = 0$, Eq. (122) becomes:

$$\begin{aligned}
 {}^2U''_{AAo} + k_p^2 {}^2U_{AAo} &= 0 \\
 {}^1V''_{AAo} + k_p^2 {}^1V_{AAo} &= 0
 \end{aligned} \tag{140}$$

The solutions of Eq. (140) can be expressed as:

$$\begin{aligned}
 {}^2U_{AAo} &= C_{1_o} \sin k_p x \\
 {}^1V_{AAo} &= C_{2_o} \sin k_p y
 \end{aligned} \tag{141}$$

where C_{1_o} and C_{2_o} are integration constants.

➤ Symmetric-antisymmetric contribution (SA)

In this case the displacements are obtained combining previously defined symmetric-symmetric and antisymmetric-antisymmetric contributions:

$$\begin{aligned}\hat{u}_{SA}(x, y) &= \sum_{m=0}^M {}^1U_{SA_m}(y) \sin \frac{m\pi x}{a} + \sum_{m=1}^M {}^2U_{SA_m}(x) \sin \frac{(2m-1)\pi y}{2b} \\ \hat{v}_{SA}(x, y) &= \sum_{m=0}^M {}^1V_{SA_m}(y) \cos \frac{m\pi x}{a} + \sum_{m=1}^M {}^2V_{SA_m}(x) \cos \frac{(2m-1)\pi y}{2b}\end{aligned}, \quad (142)$$

where ${}^1U_{SA_m}$ and ${}^2U_{SA_m}$ are odd functions, while ${}^1V_{SA_m}$ and ${}^2V_{SA_m}$ are even functions.

For $m = 0$, the solution for ${}^1V_{SA_m}$ becomes:

$${}^1V_{SA_0} = C_{3_0} \cos k_p y. \quad (143)$$

For $m > 0$, the following solutions are obtained:

$$\begin{aligned}{}^1V_{SA_m} &= C_m \cos \beta_{1_m} y + D_m \cos \gamma_{1_m} y \\ {}^2U_{SA_m} &= A_m \sin \beta_{2_m} x + B_m \sin \gamma_{2_m} x\end{aligned}, \quad (144)$$

$$\begin{aligned}{}^1U_{SA_m} &= C_m \alpha_{2_m} \sin \beta_{1_m} y + D_m \alpha_{4_m} \sin \gamma_{1_m} y \\ {}^2V_{SA_m} &= -A_m \alpha_{1_m} \cos \beta_{2_m} x - B_m \alpha_{3_m} \cos \gamma_{2_m} x\end{aligned}, \quad (145)$$

$$\begin{aligned}\alpha_{1_m} &= \frac{1}{c_{n_2}} \left(a_2 k_{b_m} + \frac{a_1 c_{n_1}}{a_2 k_{b_m}} \right) \beta_{2_m} - \frac{a_1}{a_2 k_{b_m} c_{n_2}} \beta_{2_m}^3 \\ \alpha_{2_m} &= -\frac{1}{c_{m_1}} \left(a_2 k_{a_m} + \frac{a_1 c_{m_2}}{a_2 k_{a_m}} \right) \beta_{1_m} + \frac{a_1}{a_2 k_{a_m} c_{m_1}} \beta_{1_m}^3 \\ \alpha_{3_m} &= \frac{1}{c_{n_2}} \left(a_2 k_{b_m} + \frac{a_1 c_{n_1}}{a_2 k_{b_m}} \right) \gamma_{2_m} - \frac{a_1}{a_2 k_{b_m} c_{n_2}} \gamma_{2_m}^3 \\ \alpha_{4_m} &= -\frac{1}{c_{m_1}} \left(a_2 k_{a_m} + \frac{a_1 c_{m_2}}{a_2 k_{a_m}} \right) \gamma_{1_m} + \frac{a_1}{a_2 k_{a_m} c_{m_1}} \gamma_{1_m}^3\end{aligned}, \quad (146)$$

$$\begin{aligned}
 f_{11_m}(x, y) &= \sin \beta_{2_m} x \sin \frac{(2m-1)\pi y}{2b}, & f_{21_m}(x, y) &= -\alpha_{1_m} \cos \beta_{2_m} x \cos \frac{(2m-1)\pi y}{2b} \\
 f_{12_m}(x, y) &= \sin \gamma_{2_m} x \sin \frac{(2m-1)\pi y}{2b}, & f_{22_m}(x, y) &= -\alpha_{3_m} \cos \gamma_{2_m} x \cos \frac{(2m-1)\pi y}{2b} \\
 f_{13_m}(x, y) &= \alpha_{2_m} \sin \beta_{1_m} y \sin \frac{m\pi x}{a}, & f_{23_m}(x, y) &= \cos \beta_{1_m} y \cos \frac{m\pi x}{a} \\
 f_{14_m}(x, y) &= \alpha_{4_m} \sin \gamma_{1_m} y \sin \frac{m\pi x}{a}, & f_{24_m}(x, y) &= \cos \gamma_{1_m} y \cos \frac{m\pi x}{a}
 \end{aligned} \tag{147}$$

➤ Antisymmetric-symmetric contribution (AS)

Displacements of plate element in this case are defined as:

$$\begin{aligned}
 \hat{u}_{AS}(x, y) &= \sum_{m=1}^M {}^1U_{ASm}(y) \cos \frac{(2m-1)\pi x}{2a} + \sum_{m=0}^M {}^2U_{ASm}(x) \cos \frac{m\pi y}{b} \\
 \hat{v}_{AS}(x, y) &= \sum_{m=1}^M {}^1V_{ASm}(y) \sin \frac{(2m-1)\pi x}{2a} + \sum_{m=0}^M {}^2V_{ASm}(x) \sin \frac{m\pi y}{b}
 \end{aligned} \tag{148}$$

where ${}^1U_{ASm}$ and ${}^2U_{ASm}$ are even functions, while ${}^1V_{ASm}$ and ${}^2V_{ASm}$ are odd functions.

For $m = 0$, the solution for ${}^2U_{ASm}$ becomes:

$${}^2U_{AS0} = C_{4_0} \cos k_p x. \tag{149}$$

For $m > 0$, the following solutions are obtained:

$$\begin{aligned}
 {}^1U_{ASm} &= -C_m \alpha_{2_m} \cos \beta_{1_m} y - D_m \alpha_{4_m} \cos \gamma_{1_m} y \\
 {}^2V_{ASm} &= A_m \alpha_{1_m} \sin \beta_{2_m} x + B_m \alpha_{3_m} \sin \gamma_{2_m} x
 \end{aligned} \tag{150}$$

$$\begin{aligned}
 {}^1V_{ASm} &= C_m \sin \beta_{1_m} y + D_m \sin \gamma_{1_m} y \\
 {}^2U_{ASm} &= A_m \cos \beta_{2_m} x + B_m \cos \gamma_{2_m} x
 \end{aligned} \tag{151}$$

$$\begin{aligned}
 \alpha_{1_m} &= -\frac{1}{c_{n_2}} \left(a_2 k_{b_m} + \frac{a_1 c_{n_1}}{a_2 k_{b_m}} \right) \beta_{2_m} + \frac{a_1}{a_2 k_{b_m} c_{n_2}} \beta_{2_m}^3 \\
 \alpha_{2_m} &= \frac{1}{c_{m_1}} \left(a_2 k_{a_m} + \frac{a_1 c_{m_2}}{a_2 k_{a_m}} \right) \beta_{1_m} - \frac{a_1}{a_2 k_{a_m} c_{m_1}} \beta_{1_m}^3 \\
 \alpha_{3_m} &= -\frac{1}{c_{n_2}} \left(a_2 k_{b_m} + \frac{a_1 c_{n_1}}{a_2 k_{b_m}} \right) \gamma_{2_m} + \frac{a_1}{a_2 k_{b_m} c_{n_2}} \gamma_{2_m}^3 \\
 \alpha_{4_m} &= \frac{1}{c_{m_1}} \left(a_2 k_{a_m} + \frac{a_1 c_{m_2}}{a_2 k_{a_m}} \right) \gamma_{1_m} - \frac{a_1}{a_2 k_{a_m} c_{m_1}} \gamma_{1_m}^3
 \end{aligned} \tag{152}$$

$$\begin{aligned}
 f_{11_m}(x, y) &= \cos \beta_{2_m} x \cos \frac{m\pi y}{b}, & f_{21_m}(x, y) &= \alpha_{1_m} \sin \beta_{2_m} x \sin \frac{m\pi y}{b} \\
 f_{12_m}(x, y) &= \cos \gamma_{2_m} x \cos \frac{m\pi y}{b}, & f_{22_m}(x, y) &= \alpha_{3_m} \sin \gamma_{2_m} x \sin \frac{m\pi y}{b} \\
 f_{13_m}(x, y) &= -\alpha_{2_m} \cos \beta_{1_m} y \cos \frac{(2m-1)\pi x}{2a}, & f_{23_m}(x, y) &= \sin \beta_{1_m} y \sin \frac{(2m-1)\pi x}{2a} \\
 f_{14_m}(x, y) &= -\alpha_{4_m} \cos \gamma_{1_m} y \cos \frac{(2m-1)\pi x}{2a}, & f_{24_m}(x, y) &= \sin \gamma_{1_m} y \sin \frac{(2m-1)\pi x}{2a}
 \end{aligned} \tag{153}$$

2.3.2.3 Development of the dynamic stiffness matrix

In the following, the procedure for the development of the dynamic stiffness matrix \mathbf{K}_{SS} for the double symmetric contribution will be presented, considering only one quarter of the rectangular plate element (Figure 12). The dynamic stiffness matrices of the other three contributions: \mathbf{K}_{SA} , \mathbf{K}_{AS} and \mathbf{K}_{AA} can be obtained likewise.

The in-plane displacement for the SS contribution and the corresponding force vector, for each circular frequency ω , along the boundary $x = a$ and $y = b$ of the quarter segment of rectangular plate element are defined as:

$$\begin{aligned}
 \mathbf{q}_{SS}^T &= [\hat{u}_{SS}(a, y) \quad \hat{v}_{SS}(a, y) \quad \hat{u}_{SS}(x, b) \quad \hat{v}_{SS}(x, b)] \\
 \mathbf{Q}_{SS}^T &= [\hat{N}_{x_{SS}}(a, y) \quad \hat{N}_{y_{SS}}(a, y) \quad \hat{N}_{x_{SS}}(x, b) \quad \hat{N}_{y_{SS}}(x, b)]
 \end{aligned} \tag{154}$$

Projections $\tilde{\mathbf{q}}_{SS}$ and $\tilde{\mathbf{Q}}_{SS}$ of the vectors \mathbf{q}_{SS} and \mathbf{Q}_{SS} have been obtained using the following set of projection functions:

$$\begin{aligned} {}^1h_{ss_n}(y) &= \cos\frac{(2n-1)\pi y}{2b}, & {}^2h_{ss_n}(y) &= \sin\frac{(2n-1)\pi y}{2b} \quad \text{for } x = a \\ {}^1h_{ss_n}(x) &= \cos\frac{(2n-1)\pi x}{2a}, & {}^2h_{ss_n}(x) &= \sin\frac{(2n-1)\pi x}{2a} \quad \text{for } y = b \end{aligned} \quad (155)$$

According to Eq. (51) projections of the vectors \mathbf{q}_{SS} and \mathbf{Q}_{SS} are given in the following form:

$$\begin{aligned} \tilde{\mathbf{q}}_{SS} &= \frac{2}{L_s} \int \mathbf{H}_{SS} \mathbf{q}_{SS} ds = \frac{2}{L_s} \int \mathbf{H}_{SS} \mathbf{\Phi}_b \mathbf{C} ds = \tilde{\mathbf{D}}_{SS} \mathbf{C} \\ \tilde{\mathbf{Q}}_{SS} &= \frac{2}{L_s} \int \mathbf{H}_{SS} \mathbf{Q}_{SS} ds = \frac{2}{L_s} \int \mathbf{H}_{SS} \mathbf{G}_b \mathbf{C} ds = \tilde{\mathbf{F}}_{SS} \mathbf{C}, \\ \tilde{\mathbf{D}}_{SS} &= \frac{2}{L_s} \int \mathbf{H}_{SS} \mathbf{\Phi}_b ds, & \tilde{\mathbf{F}}_{SS} &= \frac{2}{L_s} \int \mathbf{H}_{SS} \mathbf{G}_b ds \end{aligned} \quad (156)$$

where

$$\mathbf{C}^T = [A_1 \ B_1 \ C_1 \ D_1 \ \dots \ A_m \ B_m \ C_m \ D_m \ \dots \ A_M \ B_M \ C_M \ D_M], \quad (157)$$

$$\begin{aligned} \tilde{\mathbf{q}}_{SS}^T &= [\tilde{\mathbf{q}}_{SS_1} \ \tilde{\mathbf{q}}_{SS_2} \ \dots \ \tilde{\mathbf{q}}_{SS_m} \ \dots \ \tilde{\mathbf{q}}_{SS_M}]_{1 \times 4M} \\ \tilde{\mathbf{q}}_{SS_m}^T &= [{}^x u_{SS_m} \quad {}^x v_{SS_m} \quad {}^y u_{SS_m} \quad {}^y v_{SS_m}] \\ \tilde{\mathbf{Q}}_{SS}^T &= [\tilde{\mathbf{Q}}_{SS_1} \ \tilde{\mathbf{Q}}_{SS_2} \ \dots \ \tilde{\mathbf{Q}}_{SS_m} \ \dots \ \tilde{\mathbf{Q}}_{SS_M}]_{1 \times 4M} \\ \tilde{\mathbf{Q}}_{SS_m}^T &= [{}^x N_{xSS_m} \quad {}^x N_{xySS_m} \quad {}^y N_{xySS_m} \quad {}^y N_{ySS_m}] \end{aligned} \quad (158)$$

$$\mathbf{H}_{SS} = \begin{bmatrix} \mathbf{H}_1 \\ \mathbf{H}_2 \\ \vdots \\ \mathbf{H}_n \\ \vdots \\ \mathbf{H}_M \end{bmatrix}_{4M \times 4}, \quad \mathbf{H}_n = \begin{bmatrix} {}^2h_{nSS}(y) & 0 & 0 & 0 \\ 0 & {}^1h_{nSS}(y) & 0 & 0 \\ 0 & 0 & {}^1h_{nSS}(x) & 0 \\ 0 & 0 & 0 & {}^2h_{nSS}(x) \end{bmatrix}, \quad (159)$$

$$\Phi_b^T = \begin{bmatrix} \Phi_{b1} \\ \Phi_{b2} \\ \vdots \\ \Phi_{bm} \\ \vdots \\ \Phi_{bM} \end{bmatrix}_{4M \times 4}, \quad \Phi_{bm} = \begin{bmatrix} f_{11_m}(a, y) & f_{12_m}(a, y) & f_{13_m}(a, y) & f_{14_m}(a, y) \\ f_{21_m}(a, y) & f_{22_m}(a, y) & f_{23_m}(a, y) & f_{24_m}(a, y) \\ f_{11_m}(x, b) & f_{12_m}(x, b) & f_{13_m}(x, b) & f_{14_m}(x, b) \\ f_{21_m}(x, b) & f_{22_m}(x, b) & f_{23_m}(x, b) & f_{24_m}(x, b) \end{bmatrix}, \quad (160)$$

$$\mathbf{G}_b = [\mathbf{G}_{b1} \quad \mathbf{G}_{b2} \quad \dots \quad \mathbf{G}_{bm} \quad \dots \quad \mathbf{G}_{bM}]_{4 \times 4M}$$

$$\mathbf{G}_{bm} = D \begin{bmatrix} \frac{\partial \hat{f}_{11}}{\partial x}(a, y) + v \frac{\partial \hat{f}_{21}}{\partial y}(a, y) & \frac{\partial \hat{f}_{12}}{\partial x}(a, y) + v \frac{\partial \hat{f}_{21}}{\partial y}(a, y) & \frac{\partial \hat{f}_{13}}{\partial x}(a, y) + v \frac{\partial \hat{f}_{23}}{\partial y}(a, y) & \frac{\partial \hat{f}_{14}}{\partial x}(a, y) + v \frac{\partial \hat{f}_{24}}{\partial y}(a, y) \\ \frac{\partial \hat{f}_{11}}{\partial y}(a, y) + \frac{\partial \hat{f}_{21}}{\partial x}(a, y) & \frac{\partial \hat{f}_{12}}{\partial y}(a, y) + \frac{\partial \hat{f}_{22}}{\partial x}(a, y) & \frac{\partial \hat{f}_{13}}{\partial y}(a, y) + \frac{\partial \hat{f}_{23}}{\partial x}(a, y) & \frac{\partial \hat{f}_{14}}{\partial y}(a, y) + \frac{\partial \hat{f}_{24}}{\partial x}(a, y) \\ \frac{\partial \hat{f}_{11}}{\partial y}(x, b) + \frac{\partial \hat{f}_{21}}{\partial x}(x, b) & \frac{\partial \hat{f}_{12}}{\partial y}(x, b) + \frac{\partial \hat{f}_{22}}{\partial x}(x, b) & \frac{\partial \hat{f}_{13}}{\partial y}(x, b) + \frac{\partial \hat{f}_{23}}{\partial x}(x, b) & \frac{\partial \hat{f}_{14}}{\partial y}(x, b) + \frac{\partial \hat{f}_{24}}{\partial x}(x, b) \\ v \frac{\partial \hat{f}_{11}}{\partial x}(x, b) + v \frac{\partial \hat{f}_{21}}{\partial y}(x, b) & v \frac{\partial \hat{f}_{12}}{\partial x}(x, b) + \frac{\partial \hat{f}_{21}}{\partial y}(x, b) & v \frac{\partial \hat{f}_{13}}{\partial x}(x, b) + \frac{\partial \hat{f}_{23}}{\partial y}(x, b) & v \frac{\partial \hat{f}_{14}}{\partial x}(x, b) + \frac{\partial \hat{f}_{24}}{\partial y}(x, b) \end{bmatrix}, \quad (161)$$

$$L = \begin{cases} 2b, & \text{for } x = a \\ 2a, & \text{for } y = b \end{cases} \quad ds = \begin{cases} dy, & \text{for } x = a \\ dx, & \text{for } y = b \end{cases} \quad (162)$$

Now, the dynamic stiffness matrix for the double symmetry contribution is obtained as:

$$\tilde{\mathbf{K}}_{D_{SS}}(\omega) = \tilde{\mathbf{F}}_{SS} \tilde{\mathbf{D}}_{SS}^{-1}. \quad (163)$$

The size of the dynamic stiffness matrix $\tilde{\mathbf{K}}_{D_{SS}}$ is $4M$. The dynamic stiffness matrices of other three contributions: $\tilde{\mathbf{K}}_{D_{SA}}(\omega)$, $\tilde{\mathbf{K}}_{D_{AS}}(\omega)$ and $\tilde{\mathbf{K}}_{D_{AA}}(\omega)$ are obtained likewise, using the corresponding base functions $f_{i_m}(x, y)$ defined previously and the projection functions $h_n(x)$ and $h_n(y)$:

$$\begin{aligned}
 {}^1h_{SA_n}(y) &= \cos \frac{(2n-1)\pi y}{2b}, & {}^2h_{SA_n}(y) &= \sin \frac{(2n-1)\pi y}{2b}, \\
 {}^1h_{SA_n}(x) &= \cos \frac{n\pi x}{a}, & {}^2h_{SA_n}(x) &= \sin \frac{n\pi x}{a}, \\
 {}^1h_{AS_n}(y) &= \cos \frac{n\pi y}{b}, & {}^2h_{AS_n}(y) &= \sin \frac{n\pi y}{b}, \\
 {}^1h_{AS_n}(x) &= \cos \frac{(2n-1)\pi x}{2a}, & {}^2h_{AS_n}(x) &= \sin \frac{(2n-1)\pi x}{2a}, \\
 {}^1h_{AA_n}(y) &= \cos \frac{n\pi y}{b}, & {}^2h_{AA_n}(y) &= \sin \frac{n\pi y}{b}, \\
 {}^1h_{AA_n}(x) &= \cos \frac{n\pi x}{a}, & {}^2h_{AA_n}(x) &= \sin \frac{n\pi x}{a}
 \end{aligned} \tag{164}$$

The size of the matrices $\tilde{\mathbf{K}}_{D_{SA}}$ and $\tilde{\mathbf{K}}_{D_{AS}}$ are $4M+1$, while the size of matrix $\tilde{\mathbf{K}}_{D_{AA}}$ is $4M+2$, since the term $m=0$ exists in the antisymmetric contribution. Consequently, the size of the dynamic stiffness matrix $\tilde{\mathbf{K}}_0$, which relates the vectors $\tilde{\mathbf{Q}}_0^T = [\tilde{\mathbf{Q}}_{SS} \quad \tilde{\mathbf{Q}}_{SA} \quad \tilde{\mathbf{Q}}_{AS} \quad \tilde{\mathbf{Q}}_{AA}]$ and $\tilde{\mathbf{q}}_0^T = [\tilde{\mathbf{q}}_{SS} \quad \tilde{\mathbf{q}}_{SA} \quad \tilde{\mathbf{q}}_{AS} \quad \tilde{\mathbf{q}}_{AA}]$ is $4M+4$.

Dynamic stiffness matrix of completely free rectangular plate

The dynamic stiffness matrix $\tilde{\mathbf{K}}_D$ of completely free plate is obtained similarly as for the case of transverse plate vibrations. The in-plane displacements along the plate edges 1, 2, 3 and 4 are given as:

$$\begin{aligned}
 \hat{u}(a, y) &= {}^1u_{S_o} + \sum_{m=1}^M {}^1u_{S_m} \cos \frac{m\pi y}{b} + \sum_{m=1}^M {}^1u_{A_m} \sin \frac{(2m-1)\pi y}{2b} \\
 \hat{v}(a, y) &= \sum_{m=1}^M {}^1v_{S_m} \cos \frac{(2m-1)\pi y}{2b} + \sum_{m=1}^M {}^1v_{A_m} \sin \frac{m\pi y}{b} \\
 \hat{u}(x, b) &= \sum_{m=1}^M {}^2u_{S_m} \cos \frac{(2m-1)\pi y}{2b} + \sum_{m=1}^M {}^2u_{A_m} \sin \frac{m\pi y}{b} \\
 \hat{v}(x, b) &= {}^2v_{S_o} + \sum_{m=1}^M {}^2v_{S_m} \cos \frac{m\pi y}{b} + \sum_{m=1}^M {}^2v_{A_m} \sin \frac{(2m-1)\pi y}{2b} \\
 \hat{u}(-a, y) &= {}^3u_{S_o} + \sum_{m=1}^M {}^3u_{S_m} \cos \frac{m\pi y}{b} + \sum_{m=1}^M {}^3u_{A_m} \sin \frac{(2m-1)\pi y}{2b} \\
 \hat{v}(-a, y) &= \sum_{m=1}^M {}^3v_{S_m} \cos \frac{(2m-1)\pi y}{2b} + \sum_{m=1}^M {}^3v_{A_m} \sin \frac{m\pi y}{b} \\
 \hat{u}(x, -b) &= \sum_{m=1}^M {}^4u_{S_m} \cos \frac{(2m-1)\pi y}{2b} + \sum_{m=1}^M {}^4u_{A_m} \sin \frac{m\pi y}{b} \\
 \hat{v}(x, -b) &= {}^4v_{S_o} + \sum_{m=1}^M {}^4v_{S_m} \cos \frac{m\pi y}{b} + \sum_{m=1}^M {}^4v_{A_m} \sin \frac{(2m-1)\pi y}{2b} .
 \end{aligned} \tag{165}$$

Terms ${}^i u_{S_m}$, ${}^i u_{A_m}$, ${}^i v_{S_m}$ and ${}^i v_{A_m}$ ($i = 1, 2, 3, 4$) are the projections of the in-plane displacements along the plate edges, which are collected into the vector $\tilde{\mathbf{q}}_m$, i.e. into the vector $\tilde{\mathbf{q}}$:

$$\begin{aligned}
 \tilde{\mathbf{q}}_m^T &= [{}^1u_{S_m} \quad {}^1u_{A_m} \quad {}^1v_{S_m} \quad {}^1v_{A_m} \quad \dots \quad {}^4u_{S_m} \quad {}^4u_{A_m} \quad {}^4v_{S_m} \quad {}^4v_{A_m}]_{1 \times 16} \\
 \tilde{\mathbf{q}}_o^T &= [{}^1u_{S_o} \quad {}^2v_{S_o} \quad {}^3u_{S_o} \quad {}^4v_{S_o}]_{1 \times 4} \\
 \tilde{\mathbf{q}}^T &= [\tilde{\mathbf{q}}_o \quad \tilde{\mathbf{q}}_1 \quad \dots \quad \tilde{\mathbf{q}}_m \quad \dots \quad \tilde{\mathbf{q}}_M]_{1 \times (16M+4)}
 \end{aligned} \tag{166}$$

According to Eq. (124) and (158)-(b) the displacements of the double symmetry contribution are given as:

$$\begin{aligned}
 \hat{u}_{SS}(a, y) &= \sum_{m=1}^M {}^x u_{SS_m} \sin \frac{(2m-1)\pi y}{2b} \\
 \hat{v}_{SS}(a, y) &= \sum_{m=1}^M {}^x v_{SS_m} \cos \frac{(2m-1)\pi y}{2b} \\
 \hat{u}_{SS}(x, b) &= \sum_{m=1}^M {}^y u_{SS_m} \cos \frac{(2m-1)\pi x}{2a} . \\
 \hat{v}_{SS}(x, b) &= \sum_{m=1}^M {}^y v_{SS_m} \sin \frac{(2m-1)\pi x}{2a}
 \end{aligned} \tag{167}$$

The projections of these displacements are collected into the vector $\tilde{\mathbf{q}}_{SS}$:

$$\begin{aligned}\tilde{\mathbf{q}}_{SS}^T &= \left[\tilde{\mathbf{q}}_{SS_1} \quad \cdots \quad \tilde{\mathbf{q}}_{SS_m} \quad \tilde{\mathbf{q}}_{SS_M} \right]_{1 \times 4M} \\ \tilde{\mathbf{q}}_{SS_m}^T &= \left[\begin{matrix} x u_{SS_m} & x v_{SS_m} & y u_{SS_m} & y v_{SS_m} \end{matrix} \right]\end{aligned}\quad (168)$$

The vectors $\tilde{\mathbf{q}}_{SA}$, $\tilde{\mathbf{q}}_{AS}$, $\tilde{\mathbf{q}}_{AA}$ of SA, AS and AA contributions can be expressed likewise.

They are collected into vector $\tilde{\mathbf{q}}_0$:

$$\tilde{\mathbf{q}}_0^T = \left[\tilde{\mathbf{q}}_{SS} \quad \tilde{\mathbf{q}}_{SA} \quad \tilde{\mathbf{q}}_{AS} \quad \tilde{\mathbf{q}}_{AA} \right]. \quad (169)$$

Using Gorman's superposition method the displacements along the plate edge $y = a$ can be written as:

$$\begin{aligned}\hat{u}(a, y) &= \hat{u}_{SS}(a, y) + \hat{u}_{SA}(a, y) + \hat{u}_{AS}(a, y) + \hat{u}_{AA}(a, y) \\ \hat{u}(-a, y) &= \hat{u}_{SS}(-a, y) + \hat{u}_{SA}(-a, y) + \hat{u}_{AS}(-a, y) + \hat{u}_{AA}(-a, y) \\ \hat{u}(a, -y) &= \hat{u}_{SS}(a, -y) + \hat{u}_{SA}(a, -y) + \hat{u}_{AS}(a, -y) + \hat{u}_{AA}(a, -y) \\ \hat{u}(-a, -y) &= \hat{u}_{SS}(-a, -y) + \hat{u}_{SA}(-a, -y) + \hat{u}_{AS}(-a, -y) + \hat{u}_{AA}(-a, -y)\end{aligned}\quad (170)$$

$$\begin{aligned}\hat{v}(a, y) &= \hat{v}_{SS}(a, y) + \hat{v}_{SA}(a, y) + \hat{v}_{AS}(a, y) + \hat{v}_{AA}(a, y) \\ \hat{v}(-a, y) &= \hat{v}_{SS}(-a, y) + \hat{v}_{SA}(-a, y) + \hat{v}_{AS}(-a, y) + \hat{v}_{AA}(-a, y) \\ \hat{v}(a, -y) &= \hat{v}_{SS}(a, -y) + \hat{v}_{SA}(a, -y) + \hat{v}_{AS}(a, -y) + \hat{v}_{AA}(a, -y) \\ \hat{v}(-a, -y) &= \hat{v}_{SS}(-a, -y) + \hat{v}_{SA}(-a, -y) + \hat{v}_{AS}(-a, -y) + \hat{v}_{AA}(-a, -y)\end{aligned}$$

Since

$$\begin{aligned}\hat{u}_{SS}(a, y) &= -\hat{u}_{SS}(a, -y) = \hat{u}_{SS}(-a, y) = -\hat{u}_{SS}(-a, -y) \\ \hat{u}_{SA}(a, y) &= -\hat{u}_{SA}(-a, y) = \hat{u}_{SA}(a, -y) = -\hat{u}_{SA}(-a, -y) \\ \hat{u}_{AS}(a, y) &= \hat{u}_{AS}(a, -y) = \hat{u}_{AS}(-a, y) = \hat{u}_{AS}(-a, -y) \\ \hat{u}_{AA}(a, y) &= -\hat{u}_{AA}(-a, y) = \hat{u}_{AA}(a, -y) = -\hat{u}_{AA}(-a, -y)\end{aligned}, \quad (171)$$

$$\begin{aligned}\hat{v}_{SS}(a, y) &= \hat{v}_{SS}(a, -y) = -\hat{v}_{SS}(-a, y) = \hat{v}_{SS}(-a, -y) \\ \hat{v}_{SA}(a, y) &= \hat{v}_{SA}(-a, y) = \hat{v}_{SA}(a, -y) = \hat{v}_{SA}(-a, -y) \\ \hat{v}_{AS}(a, y) &= -\hat{v}_{AS}(a, -y) = \hat{v}_{AS}(-a, y) = -\hat{v}_{AS}(-a, -y) \\ \hat{v}_{AA}(a, y) &= \hat{v}_{AA}(-a, y) = -\hat{v}_{AA}(a, -y) = \hat{v}_{AA}(-a, -y)\end{aligned}$$

the fully symmetric displacements are given by:

$$\begin{aligned}\hat{u}_{SS}(a, y) &= \frac{1}{4}(\hat{u}(a, y) + \hat{u}(-a, y) - \hat{u}(a, -y) - \hat{u}(-a, -y)) \\ \hat{v}_{SS}(a, y) &= \frac{1}{4}(\hat{v}(a, y) + \hat{v}(a, -y) - \hat{v}(-a, y) - \hat{v}(-a, -y))\end{aligned}\quad (172)$$

For displacement components at the edge $y = b$ similar expressions can be obtained:

$$\begin{aligned}\hat{u}_{SS}(x, b) &= \frac{1}{4}(\hat{u}(x, b) + \hat{u}(-x, b) - \hat{u}(x, -b) - \hat{u}(-x, -b)) \\ \hat{v}_{SS}(x, b) &= \frac{1}{4}(\hat{v}(x, b) - \hat{v}(-x, b) + \hat{v}(x, -b) - \hat{v}(-x, -b))\end{aligned}\quad (173)$$

From Eqs. (165), (167) and (172) the following expressions are obtained:

$$\begin{aligned}u_{SS_m}(a, y) &= \frac{1}{2}({}^1u_{A_m} + {}^3u_{A_m}) \\ v_{SS_m}(a, y) &= \frac{1}{2}({}^1v_{S_m} - {}^3v_{S_m}) \\ u_{SS_m}(x, b) &= \frac{1}{2}({}^2u_{S_m} - {}^4u_{S_m}) \\ v_{SS_m}(x, b) &= \frac{1}{2}({}^2v_{A_m} + {}^4v_{A_m})\end{aligned}, m = 1, \dots, M. \quad (174)$$

Eq. (174) can be written in the matrix form as:

$$\tilde{\mathbf{q}}_{SS_m} = \frac{1}{2} \mathbf{t}_{SS} \tilde{\mathbf{q}}_m, m = 1, \dots, M, \quad (175)$$

where

$$\mathbf{t}_{SS} = \begin{bmatrix} 0 & 1 & 0 & 0 & 0 & 0 & 0 & 0 & 0 & 1 & 0 & 0 & 0 & 0 & 0 \\ 0 & 0 & 1 & 0 & 0 & 0 & 0 & 0 & 0 & 0 & -1 & 0 & 0 & 0 & 0 \\ 0 & 0 & 0 & 0 & 1 & 0 & 0 & 0 & 0 & 0 & 0 & 0 & -1 & 0 & 0 \\ 0 & 0 & 0 & 0 & 0 & 0 & 0 & 1 & 0 & 0 & 0 & 0 & 0 & 0 & 1 \end{bmatrix}. \quad (176)$$

Now, the relation between the vectors $\tilde{\mathbf{q}}_{SS}$ and $\tilde{\mathbf{q}}_0$ is given as:

$$\tilde{\mathbf{q}}_{SS} = \frac{1}{2} \mathbf{T}_{SS} \tilde{\mathbf{q}}_0, \quad (177)$$

where

$$\mathbf{T}_{SS} = \begin{bmatrix} \mathbf{t}_{SS} & & & \\ & \ddots & & \\ & & \mathbf{t}_{SS} & \\ & & & \ddots \\ & & & & \mathbf{t}_{SS} \end{bmatrix}_{4M \times 16M} \quad (178)$$

The above procedure is carried out for vectors $\tilde{\mathbf{q}}_{SA}$, $\tilde{\mathbf{q}}_{AS}$, $\tilde{\mathbf{q}}_{AA}$ and the following relations are obtained:

$$\begin{aligned} \tilde{\mathbf{q}}_{SA} &= \frac{1}{2} \mathbf{T}_{SA} \tilde{\mathbf{q}} \\ \tilde{\mathbf{q}}_{AS} &= \frac{1}{2} \mathbf{T}_{AS} \tilde{\mathbf{q}} \\ \tilde{\mathbf{q}}_{AA} &= \frac{1}{2} \mathbf{T}_{AA} \tilde{\mathbf{q}} \end{aligned} \quad (179)$$

From Eq. (177)-(179) the relation between vectors $\tilde{\mathbf{q}}_0$ and $\tilde{\mathbf{q}}$ is given as:

$$\tilde{\mathbf{q}}_0 = \frac{1}{2} \mathbf{T} \tilde{\mathbf{q}}, \quad (180)$$

where

$$\mathbf{T} = \begin{bmatrix} \mathbf{T}_{SS} \\ \mathbf{T}_{SA} \\ \mathbf{T}_{AS} \\ \mathbf{T}_{AA} \end{bmatrix}_{16M \times 16M} \quad (181)$$

Similarly, the reverse procedure is carried out for the force components. For example, the in-plane normal force on edge 1 is given by:

$$N_x(a, y) = N_{x_{SS}}(a, y) + N_{x_{SA}}(a, y) + N_{x_{AS}}(a, y) + N_{x_{AA}}(a, y), \quad (182)$$

where

$$\begin{aligned}
 N_x(a, y) &= {}^1N_{x_o} + \sum_{m=1}^M {}^1N_{x_{S_m}} \cos \frac{m\pi y}{b} + \sum_{m=1}^M {}^1N_{x_{A_m}} \sin \frac{(2m-1)\pi y}{2b} \\
 N_{x_{SS}}(a, y) &= \sum_{m=1}^M {}^xN_{x_{SS_m}} \sin \frac{(2m-1)\pi y}{2b} \\
 N_{x_{SA}}(a, y) &= \sum_{m=1}^M {}^xN_{x_{SA_m}} \sin \frac{(2m-1)\pi y}{2b} \\
 N_{x_{AS}}(a, y) &= {}^xN_{x_{AS_o}} + \sum_{m=1}^M {}^xN_{x_{AS_m}} \cos \frac{m\pi y}{b} \\
 N_{x_{AA}}(a, y) &= {}^xN_{x_{AA_o}} + \sum_{m=1}^M {}^xN_{x_{AA_m}} \cos \frac{m\pi y}{b}
 \end{aligned} \tag{183}$$

Substituting Eq. (183) into (182) the following expressions are obtained:

$$\begin{aligned}
 {}^1N_{x_{S_m}} &= {}^xN_{x_{AS_m}} + {}^xN_{x_{AA_m}} \\
 {}^1N_{x_{A_m}} &= {}^xN_{x_{SS_m}} + {}^xN_{x_{SA_m}}
 \end{aligned} \tag{184}$$

Similar expressions can be obtained for other forces along plate boundary:

$$\begin{aligned}
 {}^1N_{xy_{S_m}} &= {}^xN_{xy_{SS_m}} + {}^xN_{xy_{SA_m}} \\
 {}^1N_{xy_{A_m}} &= {}^xN_{xy_{AS_m}} + {}^xN_{xy_{AA_m}} \\
 {}^2N_{xy_{S_m}} &= {}^yN_{xy_{SS_m}} + {}^yN_{xy_{AS_m}} & {}^2N_{y_{S_m}} &= {}^yN_{y_{SA_m}} + {}^yN_{y_{AA_m}} \\
 {}^2N_{xy_{A_m}} &= {}^yN_{xy_{SA_m}} + {}^yN_{xy_{AA_m}} & {}^2N_{y_{A_m}} &= {}^yN_{y_{SS_m}} + {}^yN_{y_{AS_m}} \\
 {}^3N_{x_{S_m}} &= {}^xN_{x_{AS_m}} - {}^xN_{x_{AA_m}} & {}^3N_{xy_{S_m}} &= -{}^xN_{xy_{SS_m}} + {}^xN_{xy_{SA_m}} \\
 {}^3N_{x_{A_m}} &= {}^xN_{x_{SS_m}} - {}^xN_{x_{SA_m}} & {}^3N_{xy_{A_m}} &= {}^xN_{xy_{AS_m}} - {}^xN_{xy_{AA_m}} \\
 {}^4N_{xy_{S_m}} &= -{}^yN_{xy_{SS_m}} + {}^yN_{xy_{AS_m}} & {}^4N_{y_{S_m}} &= {}^yN_{y_{SA_m}} - {}^yN_{y_{AA_m}} \\
 {}^4N_{xy_{A_m}} &= -{}^yN_{xy_{SA_m}} + {}^yN_{xy_{AA_m}} & {}^4N_{y_{A_m}} &= {}^yN_{y_{SS_m}} - {}^yN_{y_{AS_m}}
 \end{aligned} \tag{185}$$

These relations can be written in the matrix form as:

$$\tilde{\mathbf{Q}} = \mathbf{T}^T \tilde{\mathbf{Q}}_o, \tag{186}$$

where

$$\begin{aligned}
 \tilde{\mathbf{Q}}_o^T &= [\tilde{\mathbf{Q}}_{SS} \quad \tilde{\mathbf{Q}}_{SA} \quad \tilde{\mathbf{Q}}_{AS} \quad \tilde{\mathbf{Q}}_{AA}], \\
 \tilde{\mathbf{Q}}^T &= [\tilde{\mathbf{Q}}_o \quad \tilde{\mathbf{Q}}_1 \quad \dots \quad \tilde{\mathbf{Q}}_m \quad \dots \quad \tilde{\mathbf{Q}}_M], \\
 \tilde{\mathbf{Q}}_m^T &= [{}^1N_{xS_m} \quad {}^1N_{xA_m} \quad {}^1N_{xyS_m} \quad {}^1N_{xyA_m} \quad \dots \quad {}^4N_{xyS_m} \quad {}^4N_{xyA_m} \quad {}^4N_{yS_m} \quad {}^4N_{yA_m}]
 \end{aligned} \tag{187}$$

According to the relation between the vectors $\tilde{\mathbf{Q}}_o$ and $\tilde{\mathbf{q}}_o$:

$$\tilde{\mathbf{Q}}_o = \tilde{\mathbf{K}}_o \tilde{\mathbf{q}}_o = \begin{bmatrix} \tilde{\mathbf{K}}_{D_{SS}} & 0 & 0 & 0 \\ 0 & \tilde{\mathbf{K}}_{D_{SA}} & 0 & 0 \\ 0 & 0 & \tilde{\mathbf{K}}_{D_{AS}} & 0 \\ 0 & 0 & 0 & \tilde{\mathbf{K}}_{D_{AA}} \end{bmatrix} \tilde{\mathbf{q}}_o, \tag{188}$$

and considering Eqs. (180) and (186), the dynamic stiffness matrix of the completely free rectangular plate element is given by:

$$\tilde{\mathbf{K}}_D = \frac{1}{2} \mathbf{T}^T \tilde{\mathbf{K}}_o \mathbf{T}. \tag{189}$$

The size of the dynamic stiffness matrix is $16M+4$. In order to make it square, the number of terms in the general solution defined by Eq. (64) has to be the same as the number of projection functions. The described method allows the in-plane vibration analysis of rectangular plate and plate assemblies with arbitrary boundary conditions. The efficiency and accuracy of the developed dynamic stiffness matrix will be showed on several examples with different type of boundary conditions. For that purpose the computer program using Matlab has been developed.

2.3.2.4 Numerical examples

➤ Free vibration analysis of completely free square plate

In order to check the convergence of the developed dynamic stiffness matrix, the dimensionless frequencies $\Omega = \omega a / c_p$ of square plate with free boundaries are calculated for different value of M – the number of terms in the general solution, and presented in Table 6. It can be seen that the results obtained using the SEM show a very high rate of convergence, especially for the lower vibration modes. In addition, an excellent agreement is achieved between the present solution and the solutions obtained by Gorman (2004) and Bardell at al. (1996).

Table 6. Dimensionless frequencies of completely free square plate

Mode No.	SEM					Gorman	Bardell
	M=1	M=2	M=3	M=4	M=5		
1	1.167	1.160	1.160	1.160	1.160	1.160	1.160
2*	1.266	1.245	1.241	1.238	1.237	1.236	1.236
3	1.325	1.319	1.317	1.316	1.315	1.314	1.314
4	1.529	1.507	1.501	1.498	1.497	1.494	1.493
5	1.726	1.726	1.726	1.726	1.726	1.726	1.726
6*	1.949	1.876	1.868	1.865	1.864	1.862	1.868
7	2.508	2.205	2.177	2.166	2.161	2.153	2.177

* Double frequency due to symmetry

Natural frequencies calculated using the FEM for different number of finite elements are presented in Table 7. As the number of finite elements increase, the natural frequencies converge to the more accurate solutions (SEM and Gorman's analytical solution). The first four mode shapes are given in Figure 16.

Table 7. Dimensionless frequencies of completely free square plate using FEM

Mode No.	Number of FE			Gorman	Bardell
	10x10	20x20	40x40		
1	1.162	1.160	1.160	1.160	1.160
2*	1.213	1.236	1.236	1.230	1.234
3	1.298	1.314	1.314	1.310	1.313
4	1.442	1.494	1.493	1.480	1.490
5	1.721	1.726	1.726	1.725	1.726
6*	1.820	1.862	1.868	1.851	1.859
7	2.041	2.153	2.177	2.124	2.144

* Double frequency due to symmetry

➤ Free vibration analysis rectangular plate with different boundary conditions

Application of different types of boundary conditions has been illustrated on the example of rectangular plate with aspect ratio $b/a = 1.2$. The mass density, Young's modulus and Poisson's ratio are respectively 2.8 t/m^3 , $72 \cdot 10^6 \text{ kN/m}^2$ and 0.3. The following boundary conditions have been assigned to plate boundary:

- simply supported edge - S1 ($u \neq 0, v = 0$ for $x = \pm a$ and $u = 0, v \neq 0$ for $y = \pm b$),
- simply supported edge – S2 ($u = 0, v \neq 0$ for $x = \pm a$ and $u \neq 0, v = 0$ for $y = \pm b$),
- clamped edge – C ($u = 0, v = 0$),
- free edge – F ($u \neq 0, v \neq 0$).

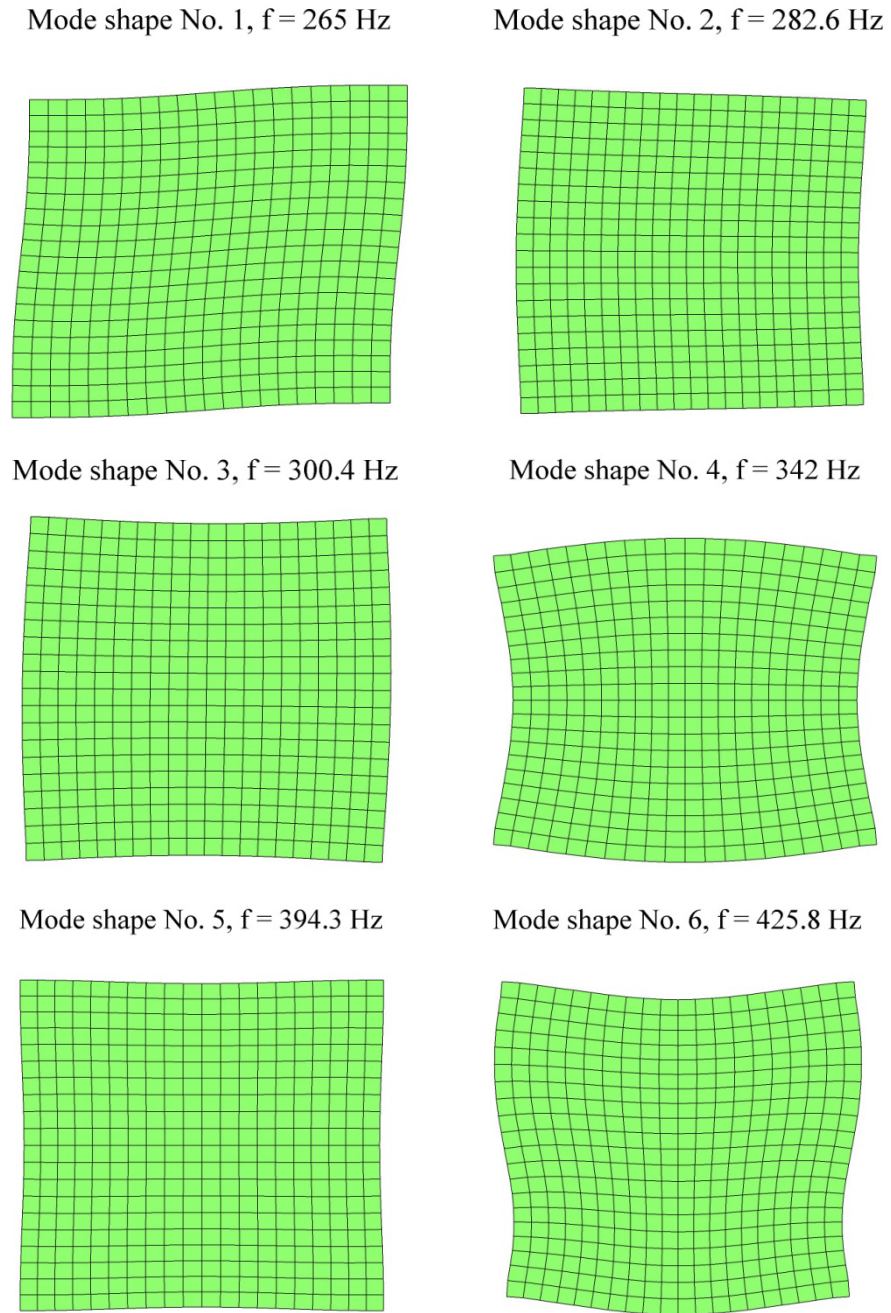


Figure 16. Mode shapes of completely free square plate

The natural frequencies obtained using the SEM, have been compared with those obtained from the exact solution proposed by Xing and Liu (2009) and Boscolo and Banerjee, (2011) - b. The results are given in Table 8. Again, an excellent agreement is achieved between the present solution and the solutions obtained by Xing and Boscolo.

Table 8. Dimensionless frequencies of rectangular plate

<i>Boundary conditions</i>	<i>Present solution using SEM</i>	<i>Boscolo</i>	<i>Xing</i>
S1-S1-S1-S1	0.773	0.774	0.774
	0.926	0.929	0.929
	1.210	1.210	1.210
	1.545	1.549	1.549
	1.807	1.806	1.806
	1.853	1.859	1.859
	2.010	2.013	2.013
	2.041	2.044	2.044
	2.318	2.323	2.323
	2.421	2.419	2.419
S1-C-S1-C	0.773		0.774
	1.431		1.432
	1.547		1.549
	1.658		1.658
	2.089	-	2.090
	2.222		2.222
	2.320		2.323
	2.388		2.392
2.579		2.581	
S2-F-S1-C	0.685		0.684
	0.837		0.839
	1.302		1.298
	1.420		1.417
	1.817		1.821
	1.895	-	1.896
	2.134		2.130
	2.240		2.242
	2.381		2.384
2.441		2.445	

3. Coupling of spectral elements

Structures consisting of two-dimensional elements like plates and one-dimensional elements like beams and columns are widely used in civil engineering practice (for example, column supported reinforced floor slabs), aerospace industry (beam reinforced panels), etc. In order to solve the vibration problems of these types of structures using the SEM, the method for coupling different types of spectral elements has to be developed. In this section the dynamic stiffness matrix for plate element with edge beams is developed. In this section the dynamic stiffness matrix for plate element with

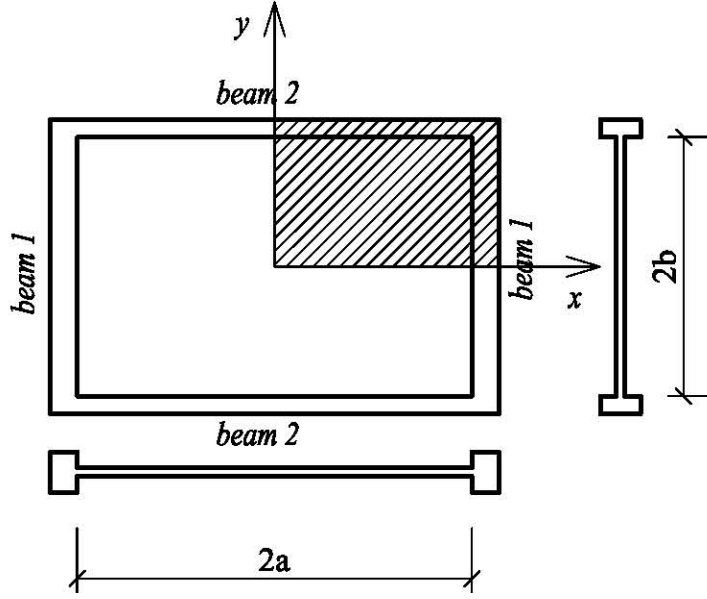


Figure 17. Rectangular plate with edge beams

edge beams will be developed. In addition, the method for obtaining the dynamic stiffness matrix for structural system consisting of plates supported by columns is presented. The accuracy and efficiency of the method is demonstrated on several numerical examples.

3.1 Dynamic stiffness matrix for plate element with edge beams

Rectangular plate with reinforcing edge beams symmetrically distributed along plate edges is presented in Figure 17. Only one quarter of the plate will be analyzed, as explained in the previous section. It is assumed that beams are ideally attached to the plate, which means that the displacements and rotations of the beams and the edge of the plate are equal at all points along the beam, i.e.

$$\begin{aligned}
 u^P(\pm a, y) &= u^B(y) & u^P(x, \pm b) &= u^B(x) \\
 v^P(\pm a, y) &= v^B(y) & v^P(x, \pm b) &= v^B(x) \\
 w^P(\pm a, y) &= w^B(y) & w^P(x, \pm b) &= w^B(x) \quad , \\
 \frac{\partial w^P(\pm a, y)}{\partial x} &= \phi_y^B(y) & \frac{\partial w^P(x, \pm b)}{\partial y} &= \phi_x^B(x)
 \end{aligned} \quad (190)$$

where $\phi_y^B(y)$ and $\phi_x^B(x)$ are beam torsional rotations. The superscripts P and B in the above equations refer to the plate and beam displacements and rotations, respectively.

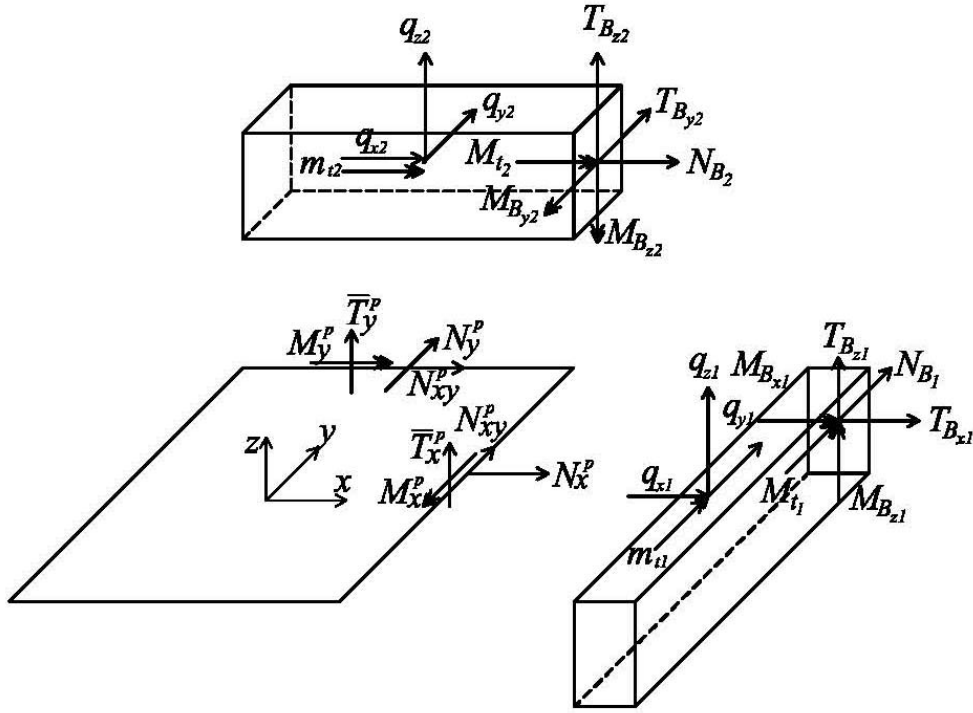


Figure 18. Plate and beam forces

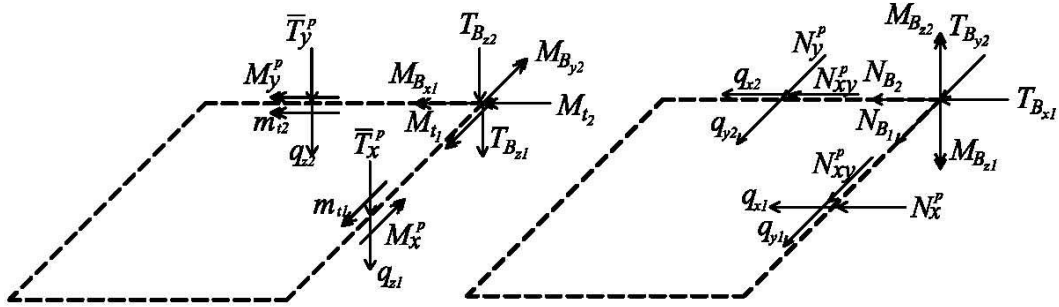


Figure 19. Resultant forces acting on the plate boundary

Consequently, the moments and forces at the boundaries of the plate are equal to those in the beams. Plate and beam forces are given in Figure 18. Resultant forces acting on the plate boundary are described in Figure 19, from which new boundary conditions are defined, (Campos and Arruda 2008):

$$\begin{aligned} \bar{T}_x(a, y) &= \bar{T}_x^p + q_{z1} + T_{Bz2} \delta(y-b) = \\ &= -D \left(\frac{\partial^3 w}{\partial x^3} + (2-\nu) \frac{\partial^3 w}{\partial x \partial y^2} \right) + E_{B1} I_{x1} \frac{\partial^4 w}{\partial y^4} - \rho A_1 \omega^2 w - E_{B2} I_{y2} \frac{\partial^3 w}{\partial x^3} \delta(y-b) \end{aligned} \quad (191)$$

$$\begin{aligned}
 M_x(a, y) &= M_x^P - m_{t1} + M_{B_{y2}} \delta(y-b) = \\
 &= D \left(\frac{\partial^2 w}{\partial x^2} + \nu \frac{\partial^2 w}{\partial y^2} \right) - G_{B1} I_{t1} \frac{\partial^3 w}{\partial x \partial y^2} - \rho I_{t1} \omega^2 \frac{\partial w}{\partial x} + E_{B2} I_{y2} \frac{\partial^2 w}{\partial x^2} \delta(y-b) \quad (192)
 \end{aligned}$$

$$\begin{aligned}
 N_x(a, y) &= N_x^P + q_{x1} + N_{B2} \delta(y-b) = \\
 &= D_1 \left(\frac{\partial u}{\partial x} + \nu \frac{\partial v}{\partial y} \right) + E_{B1} I_{z1} \frac{\partial^4 u}{\partial y^4} - \rho A_1 \omega^2 u + E_{B2} A_2 \frac{\partial u}{\partial x} \delta(y-b) \quad (193)
 \end{aligned}$$

$$\begin{aligned}
 N_{xy}(a, y) &= N_{xy}^P + q_{y1} + T_{B_{y2}} \delta(y-b) = \\
 &= D_1 a_1 \left(\frac{\partial u}{\partial y} + \frac{\partial v}{\partial x} \right) - E_{B1} A_1 \frac{\partial^2 v}{\partial y^2} - \rho A_1 \omega^2 v - E_{B2} I_{z2} \frac{\partial^3 v}{\partial x^3} \delta(y-b) \quad (194)
 \end{aligned}$$

$$\begin{aligned}
 \bar{T}_y(x, b) &= \bar{T}_y^P + q_{z2} + T_{B_{z1}} \delta(x-a) = \\
 &= -D \left(\frac{\partial^3 w}{\partial y^3} + (2-\nu) \frac{\partial^3 w}{\partial x^2 \partial y} \right) + E_{B2} I_{y2} \frac{\partial^4 w}{\partial x^4} - \rho A_2 \omega^2 w - E_{B1} I_{x1} \frac{\partial^3 w}{\partial y^3} \delta(x-a) \quad (195)
 \end{aligned}$$

$$\begin{aligned}
 M_y(x, b) &= M_y^P + m_{t2} + M_{B_{x1}} \delta(x-a) = \\
 &= D \left(\frac{\partial^2 w}{\partial y^2} + \nu \frac{\partial^2 w}{\partial x^2} \right) - G_{B2} I_{t2} \frac{\partial^3 w}{\partial x^2 \partial y} - \rho I_{t2} \omega^2 \frac{\partial w}{\partial y} + E_{B1} I_{x1} \frac{\partial^2 w}{\partial y^2} \delta(x-a) \quad (196)
 \end{aligned}$$

$$\begin{aligned}
 N_y(x, b) &= N_y^P + q_{y2} + N_{B1} \delta(x-a) = \\
 &= D_1 \left(\frac{\partial u}{\partial x} \nu + \frac{\partial v}{\partial y} \right) + E_{B2} I_{z2} \frac{\partial^4 v}{\partial x^4} - \rho A_2 \omega^2 v + E_{B1} A_1 \frac{\partial u}{\partial y} \delta(x-a) \quad (197)
 \end{aligned}$$

$$\begin{aligned}
 N_{xy}(x, b) &= N_{xy}^P + q_{x2} + T_{B_{x1}} \delta(x-a) = \\
 &= D_1 a_1 \left(\frac{\partial u}{\partial y} + \frac{\partial v}{\partial x} \right) - E_{B2} A_2 \frac{\partial^2 u}{\partial x^2} - \rho A_2 \omega^2 u - E_{B1} I_{z1} \frac{\partial^3 u}{\partial y^3} \delta(x-a) \quad (198)
 \end{aligned}$$

where $E_{B1}I_{x1}$, $E_{B1}I_{z1}$, $E_{B2}I_{y2}$ and $E_{B2}I_{z2}$ are the flexural beam stiffness, $G_{B1}I_{t1}$ and $G_{B2}I_{t2}$ are the torsional beam stiffness, $E_{B1}A_1$ and $E_{B2}A_2$ are the axial beam stiffness, ρA_1 , ρA_2 , ρI_{t1} and ρI_{t2} are the mass and polar mass moment of inertia per unit length, respectively and δ is Dirac delta function.

Using the modified boundary conditions defined by Eq. (191)-(198), the dynamic stiffness matrix of plate element with edge beams for transverse and in-plane vibration

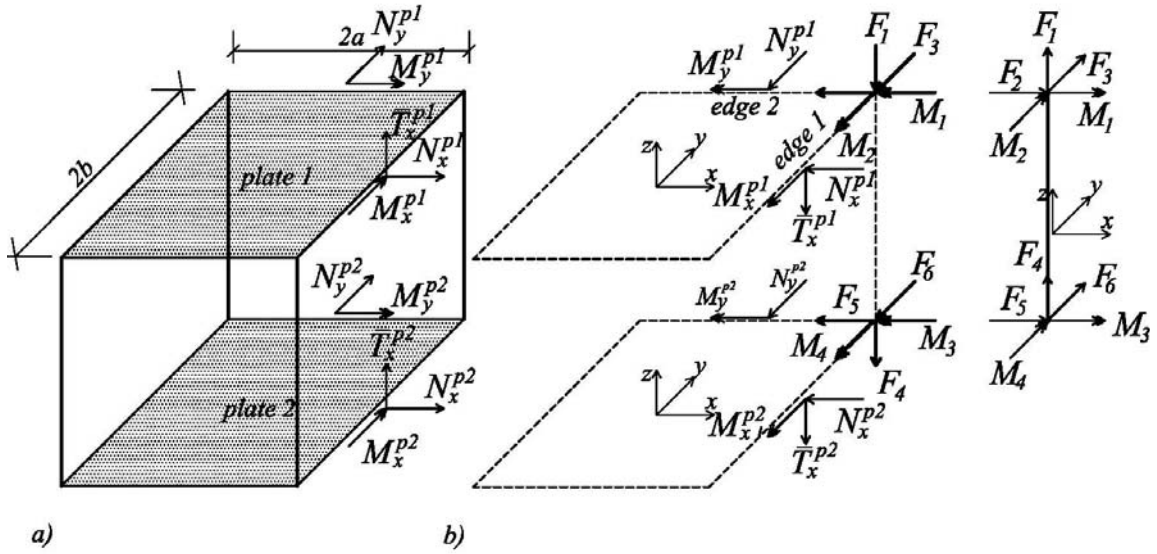


Figure 20. Column supported plate: a) Geometry, b) Resultant forces

is obtained. The matrices $\tilde{\mathbf{D}}$ relating the vector of the displacement projections $\tilde{\mathbf{q}}$ and the vector of integration coefficients \mathbf{C} remain unchanged, while the matrices $\tilde{\mathbf{F}}$ are modified according to Eq. (191)-(198).

3.2. Column supported plate element

In order to apply the SEM in the analysis of structures consisting of floor slabs and columns, the method for coupling columns and plates has to be developed. The assembly consisting of two plates supported by columns at the plate edges is given in Figure 20a). Resultant forces in the column acting on the plate edges are presented in Figure 20b). It is assumed that torsional effects of the column can be neglected and that plate and column displacements and rotations at the junction point (x_o, y_o) are equal. Consequently, according to Eq. (33), forces acting on the plate boundary can be written as:

$$\begin{aligned}
 F_1 &= \left[k_{11}^c w^{p1}(x_o, y_o) + k_{17}^c w^{p2}(x_o, y_o) \right] \delta(y - y_o) \\
 F_2 &= \left[k_{22}^c u^{p1}(x_o, y_o) + k_{26}^c \left(\frac{\partial w}{\partial x} \right)_{(x_o, y_o)}^{p1} + k_{28}^c u^{p2}(x_o, y_o) + k_{2,12}^c \left(\frac{\partial w}{\partial x} \right)_{(x_o, y_o)}^{p2} \right] \delta(y - y_o) \\
 F_3 &= \left[k_{33}^c v^{p1}(x_o, y_o) + k_{35}^c \left(\frac{\partial w}{\partial y} \right)_{(x_o, y_o)}^{p1} + k_{39}^c v^{p2}(x_o, y_o) + k_{3,11}^c \left(\frac{\partial w}{\partial y} \right)_{(x_o, y_o)}^{p2} \right] \delta(x - x_o)
 \end{aligned} \tag{199}$$

$$\begin{aligned}
 F_4 &= \left[k_{71}^c w^{p1}(x_o, y_o) + k_{77}^c w^{p2}(x_o, y_o) \right] \delta(y - y_o) \\
 F_5 &= \left[k_{82}^c u^{p1}(x_o, y_o) + k_{86}^c \left(\frac{\partial w}{\partial x} \right)_{(x_o, y_o)}^{p1} + k_{88}^c u^{p2}(x_o, y_o) + k_{8,12}^c \left(\frac{\partial w}{\partial x} \right)_{(x_o, y_o)}^{p2} \right] \delta(y - y_o) \\
 F_6 &= \left[k_{93}^c v^{p1}(x_o, y_o) + k_{95}^c \left(\frac{\partial w}{\partial y} \right)_{(x_o, y_o)}^{p1} + k_{99}^c v^{p2}(x_o, y_o) + k_{9,11}^c \left(\frac{\partial w}{\partial y} \right)_{(x_o, y_o)}^{p2} \right] \delta(x - x_o)
 \end{aligned} \tag{200}$$

$$\begin{aligned}
 M_1 &= \left[k_{53}^c v^{p1}(x_o, y_o) + k_{55}^c \left(\frac{\partial w}{\partial y} \right)_{(x_o, y_o)}^{p1} + k_{59}^c v^{p2}(x_o, y_o) + k_{5,11}^c \left(\frac{\partial w}{\partial y} \right)_{(x_o, y_o)}^{p2} \right] \delta(x - x_o) \\
 M_2 &= \left[k_{62}^c u^{p1}(x_o, y_o) + k_{66}^c \left(\frac{\partial w}{\partial x} \right)_{(x_o, y_o)}^{p1} + k_{68}^c u^{p2}(x_o, y_o) + k_{6,12}^c \left(\frac{\partial w}{\partial x} \right)_{(x_o, y_o)}^{p2} \right] \delta(y - y_o)
 \end{aligned} \tag{201}$$

$$\begin{aligned}
 M_3 &= \left[k_{11,3}^c v^{p1}(x_o, y_o) + k_{11,5}^c \left(\frac{\partial w}{\partial y} \right)_{(x_o, y_o)}^{p1} + k_{11,9}^c v^{p2}(x_o, y_o) + k_{11,11}^c \left(\frac{\partial w}{\partial y} \right)_{(x_o, y_o)}^{p2} \right] \delta(x - x_o) \\
 M_4 &= \left[k_{12,2}^c u^{p1}(x_o, y_o) + k_{12,6}^c \left(\frac{\partial w}{\partial x} \right)_{(x_o, y_o)}^{p1} + k_{12,8}^c u^{p2}(x_o, y_o) + k_{12,12}^c \left(\frac{\partial w}{\partial x} \right)_{(x_o, y_o)}^{p2} \right] \delta(y - y_o)
 \end{aligned} \tag{202}$$

where k_{ij}^c are the corresponding elements of the dynamic stiffness matrix of the column member defined in Section 2.2.4, while $u(x_o, y_o)$, $v(x_o, y_o)$, $w(x_o, y_o)$, $\left(\frac{\partial w}{\partial x} \right)_{(x_o, y_o)}$ and

$\left(\frac{\partial w}{\partial y}\right)_{(x_o, y_o)}$ are the displacements and rotations of the plate at the junction point (x_o, y_o)

. Superscripts p1 and p2 refer to the plate 1 and plate 2, respectively. Now, the equilibrium equations along the boundary of plate 1 are given as:

$$\begin{aligned} N_x^{p1} + F_2 &= 0 \\ \bar{T}_x^{p1} + F_1 &= 0 \\ M_x^{p1} + M_2 &= 0. \\ N_y^{p1} + F_3 &= 0 \\ M_y^{p1} + M_1 &= 0 \end{aligned} \quad (203)$$

Forces F_i , $i = 1, \dots, 6$ and moments M_i , $i = 1, \dots, 4$ have to be projected onto a set of corresponding projection functions:

$$\begin{aligned} h_m^S(x) &= \cos \frac{m\pi x}{a}, \quad h_m^S(y) = \cos \frac{m\pi y}{b} \\ h_m^A(x) &= \sin \frac{(2m-1)\pi x}{2a}, \quad h_m^A(y) = \sin \frac{(2m-1)\pi y}{2b}, \quad m = 0, 1, \dots, M. \end{aligned} \quad (204)$$

Now, the projections of the forces F_i and moments M_i are:

$$\begin{aligned} \tilde{F}_{i_m}^S &= \langle F_i, h_m^S(s) \rangle = \frac{2}{L} \int_{-L/2}^{L/2} F_i \delta\left(s - \frac{L}{2}\right) h_m^S(s) ds = \frac{2}{L} (-1)^m F_i \\ \tilde{F}_{i_m}^A &= \langle F_i, h_m^A(s) \rangle = \frac{2}{L} \int_{-L/2}^{L/2} F_i \delta\left(s - \frac{L}{2}\right) h_m^A(s) ds = \frac{2}{L} (-1)^{m-1} F_i \\ \tilde{M}_{i_m}^S &= \langle M_i, h_m^S(s) \rangle = \frac{2}{L} \int_{-L/2}^{L/2} M_i \delta\left(s - \frac{L}{2}\right) h_m^S(s) ds = \frac{2}{L} (-1)^m M_i \\ \tilde{M}_{i_m}^A &= \langle M_i, h_m^A(s) \rangle = \frac{2}{L} \int_{-L/2}^{L/2} M_i \delta\left(s - \frac{L}{2}\right) h_m^A(s) ds = \frac{2}{L} (-1)^{m-1} M_i \end{aligned} \quad (205)$$

where

$$L = \begin{cases} 2b & \text{for edges 1 and 3} \\ 2a & \text{for edges 2 and 4} \end{cases}, \quad s = \begin{cases} y & \text{for edges 1 and 3} \\ x & \text{for edges 2 and 4} \end{cases}. \quad (206)$$

The displacements and rotations $u(x_o, y_o)$, $v(x_o, y_o)$, $w(x_o, y_o)$, $\left(\frac{\partial w}{\partial x}\right)_{(x_o, y_o)}$ and

$\left(\frac{\partial w}{\partial y}\right)_{(x_o, y_o)}$ are obtained from Eq. (91) and (165), setting $x = x_o$ and $y = y_o$. Substituting

these expressions into Eq. (205) and using Eq. (199)-(202), the relations between the force and displacement projections of the plate spectral element are obtained. For example, the relations for forces F_1 , F_2 and moment M_3 are given by the following expressions:

$$\begin{aligned}
 \tilde{F}_{1_o} &= \frac{1}{2b} \left[k_{11}^c \left({}^1w_o^{p1} + \sum_{n=1}^M {}^1w_{S_n}^{p1} \cos \frac{n\pi y_o}{b} + \sum_{n=1}^M {}^1w_{A_n}^{p1} \sin \frac{(2n-1)\pi y_o}{b} \right) + \right. \\
 &\quad \left. + k_{17}^c \left({}^1w_o^{p2} + \sum_{n=1}^M {}^1w_{S_n}^{p2} \cos \frac{n\pi y_o}{b} + \sum_{n=1}^M {}^1w_{A_n}^{p2} \sin \frac{(2n-1)\pi y_o}{b} \right) \right] \\
 \tilde{F}_{1_m}^S &= \frac{1}{b} \cos \frac{m\pi y_o}{b} \left[k_{11}^c \left({}^1w_o^{p1} + \sum_{n=1}^M {}^1w_{S_n}^{p1} \cos \frac{n\pi y_o}{b} + \sum_{n=1}^M {}^1w_{A_n}^{p1} \sin \frac{(2n-1)\pi y_o}{b} \right) + \right. \\
 &\quad \left. + k_{17}^c \left({}^1w_o^{p2} + \sum_{n=1}^M {}^1w_{S_n}^{p2} \cos \frac{n\pi y_o}{b} + \sum_{n=1}^M {}^1w_{A_n}^{p2} \sin \frac{(2n-1)\pi y_o}{b} \right) \right] \\
 \tilde{F}_{1_m}^A &= \frac{1}{b} \sin \frac{(2m-1)\pi y_o}{b} \left[k_{11}^c \left({}^1w_o^{p1} + \sum_{n=1}^M {}^1w_{S_n}^{p1} \cos \frac{n\pi y_o}{b} + \sum_{n=1}^M {}^1w_{A_n}^{p1} \sin \frac{(2n-1)\pi y_o}{b} \right) + \right. \\
 &\quad \left. + k_{17}^c \left({}^1w_o^{p2} + \sum_{n=1}^M {}^1w_{S_n}^{p2} \cos \frac{n\pi y_o}{b} + \sum_{n=1}^M {}^1w_{A_n}^{p2} \sin \frac{(2n-1)\pi y_o}{b} \right) \right]
 \end{aligned} \tag{207}$$

$$\begin{aligned}
 \tilde{F}_{2_o} &= \frac{1}{2b} \left[k_{22}^c \left({}^1u_o^{p1} + \sum_{n=1}^M {}^1u_{S_n}^{p1} \cos \frac{n\pi y_o}{b} + \sum_{n=1}^M {}^1u_{A_n}^{p1} \sin \frac{(2n-1)\pi y_o}{2b} \right) + \right. \\
 &+ k_{26}^c \left({}^1 \left(\frac{\partial w}{\partial x} \right)_o^{p1} + \sum_{n=1}^M {}^1 \left(\frac{\partial w}{\partial x} \right)_{S_n}^{p1} \cos \frac{n\pi y_o}{b} + \sum_{n=1}^M {}^1 \left(\frac{\partial w}{\partial x} \right)_{A_n}^{p1} \sin \frac{(2n-1)\pi y_o}{2b} \right) + \\
 &+ k_{28}^c \left({}^1u_o^{p2} + \sum_{n=1}^M {}^1u_{S_n}^{p2} \cos \frac{n\pi y_o}{b} + \sum_{n=1}^M {}^1u_{A_n}^{p2} \sin \frac{(2n-1)\pi y_o}{2b} \right) + \\
 &\left. + k_{2,12}^c \left({}^1 \left(\frac{\partial w}{\partial x} \right)_o^{p2} + \sum_{n=1}^M {}^1 \left(\frac{\partial w}{\partial x} \right)_{S_n}^{p2} \cos \frac{n\pi y_o}{b} + \sum_{n=1}^M {}^1 \left(\frac{\partial w}{\partial x} \right)_{A_n}^{p2} \sin \frac{(2n-1)\pi y_o}{2b} \right) \right] \\
 \\
 \tilde{F}_{2_m}^S &= \frac{1}{b} \cos \frac{m\pi y_o}{b} \left[k_{22}^c \left({}^1u_o^{p1} + \sum_{n=1}^M {}^1u_{S_n}^{p1} \cos \frac{n\pi y_o}{b} + \sum_{n=1}^M {}^1u_{A_n}^{p1} \sin \frac{(2n-1)\pi y_o}{2b} \right) + \right. \\
 &+ k_{26}^c \left({}^1 \left(\frac{\partial w}{\partial x} \right)_o^{p1} + \sum_{n=1}^M {}^1 \left(\frac{\partial w}{\partial x} \right)_{S_n}^{p1} \cos \frac{n\pi y_o}{b} + \sum_{n=1}^M {}^1 \left(\frac{\partial w}{\partial x} \right)_{A_n}^{p1} \sin \frac{(2n-1)\pi y_o}{2b} \right) + \\
 &+ k_{28}^c \left({}^1u_o^{p2} + \sum_{n=1}^M {}^1u_{S_n}^{p2} \cos \frac{n\pi y_o}{b} + \sum_{n=1}^M {}^1u_{A_n}^{p2} \sin \frac{(2n-1)\pi y_o}{2b} \right) + \\
 &\left. + k_{2,12}^c \left({}^1 \left(\frac{\partial w}{\partial x} \right)_o^{p2} + \sum_{n=1}^M {}^1 \left(\frac{\partial w}{\partial x} \right)_{S_n}^{p2} \cos \frac{n\pi y_o}{b} + \sum_{n=1}^M {}^1 \left(\frac{\partial w}{\partial x} \right)_{A_n}^{p2} \sin \frac{(2n-1)\pi y_o}{2b} \right) \right] \quad (208) \\
 \\
 \tilde{F}_{2_m}^A &= \frac{1}{b} \sin \frac{(2m-1)\pi y_o}{2b} \left[k_{22}^c \left({}^1u_o^{p1} + \sum_{n=1}^M {}^1u_{S_n}^{p1} \cos \frac{n\pi y_o}{b} + \sum_{n=1}^M {}^1u_{A_n}^{p1} \sin 2 \frac{(2n-1)\pi y_o}{b} \right) + \right. \\
 &+ k_{26}^c \left({}^1 \left(\frac{\partial w}{\partial x} \right)_o^{p1} + \sum_{n=1}^M {}^1 \left(\frac{\partial w}{\partial x} \right)_{S_n}^{p1} \cos \frac{n\pi y_o}{b} + \sum_{n=1}^M {}^1 \left(\frac{\partial w}{\partial x} \right)_{A_n}^{p1} \sin \frac{(2n-1)\pi y_o}{2b} \right) + \\
 &+ k_{28}^c \left({}^1u_o^{p2} + \sum_{n=1}^M {}^1u_{S_n}^{p2} \cos \frac{n\pi y_o}{b} + \sum_{n=1}^M {}^1u_{A_n}^{p2} \sin \frac{(2n-1)\pi y_o}{2b} \right) + \\
 &\left. + k_{2,12}^c \left({}^1 \left(\frac{\partial w}{\partial x} \right)_o^{p2} + \sum_{n=1}^M {}^1 \left(\frac{\partial w}{\partial x} \right)_{S_n}^{p2} \cos \frac{n\pi y_o}{b} + \sum_{n=1}^M {}^1 \left(\frac{\partial w}{\partial x} \right)_{A_n}^{p2} \sin \frac{(2n-1)\pi y_o}{2b} \right) \right]
 \end{aligned}$$

$$\begin{aligned}
 \tilde{M}_{3_o} = & \frac{1}{2a} \left[k_{11,3}^c \left(2v_o^{p1} + \sum_{n=1}^M 2v_{S_n}^{p1} \cos \frac{n\pi x_o}{a} + \sum_{n=1}^M 2v_{A_n}^{p1} \sin \frac{(2n-1)\pi x_o}{2a} \right) + \right. \\
 & + k_{11,5}^c \left(2 \left(\frac{\partial w}{\partial y} \right)_o^{p1} + \sum_{n=1}^M 2 \left(\frac{\partial w}{\partial y} \right)_{S_n}^{p1} \cos \frac{n\pi x_o}{a} + \sum_{n=1}^M 2 \left(\frac{\partial w}{\partial y} \right)_{A_n}^{p1} \sin \frac{(2n-1)\pi x_o}{2a} \right) + \\
 & + k_{11,9}^c \left(2v_o^{p2} + \sum_{n=1}^M 2v_{S_n}^{p2} \cos \frac{n\pi x_o}{a} + \sum_{n=1}^M 2v_{A_n}^{p2} \sin \frac{(2n-1)\pi x_o}{2a} \right) + \\
 & \left. + k_{11,11}^c \left(2 \left(\frac{\partial w}{\partial y} \right)_o^{p2} + \sum_{n=1}^M 2 \left(\frac{\partial w}{\partial y} \right)_{S_n}^{p2} \cos \frac{n\pi x_o}{a} + \sum_{n=1}^M 2 \left(\frac{\partial w}{\partial y} \right)_{A_n}^{p2} \sin \frac{(2n-1)\pi x_o}{2a} \right) \right] \\
 \tilde{M}_{3_m}^S = & \frac{1}{a} \cos \frac{m\pi x_o}{a} \left[k_{11,3}^c \left(2v_o^{p1} + \sum_{n=1}^M 2v_{S_n}^{p1} \cos \frac{n\pi x_o}{a} + \sum_{n=1}^M 2v_{A_n}^{p1} \sin \frac{(2n-1)\pi x_o}{2a} \right) + \right. \\
 & + k_{11,5}^c \left(2 \left(\frac{\partial w}{\partial y} \right)_o^{p1} + \sum_{n=1}^M 2 \left(\frac{\partial w}{\partial y} \right)_{S_n}^{p1} \cos \frac{n\pi x_o}{a} + \sum_{n=1}^M 2 \left(\frac{\partial w}{\partial y} \right)_{A_n}^{p1} \sin \frac{(2n-1)\pi x_o}{2a} \right) + \\
 & + k_{11,9}^c \left(2v_o^{p2} + \sum_{n=1}^M 2v_{S_n}^{p2} \cos \frac{n\pi x_o}{a} + \sum_{n=1}^M 2v_{A_n}^{p2} \sin \frac{(2n-1)\pi x_o}{2a} \right) + \\
 & \left. + k_{11,11}^c \left(2 \left(\frac{\partial w}{\partial y} \right)_o^{p2} + \sum_{n=1}^M 2 \left(\frac{\partial w}{\partial y} \right)_{S_n}^{p2} \cos \frac{n\pi x_o}{a} + \sum_{n=1}^M 2 \left(\frac{\partial w}{\partial y} \right)_{A_n}^{p2} \sin \frac{(2n-1)\pi x_o}{2a} \right) \right] \tag{209}
 \end{aligned}$$

$$\begin{aligned}
 \tilde{M}_{3_m}^A = & \frac{1}{a} \sin \frac{(2m-1)\pi x_o}{2a} \left[k_{11,3}^c \left(2v_o^{p1} + \sum_{n=1}^M 2v_{S_n}^{p1} \cos \frac{n\pi x_o}{a} + \sum_{n=1}^M 2v_{A_n}^{p1} \sin \frac{(2n-1)\pi x_o}{2a} \right) + \right. \\
 & + k_{11,5}^c \left(2 \left(\frac{\partial w}{\partial y} \right)_o^{p1} + \sum_{n=1}^M 2 \left(\frac{\partial w}{\partial y} \right)_{S_n}^{p1} \cos \frac{n\pi x_o}{a} + \sum_{n=1}^M 2 \left(\frac{\partial w}{\partial y} \right)_{A_n}^{p1} \sin \frac{(2n-1)\pi x_o}{2a} \right) + \\
 & + k_{11,9}^c \left(2v_o^{p2} + \sum_{n=1}^M 2v_{S_n}^{p2} \cos \frac{n\pi x_o}{a} + \sum_{n=1}^M 2v_{A_n}^{p2} \sin \frac{(2n-1)\pi x_o}{2a} \right) + \\
 & \left. + k_{11,11}^c \left(2 \left(\frac{\partial w}{\partial y} \right)_o^{p2} + \sum_{n=1}^M 2 \left(\frac{\partial w}{\partial y} \right)_{S_n}^{p2} \cos \frac{n\pi x_o}{a} + \sum_{n=1}^M 2 \left(\frac{\partial w}{\partial y} \right)_{A_n}^{p2} \sin \frac{(2n-1)\pi x_o}{2a} \right) \right]
 \end{aligned}$$

where ${}^j u_{S_n}^{pi}$, ${}^j u_{A_n}^{pi}$, ..., $\left(\frac{\partial w}{\partial y} \right)_{S_n}^{pi}$, $\left(\frac{\partial w}{\partial y} \right)_{A_n}^{pi}$, $i = 1, 2$ are the corresponding components

of the projection vectors $\tilde{\mathbf{q}}^t$ and $\tilde{\mathbf{q}}^i$ for transverse and in-plane vibration, respectively

defined by Eq. (92) and (166). Similar expressions can be developed for the other components of the column force vector and the following relation is obtained:

$$\tilde{\mathbf{Q}}^c = \mathbf{K}_D^c \tilde{\mathbf{q}}, \quad (210)$$

$$\tilde{\mathbf{Q}}^{cT} = \begin{bmatrix} \tilde{F}_{1_m}^S & \tilde{F}_{1_m}^A & \dots & \tilde{M}_{1_m}^S & \tilde{M}_{1_m}^A \end{bmatrix}, \quad \tilde{\mathbf{q}} = \begin{bmatrix} \tilde{\mathbf{q}}^t \\ \tilde{\mathbf{q}}^i \end{bmatrix}, \quad (211)$$

where \mathbf{K}_D^c is the modified dynamic stiffness matrix of the column member, $\tilde{\mathbf{Q}}^c$ is the modified force vector of the column and $\tilde{\mathbf{q}}$ is the displacement vector of plate element. Setting the equilibrium equations for each edge of the plate assemblies (Figure 20b), the dynamic stiffness matrix \mathbf{K}_D^c is superimposed to the global dynamic stiffness matrix of the plate spectral element \mathbf{K}_D^p , which comprises the transverse and in-plane vibration:

$$\mathbf{K}_D = \mathbf{K}_D^p + \mathbf{K}_D^c = \begin{bmatrix} \mathbf{K}_D^t & 0 \\ 0 & \mathbf{K}_D^i \end{bmatrix} + \mathbf{K}_D^c. \quad (212)$$

3.3 Numerical examples

Validation of the spectral element coupling presented in the previous section will be carried out on several numerical examples. The results will be compared with the results obtained using the FEM software SAP2000.

3.3.1. Transverse free vibrations of completely free square plate with edge beams

Consider a square plate with a span-to-thickness ratio of 20, with edge beams of rectangular cross section with a depth-to-width ratio of 5/3. The beam's width equals the plate thickness. Both plate and beams are made of the same isotropic material whose Poisson's ratio is 0.15. The first eight natural frequencies have been computed using the SEM for different number of terms – M in the general solution. The results are compared with the results obtained using the FEM software SAP2000 for several mesh sizes. Dimensionless frequencies $\lambda^2 = \omega a^2 \sqrt{\frac{\rho h}{D}}$ are given in Table 9. The first four mode shapes have been presented in Figure 21. It can be seen that the SEM results

rapidly converge. Also, the agreement between the SEM and FEM results is quite satisfactory.

Table 9. Dimensionless frequencies λ^2 of square plate with edge beams for transverse vibration

Mode No.	SEM			SAP2000		
	M=3	M=5	M=10	Mesh size		
				10x10	20x20	40x40
1	3.1	3.0	3.0	2.9	2.9	2.9
2	4.8	4.8	4.8	4.7	4.7	4.7
3	5.3	5.3	5.3	5.2	5.3	5.3
4*	8.4	8.4	8.4	8.0	8.2	8.2
5*	14.0	14.0	14.0	13.7	14.0	14.0
6	15.1	15.1	15.0	14.1	14.5	14.6
7	17.9	17.8	17.7	17.2	17.6	17.6
8	18.5	18.6	18.5	17.9	18.4	18.4

* Double frequency due to symmetry

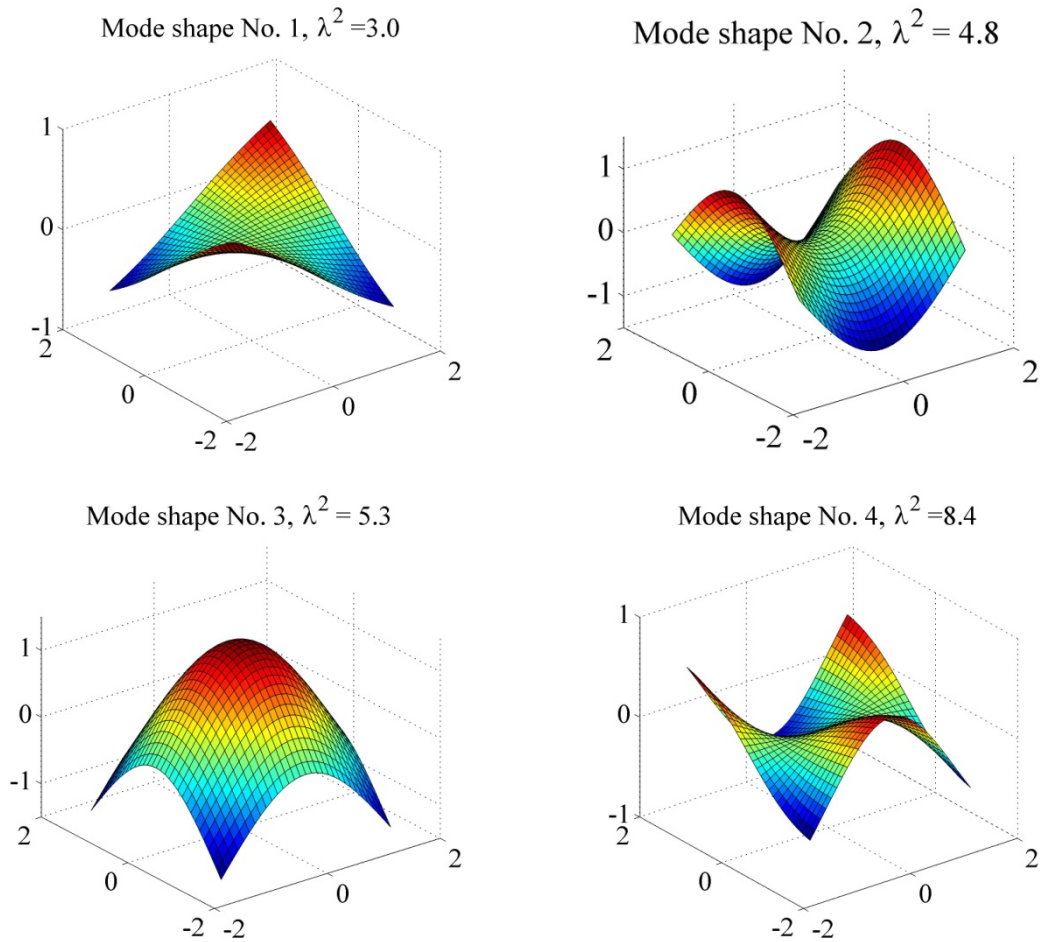


Figure 21. First four transverse mode shapes of completely free square plate with edge beams

3.2.2. In-plane free vibrations of completely free square plate with edge beams

The dimensionless frequencies $\lambda^2 = \omega a \sqrt{\frac{\rho h}{D_1}}$ of square plate having the same geometrical and material properties as in the previous example are given in Table 10. The first four mode shapes have been presented in Figure 22. Again, an excellent agreement is obtained between the SEM and FEM results.

Table 10. Dimensionless frequencies λ^2 of square plate with edge beams for in-plane vibration

Mode No.	SEM			SAP2000		
	M=3	M=5	M=10	Mesh size		
				10x10	20x20	40x40
1	1.09	1.09	1.09	1.09	1.09	1.09
2*	1.17	1.17	1.17	1.15	1.16	1.16
3	1.25	1.25	1.25	1.23	1.24	1.24
4	1.44	1.43	1.43	1.39	1.41	1.42
5	1.45	1.45	1.45	1.44	1.45	1.45
6*	1.74	1.74	1.73	1.70	1.72	1.73
7	2.10	2.08	2.07	1.96	2.02	2.04
8	2.28	2.28	2.28	2.23	2.27	2.28
9*	2.37	2.36	2.36	2.26	2.32	2.34
10	2.41	2.39	2.39	2.34	2.37	2.38

* Double frequency due to symmetry

3.3.3 Free vibrations of column supported square plate

A square plate having the same properties as in the previous examples is supported at its corners by columns of rectangular cross section with width-to-depth ratio of 1. Column width-to-plate thickness ratio equals 2. The plate and the columns are made of the same isotropic material ($E = 30GPa$, $\nu = 0.15$, $\rho = 2.5 t/m^3$). The first ten natural frequencies are calculated using the SEM and FEM software SAP2000. The results are given in Table 11, and first three mode shapes are presented in Figure 23. In this case, more terms in the general solution – M are required in order to obtain accurate natural frequencies.

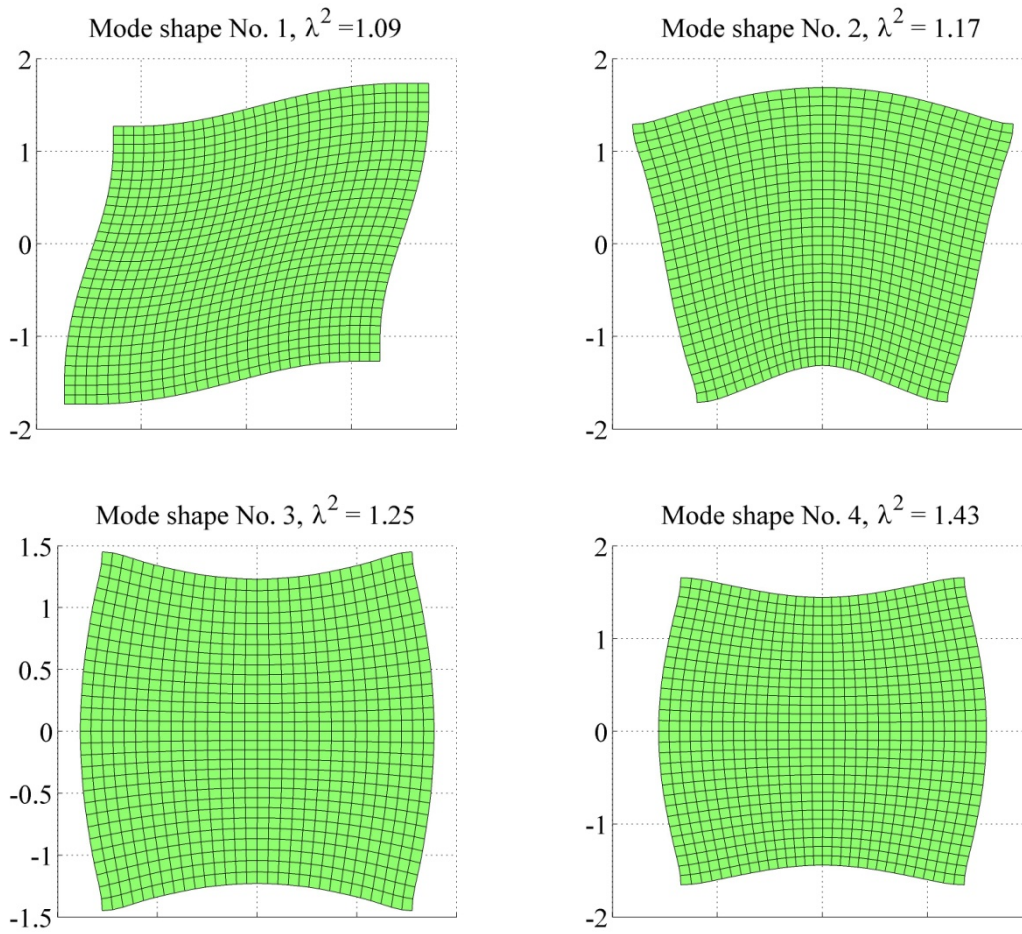


Figure 22. First four in-plane mode shapes of completely free plate with edge beams

Table 11. Natural frequencies (in Hz) of column supported square plate

Mode No.	SEM			SAP2000		
	M=5	M=10	M=15	Mesh size		
	10x10	20x20	40x40			
1	9.4*	9.1*	8.9*	9.0*	8.8*	8.7*
2	16.2	13.7	13.1	13.3	13.2	13.0
3	25.4	24.1	23.6	24.4	23.6	23.0
4	51.7*	49.9*	49.1*	51.7*	50.9*	50.1*
5	65.2	64.3	63.8	64.1	64.4	64.0
6	81.9	80.8	80.2	83.6	83.1	82.35
7	83.9*	83.0*	82.5*	84.4*	83.3*	82.4*
8	87.1	85.5	84.8	84.7	83.5	82.8
9	87.9	85.9	85.1	84.9	84.0	83.5
10	90.4*	89.1*	88.5*	88.2*	87.5*	86.9*

* Double frequency due to symmetry

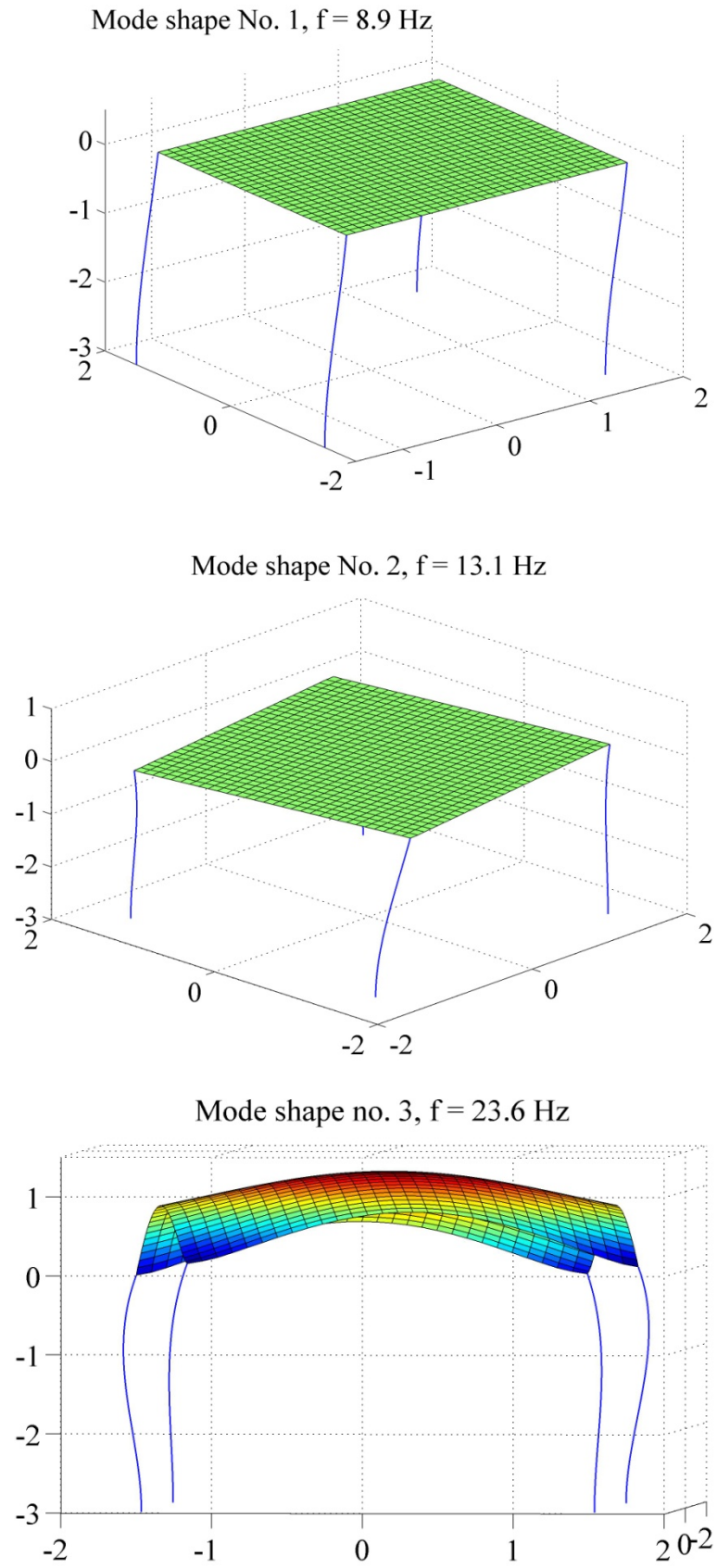


Figure 23. Mode shapes of column supported square plate

3.3.4 Transverse vibration of corner-supported square plate with edge beams

Dimensionless natural frequencies of square plate with edge beams with point supports in the plate corners are given in Table 12, exploiting the SEM and FEM (SAP2000 1996). In the SEM point supports in the plate corners have been modeled as columns having very large axial stiffness, very small bending stiffness about two principal axes and no mass. The first columns of Table 12 for the SEM and FEM correspond to the case when lateral, rotational and inertial effects of the edge beams have been taken into account, while the second columns correspond to the situation when inertial effects of edge beams have been neglected. It can be concluded that inertia effects of edge beams are very small in the first mode vibration, and become more significant in higher modes of vibration.

Verification of the proposed spectral element coupling has been demonstrated in Figure 24. Dimensionless frequency λ^2 of the first antisymmetric vibration mode has been plotted against the beam lateral stiffness-to-plate stiffness ratio (Figure 24a) and against both the lateral and rotational beam stiffness (Figure 24b). Inertia effects of the beam have been neglected. In both cases the lower frequency limit is 9.97, which is the dimensionless frequency of the point corner-supported plate. The upper frequency limit is equal 19.70 and 27.05 for the case when rotational beam stiffness is neglected and when it is equal to the lateral beam stiffness, respectively. These limit values correspond to the dimensionless frequencies of the simply supported and clamped square plate, respectively.

Table 12. Dimensionless frequencies λ^2 of corner-supported square plate with edge beams

Mode No.	SEM ($M = 15$)		SAP2000	
	$\rho_{beam} \neq 0$	$\rho_{beam} = 0$	$\rho_{beam} \neq 0$	$\rho_{beam} = 0$
1	2.2	2.3	2.2	2.3
2	4.6*	5.4*	4.4*	5.3*
3	4.8	6.5	4.8	6.5
4	10.7	13.1	10.4	12.8
5	12.2	13.4	11.9	13.1
6	13.1*	16.9*	13.1*	16.8*
7	17.7	23.6	17.8	23.2
8	20.1*	25.5*	19.7*	25.5*

* Double frequency due to symmetry

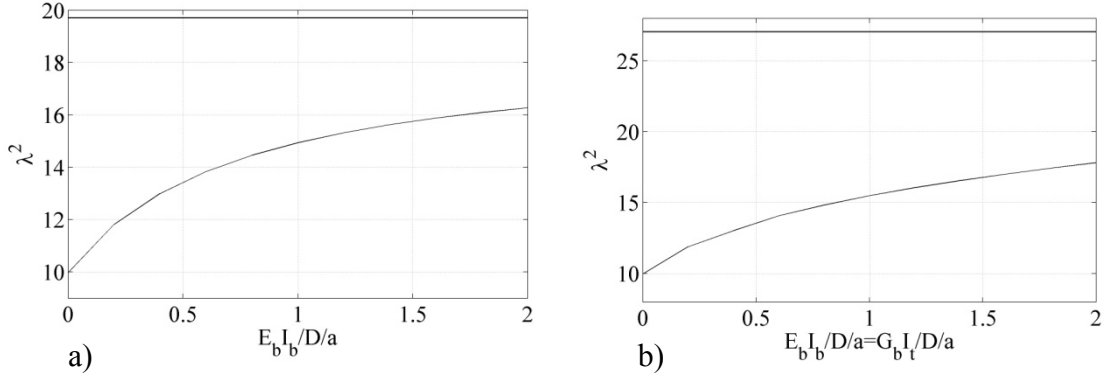


Figure 24. First antisymmetric dimensionless frequency vs. beam stiffness-to-plate stiffness ratio: a) $G_b I_t = 0$, b) $G_b I_t = E_b I_b$

4. Soil-structure interaction

In this section the coupling between the structure and the soil will be shown. It is assumed that the structure is founded on rigid surface foundations resting on homogeneous, isotropic and elastic horizontally layered half-space. The dynamic stiffness matrix of the soil will be calculated using the ITM.

4.1 Soil modeling

4.1.1 Equations of motion

The equations of motion of the infinitesimal volume of soil continuum, neglecting the body forces are given by:

$$\sigma_{ij,j} = \rho \ddot{u}_i, \quad (i = x, y, z) \quad (213)$$

where σ_{ij} are the components of the stress tensor, u_i are the components of the displacement vector \mathbf{u} , and ρ is the soil density. Using the constitutive relations for linear elastic isotropic material and kinematic relations, respectively:

$$\sigma_{ij} = \lambda \delta_{ij} \varepsilon_{kk} + 2\mu \varepsilon_{ij}, \quad (214)$$

$$\varepsilon_{ij} = \frac{1}{2} (u_{i,j} + u_{j,i}), \quad (215)$$

where ε_{ij} are the components of the deformation tensor, δ_{ij} is the Kronecker delta and λ and μ are Lamé constants, Eq. (213) become:

$$(\lambda + \mu) u_{k,ki} + \mu u_{i,kk} = \rho \ddot{u}_i. \quad (216)$$

Eq. (216) consists of three coupled differential equations with second-order derivatives in both space and time, which can be decoupled using Helmholtz's decomposition:

$$u_i = \Phi_{,i} + \varepsilon_{ijk} \Psi_{k,j}, \quad (217)$$

where $\Phi = \Phi(x, y, z, t)$ and $\Psi^T = [\Psi_x \quad \Psi_y \quad \Psi_z]^T$ are the potential functions. Since three displacement components are represented by four potential functions, additional condition which uniquely determines Ψ_i has to be satisfied:

$$\Psi_{i,i} = 0. \quad (218)$$

Substituting Eq. (217) into Eq. (216) gives two uncoupled differential equations:

$$\nabla^2 \Phi - \frac{1}{c_p^2} \ddot{\Phi} = 0, \quad (219)$$

$$\nabla^2 \Psi_i - \frac{1}{c_s^2} \ddot{\Psi}_i = 0, \quad (220)$$

where $\nabla^2 = \frac{\partial^2}{\partial x^2} + \frac{\partial^2}{\partial y^2} + \frac{\partial^2}{\partial z^2}$ and

$$c_p = \sqrt{\frac{\lambda + 2\mu}{\rho}}, \quad c_s = \sqrt{\frac{\mu}{\rho}}, \quad (221)$$

are the longitudinal and shear wave velocity, respectively. Introducing spectral representation of potential functions:

$$\begin{aligned} \Phi(x, y, z, t) &= \hat{\Phi}(k_x, k_y, z, \omega) e^{-ik_x x} e^{-ik_y y} e^{-i\omega t} \\ \Psi_i(x, y, z, t) &= \hat{\Psi}_i(k_x, k_y, z, \omega) e^{-ik_x x} e^{-ik_y y} e^{-i\omega t}, \end{aligned} \quad (222)$$

a threefold Fourier transformation $x \Leftrightarrow k_x$, $y \Leftrightarrow k_y$, $t \Leftrightarrow \omega$ of Eq. (219) and (220) gives the following equations:

$$\begin{aligned} (k_p^2 - k_x^2 - k_y^2) \hat{\Phi} + \frac{\partial^2 \hat{\Phi}}{\partial z^2} &= 0 \\ (k_s^2 - k_x^2 - k_y^2) \hat{\Psi}_i + \frac{\partial^2 \hat{\Psi}_i}{\partial z^2} &= 0 \end{aligned}, \quad (223)$$

where $k_p = \frac{\omega}{c_p}$ and $k_s = \frac{\omega}{c_s}$ are the wave numbers. Solutions of the above equations are given by:

$$\begin{aligned}\hat{\Phi} &= C_1 e^{\lambda_1 z} + C_2 e^{-\lambda_1 z} \\ \hat{\Psi}_i &= D_{1i} e^{\lambda_2 z} + D_{2i} e^{-\lambda_2 z},\end{aligned}\quad (224)$$

where C_1, C_2, D_{1i} and D_{2i} are integration constants ($i = x, y, z$) and

$$\begin{aligned}\lambda_1^2 &= k_x^2 + k_y^2 - k_p^2 \\ \lambda_2^2 &= k_x^2 + k_y^2 - k_s^2.\end{aligned}\quad (225)$$

Substituting Eq. (224) into Eq. (217) and using additional condition (218) gives

$$\begin{bmatrix} \hat{u} \\ \hat{v} \\ \hat{w} \end{bmatrix} = \begin{bmatrix} -ik_x e^{\lambda_1 z} & -ik_x e^{-\lambda_1 z} & \frac{k_x k_y}{\lambda_2} e^{\lambda_2 z} & -\frac{k_x k_y}{\lambda_2} e^{-\lambda_2 z} & \left(\frac{k_y^2}{\lambda_2} - \lambda_2\right) e^{\lambda_2 z} & -\left(\frac{k_y^2}{\lambda_2} - \lambda_2\right) e^{-\lambda_2 z} \\ -ik_y e^{\lambda_1 z} & -ik_y e^{-\lambda_1 z} & -\left(\frac{k_x^2}{\lambda_2} - \lambda_2\right) e^{\lambda_2 z} & \left(\frac{k_x^2}{\lambda_2} - \lambda_2\right) e^{-\lambda_2 z} & -\frac{k_x k_y}{\lambda_2} e^{\lambda_2 z} & \frac{k_x k_y}{\lambda_2} e^{-\lambda_2 z} \\ \lambda_1 e^{\lambda_1 z} & \lambda_1 e^{-\lambda_1 z} & ik_y e^{\lambda_2 z} & ik_y e^{-\lambda_2 z} & -ik_x e^{\lambda_2 z} & -ik_x e^{-\lambda_2 z} \end{bmatrix} \begin{bmatrix} C_1 \\ C_2 \\ D_{1x} \\ D_{2x} \\ D_{1y} \\ D_{2y} \end{bmatrix}. \quad (226)$$

4.1.2 Dynamic stiffness matrix of a single soil layer

A horizontal soil layer of thickness h with stress and displacement vectors at the boundaries is given in Figure 25a. The relation between the displacement vector $\hat{\mathbf{q}}_e^T = [\hat{u}_1 \quad \hat{v}_1 \quad \hat{w}_1 \quad \hat{u}_2 \quad \hat{v}_2 \quad \hat{w}_2]$ and the force vector $\hat{\mathbf{P}}_e^T = [\hat{P}_1 \quad \hat{P}_2 \quad \hat{P}_3 \quad \hat{P}_4 \quad \hat{P}_5 \quad \hat{P}_6]$

is given through the dynamic stiffness matrix $\hat{\mathbf{K}}_D^e$:

$$\hat{\mathbf{P}}_e = \hat{\mathbf{K}}_D^e \hat{\mathbf{q}}_e. \quad (227)$$

The dynamic stiffness matrix of soil layer is obtained similarly as dynamic stiffness matrices of beam spectral element:

$$\hat{\mathbf{K}}_D^e = \hat{\mathbf{D}}^{-1} \hat{\mathbf{F}}, \quad (228)$$

where $\hat{\mathbf{D}}$ is matrix which relates the displacement vector $\hat{\mathbf{q}}_e$ and vector of integration constants \mathbf{C} , while $\hat{\mathbf{F}}$ is matrix which relates the stress vector $\hat{\mathbf{P}}_e$ and vector \mathbf{C} .

Applying the boundary conditions:

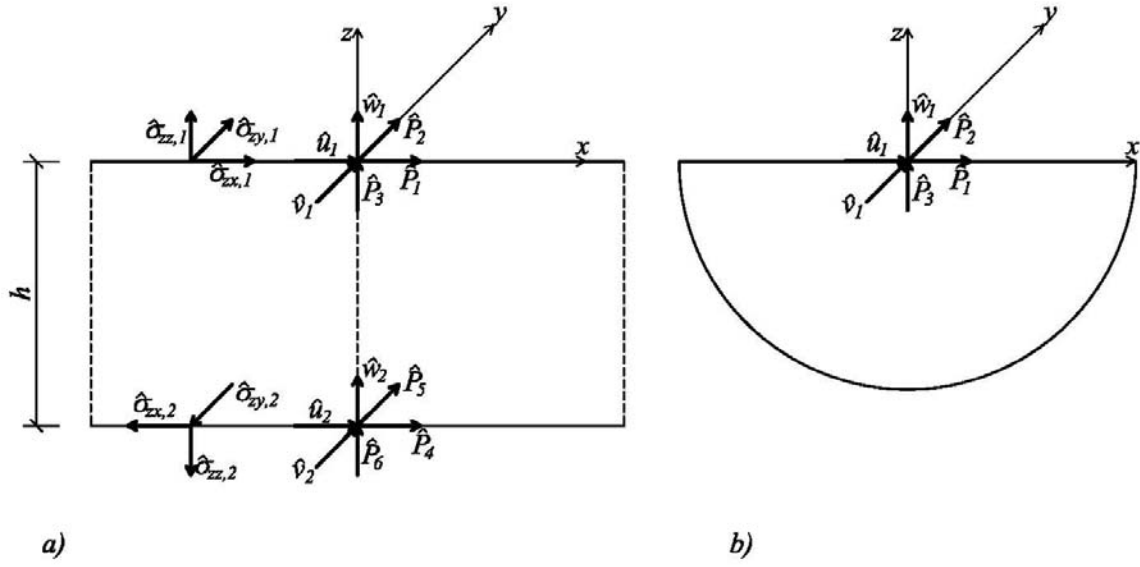


Figure 25. Displacements and stresses at the boundaries of: a) layer element, b) half-space element

$$\begin{aligned} \hat{u}_1 &= \hat{u}(0) & \hat{v}_1 &= \hat{v}(0) & \hat{w}_1 &= \hat{w}(0) \\ \hat{u}_2 &= \hat{u}(-h) & \hat{v}_2 &= \hat{v}(-h) & \hat{w}_2 &= \hat{w}(-h) \end{aligned} \quad (229)$$

matrix $\hat{\mathbf{D}}$ is obtained directly from Eq. (226):

$$\hat{\mathbf{D}} = \begin{bmatrix} -ik_x & -ik_x & \frac{k_x k_y}{\lambda_2} & -\frac{k_x k_y}{\lambda_2} & \frac{k_s^2 - k_x^2}{\lambda_2} & -\frac{k_s^2 - k_x^2}{\lambda_2} \\ -ik_y & -ik_y & -\frac{k_s^2 - k_y^2}{\lambda_2} & \frac{k_s^2 - k_y^2}{\lambda_2} & -\frac{k_x k_y}{\lambda_2} & \frac{k_x k_y}{\lambda_2} \\ \lambda_1 & -\lambda_1 & ik_y & ik_y & -ik_x & -ik_x \\ -ik_x e_1 & -ik_x e_2 & \frac{k_x k_y}{\lambda_2} e_3 & -\frac{k_x k_y}{\lambda_2} e_4 & \frac{k_s^2 - k_x^2}{\lambda_2} e_3 & -\frac{k_s^2 - k_x^2}{\lambda_2} e_4 \\ -ik_y e_1 & -ik_y e_2 & -\frac{k_s^2 - k_y^2}{\lambda_2} e_3 & \frac{k_s^2 - k_y^2}{\lambda_2} e_4 & -\frac{k_x k_y}{\lambda_2} e_3 & \frac{k_x k_y}{\lambda_2} e_4 \\ \lambda_1 e_1 & -\lambda_1 e_2 & ik_y e_3 & ik_y e_4 & -ik_x e_3 & -ik_x e_4 \end{bmatrix} \quad (230)$$

The elements of matrix $\hat{\mathbf{F}}$ are obtained using kinematic and constitutive relations (215) and (216) and setting:

$$\begin{aligned} \hat{P}_1 &= \hat{\sigma}_{xx}(0) & \hat{P}_2 &= \hat{\sigma}_{zy}(0) & \hat{P}_3 &= \hat{\sigma}_{zz}(0) \\ \hat{P}_4 &= -\hat{\sigma}_{xx}(-h) & \hat{P}_5 &= -\hat{\sigma}_{zy}(-h) & \hat{P}_6 &= -\hat{\sigma}_{zz}(-h) \end{aligned} \quad (231)$$

in the following form:

$$\hat{\mathbf{F}} = \begin{bmatrix} -2ik_x\lambda_1\mu & 2ik_x\lambda_1\mu & 2\mu k_x k_y & 2\mu k_x k_y & \mu(k_s^2 - 2k_x^2) & \mu(k_s^2 - 2k_x^2) \\ -2ik_y\lambda_1\mu & 2ik_y\lambda_1\mu & -\mu(k_s^2 - 2k_y^2) & -\mu(k_s^2 - 2k_y^2) & -2\mu k_x k_y & -2\mu k_x k_y \\ -\lambda k_p^2 + 2\mu\lambda_1^2 & -\lambda k_p^2 + 2\mu\lambda_1^2 & 2ik_y\lambda_2\mu & -2ik_y\lambda_2\mu & -2ik_x\lambda_2\mu & 2ik_x\lambda_2\mu \\ -2ik_x\lambda_1\mu e_1 & 2ik_x\lambda_1\mu e_2 & 2\mu k_x k_y e_3 & 2\mu k_x k_y e_4 & \mu(k_s^2 - 2k_x^2)e_3 & \mu(k_s^2 - 2k_x^2)e_4 \\ -2ik_y\lambda_1\mu e_1 & 2ik_y\lambda_1\mu e_2 & -\mu(k_s^2 - 2k_y^2)e_3 & -\mu(k_s^2 - 2k_y^2)e_4 & -2\mu k_x k_y e_3 & -2\mu k_x k_y e_4 \\ (-\lambda k_p^2 + 2\mu\lambda_1^2)e_1 & (-\lambda k_p^2 + 2\mu\lambda_1^2)e_2 & 2ik_y\lambda_2\mu e_3 & -2ik_y\lambda_2\mu e_4 & -2ik_x\lambda_2\mu e_3 & 2ik_x\lambda_2\mu e_4 \end{bmatrix} \quad (232)$$

where $e_1 = e^{-\lambda_1 h}$, $e_2 = e^{\lambda_1 h}$, $e_3 = e^{-\lambda_2 h}$, $e_4 = e^{\lambda_2 h}$.

The dynamic stiffness matrix $\hat{\mathbf{K}}_D^e$ is obtained from the exact solutions of the equations of motion in the transformed wave number-frequency domain. As the wave propagation is treated exactly, there is no need to divide homogeneous layers into multiple layer elements in order to obtain appropriate solution.

For a half-space element presented in Figure 25b only outgoing waves exist, so the solutions of Eq. (223) become:

$$\begin{aligned} \hat{\Phi} &= C_2 e^{-\lambda_1 z} \\ \hat{\Psi}_i &= D_{2i} e^{-\lambda_2 z} \end{aligned} \quad (233)$$

The displacement vector in this case is $\hat{\mathbf{q}}_e^T = [\hat{u}_1 \quad \hat{v}_1 \quad \hat{w}_1]$ and the corresponding force vector $\hat{\mathbf{P}}_e^T = [\hat{P}_1 \quad \hat{P}_2 \quad \hat{P}_3]$. Matrices $\hat{\mathbf{D}}$ and $\hat{\mathbf{F}}$ are given by:

$$\hat{\mathbf{D}} = \begin{bmatrix} -ik_x & \frac{k_x k_y}{\lambda_2} & \frac{k_s^2 - k_x^2}{\lambda_2} \\ -ik_y & \frac{k_y^2 - k_s^2}{\lambda_2} & -\frac{k_x k_y}{\lambda_2} \\ \lambda_1 & ik_y & -ik_x \end{bmatrix}, \quad (234)$$

$$\hat{\mathbf{F}} = \begin{bmatrix} -2ik_x\lambda_1\mu & 2\mu k_x k_y & \mu(k_s^2 - 2k_x^2) \\ -2ik_y\lambda_1\mu & -\mu(k_s^2 - 2k_y^2) & -2\mu k_x k_y \\ -\lambda k_p^2 + 2\mu\lambda_1^2 & 2\mu ik_y\lambda_2 & -2\mu ik_x\lambda_2 \end{bmatrix}. \quad (235)$$

4.2 Equations of motion of soil-structure system

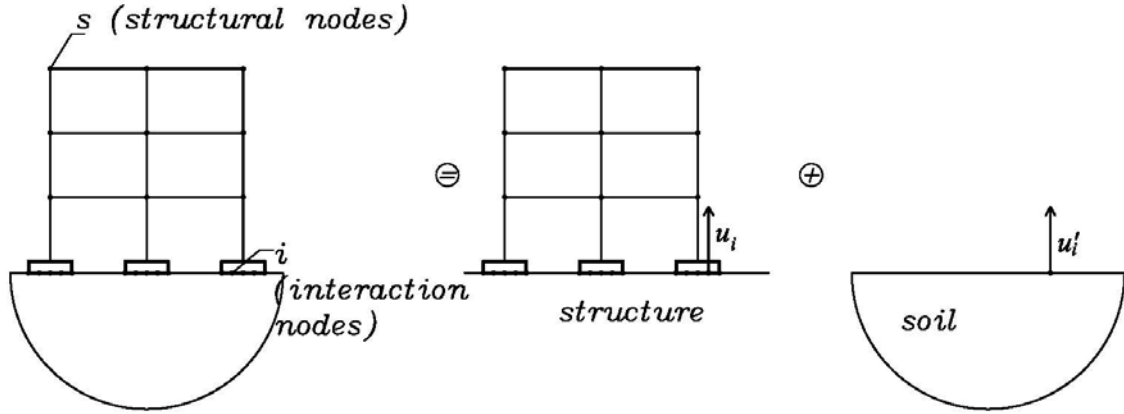


Figure 27. Soil-structure system

Soil-structure model consists of two sub-structures, the structure and the soil, described in Figure 27. Nodes at the soil-structure interface are defined as interaction nodes (i), while remaining nodes of the structure are defined as structural nodes (s). Partitioning the dynamic stiffness matrix of the structure correspondingly, the equations of motion can be written as:

$$\begin{bmatrix} \mathbf{K}_{ss}^s & \mathbf{K}_{si}^s \\ \mathbf{K}_{is}^s & \mathbf{K}_{ii}^s \end{bmatrix} \begin{bmatrix} \mathbf{u}_s \\ \mathbf{u}_i \end{bmatrix} = \begin{bmatrix} \mathbf{P}_s \\ \mathbf{P}_i^s \end{bmatrix}. \quad (237)$$

At the interaction nodes the sum of forces stemming from the soil and from the structure must be zero:

$$\begin{aligned} \mathbf{P}_i^s + \mathbf{P}_i^F &= 0 \\ \mathbf{P}_i^F &= \mathbf{K}_{ii}^F (\mathbf{u}_i - \mathbf{u}_i') \\ \mathbf{K}_{is}^s \mathbf{u}_s + \mathbf{K}_{ii}^s \mathbf{u}_i + \mathbf{K}_{ii}^F (\mathbf{u}_i - \mathbf{u}_i') &= 0 \end{aligned}, \quad (238)$$

where \mathbf{u}_i' is the free-field motion at the interface (the known wave field without the structure), \mathbf{K}_{ii}^F is the dynamic stiffness matrix of the soil – foundation interface, \mathbf{P}_i^s and \mathbf{P}_i^F are the force vectors acting in the structural and interaction nodes, respectively.

From Eq. (237) and (238) the following system of equations of the soil-structure system is obtained:

$$\begin{bmatrix} \mathbf{K}_{ss}^s & \mathbf{K}_{si}^s \\ \mathbf{K}_{is}^s & \mathbf{K}_{ii}^s + \mathbf{K}_{ii}^F \end{bmatrix} \begin{bmatrix} \mathbf{u}_s \\ \mathbf{u}_i \end{bmatrix} = \begin{bmatrix} \mathbf{P}_s \\ \mathbf{K}_{ii}^F \mathbf{u}_i' \end{bmatrix}. \quad (239)$$

4.3 Dynamic stiffness matrix for flexible foundations

The dynamic stiffness matrix \mathbf{K}_{ii}^F of the soil – foundation interface is obtained inverting the corresponding flexibility matrix \mathbf{F}_{ii}^F . Determination of the flexibility matrix \mathbf{F}_{ii}^F corresponds to the calculation of the displacements of the horizontally layered soil subjected to unit harmonic point force at the interaction nodes. The elements of the flexibility matrix are calculated using the ITM. If n is a number of interaction nodes, the size of the flexibility matrix is $3n \times 3n$.

4.4 Dynamic stiffness matrix for rigid foundations

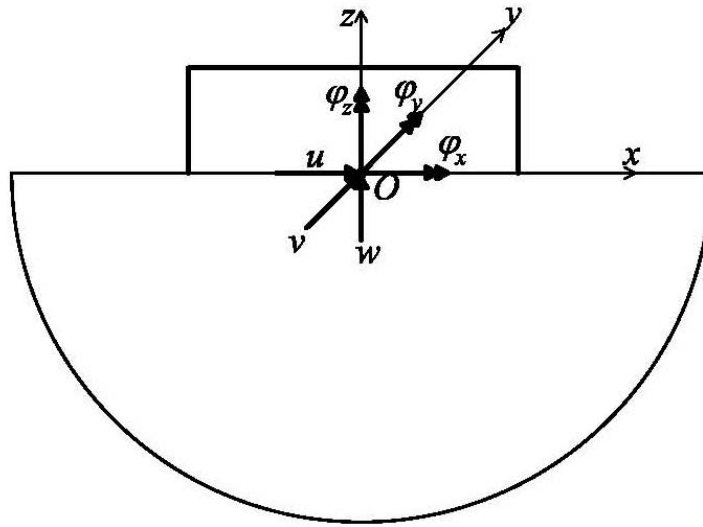


Figure 28. Rigid surface foundation – degrees of freedom

Rectangular massless rigid foundation resting on the soil surface excited by harmonic force is presented in Figure 28. Motion of the rigid basement can be described by the displacement vector $\hat{\mathbf{u}}_0$ at the center of the base interface (point O). For 3D problems, the displacement vector $\hat{\mathbf{u}}_0$ consists of three translations and three rotations. The corresponding force vector acting at the point O is $\hat{\mathbf{P}}_0$. Since dynamic properties of the

foundation depend on the frequency of excitation, force-displacement relation is given in the frequency domain through dynamic stiffness matrix of the foundation:

$$\hat{\mathbf{P}}_{\mathbf{O}} = \mathbf{K}_{\mathbf{O}} \hat{\mathbf{u}}_{\mathbf{O}}, \quad (240)$$

where:

$$\hat{\mathbf{P}}_{\mathbf{O}} = \begin{bmatrix} \hat{P}_x \\ \hat{P}_y \\ \hat{P}_z \\ \hat{M}_x \\ \hat{M}_y \\ \hat{M}_z \end{bmatrix}, \quad \hat{\mathbf{u}}_{\mathbf{O}} = \begin{bmatrix} \hat{u} \\ \hat{v} \\ \hat{w} \\ \varphi_x \\ \varphi_y \\ \varphi_z \end{bmatrix}, \quad \mathbf{K}_{\mathbf{O}} = \begin{bmatrix} k_x & 0 & 0 & 0 & k_{x,\varphi_y} & 0 \\ & k_y & 0 & k_{y,\varphi_x} & 0 & 0 \\ & & k_z & 0 & 0 & 0 \\ & & & k_{\varphi_x} & 0 & 0 \\ & & & & k_{\varphi_y} & 0 \\ & & & & & k_{\varphi_z} \end{bmatrix}. \quad (241)$$

For surface foundations, coupling terms k_{x,φ_y} and k_{y,φ_x} can be neglected, (Schmid and Tosecky 2003).

The dynamic stiffness matrix of the rigid, massless, rectangular foundation is obtained from dynamic stiffness matrix of the corresponding flexible foundation using kinematic transformation, (Schmid and Tosecky 2003). The relation between the displacement vector $\hat{\mathbf{u}}_i$ at the interaction nodes of the flexible foundation and the displacement vector $\hat{\mathbf{u}}_{\mathbf{O}}$ of the rigid foundation is given as:

$$\hat{\mathbf{u}}_i = \mathbf{a} \hat{\mathbf{u}}_{\mathbf{O}}, \quad \mathbf{a} = \begin{bmatrix} \mathbf{a}_1 \\ \vdots \\ \mathbf{a}_i \\ \vdots \\ \mathbf{a}_n \end{bmatrix}, \quad (242)$$

where \mathbf{a} is kinematic matrix, which consists of n sub-matrices \mathbf{a}_i , $i = 1, 2, \dots, n$. Each sub-matrix \mathbf{a}_i is obtained from kinematic consideration, regarding the interaction node i and the centroid of foundation O (Figure 29) as:

$$\mathbf{a}_i = \begin{bmatrix} 1 & 0 & 0 & 0 & 0 & -y_i \\ 0 & 1 & 0 & 0 & 0 & x_i \\ 0 & 0 & 1 & y_i & -x_i & 0 \end{bmatrix}. \quad (243)$$

Equating the deformation energy for flexible and rigid foundation, the dynamic stiffness matrix of rigid foundation is given as:

$$\mathbf{K}_O = \mathbf{a}^T \mathbf{K}_{ii}^F \mathbf{a}, \quad (244)$$

where \mathbf{K}_{ii}^F is the dynamic stiffness matrix of flexible foundation.

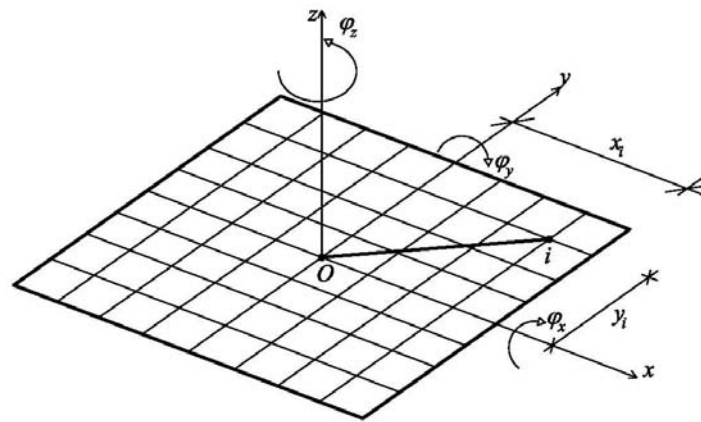


Figure 29. Interaction surface between the foundation and soil

4.5 Soil – structure coupling

Equations of motion in the frequency domain of the soil-structure system are given by Eq. (239). For structure consisting of one-dimensional spectral elements – beams and columns founded on surface rigid foundations (Figure 30) the dynamic stiffness matrix of the soil-foundation interface \mathbf{K}_O can be considered as a hyper – element matrix which can be directly superimposed to the structural dynamic stiffness matrix. The elements of the foundation dynamic stiffness matrix \mathbf{K}_O are symbolically represented by springs in Figure 30. They are complex, where the real part represents the soil stiffness and imaginary part represents the soil damping.

If the structure consists of both one-dimensional and two dimensional spectral elements, like column supported plate (Figure 31), the dynamic stiffness matrix of the soil – foundation interface is assembled with the dynamic stiffness matrix of the structure using the dynamic condensation of the column – soil springs system. The condensed

dynamic stiffness matrix of the column – soil springs system can be assembled with the dynamic stiffness matrices of plates as it was described in the previous section. The dynamic condensation is achieved using the slave and master nodes, labeled in Figure 31. Interaction nodes on the soil – foundation interface are assigned as *slave* nodes - s_i ($i = 1, 2, \dots, N_i$), while the structural nodes m_i ($i = 1, 2, \dots, N_s$) at the plate – column interface are assigned as *master* nodes.

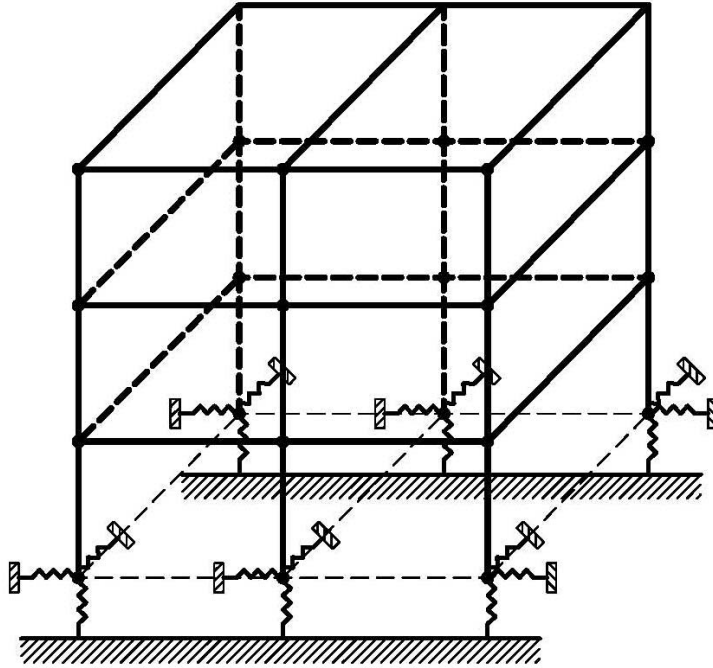


Figure 30. Numerical soil - structure model

The equations of motion of the column – soil springs system are given by:

$$\begin{bmatrix} \mathbf{K}_{mm} & \mathbf{K}_{ms} \\ \mathbf{K}_{sm} & \mathbf{K}_{ss} \end{bmatrix} \begin{bmatrix} \mathbf{u}_m \\ \mathbf{u}_s \end{bmatrix} = \begin{bmatrix} \mathbf{P}_m \\ \mathbf{P}_s \end{bmatrix}. \quad (245)$$

Eliminating the displacement vector at the slave nodes - \mathbf{u}_s from the above equation the relation between the forces and displacements at the master nodes are obtained as:

$$\begin{aligned} (\mathbf{K}_{mm} - \mathbf{K}_{ms} \mathbf{K}_{ss}^{-1} \mathbf{K}_{sm}) \mathbf{u}_m &= \mathbf{P}_m - \mathbf{K}_{ms} \mathbf{K}_{ss}^{-1} \mathbf{P}_s, \\ \mathbf{K}_c \mathbf{u}_m &= \mathbf{P}_c \end{aligned}, \quad (246)$$

where $\mathbf{K}_c = \mathbf{K}_{mm} - \mathbf{K}_{ms} \mathbf{K}_{ss}^{-1} \mathbf{K}_{sm}$ is the condensed dynamic stiffness matrix of the column – soil springs system and $\mathbf{P}_c = \mathbf{P}_m - \mathbf{K}_{ms} \mathbf{K}_{ss}^{-1} \mathbf{P}_s$ is the condensed force vector. Now, the matrix \mathbf{K}_c can be superimposed to the plate dynamic stiffness matrix \mathbf{K}_D as described in the section 3.2.

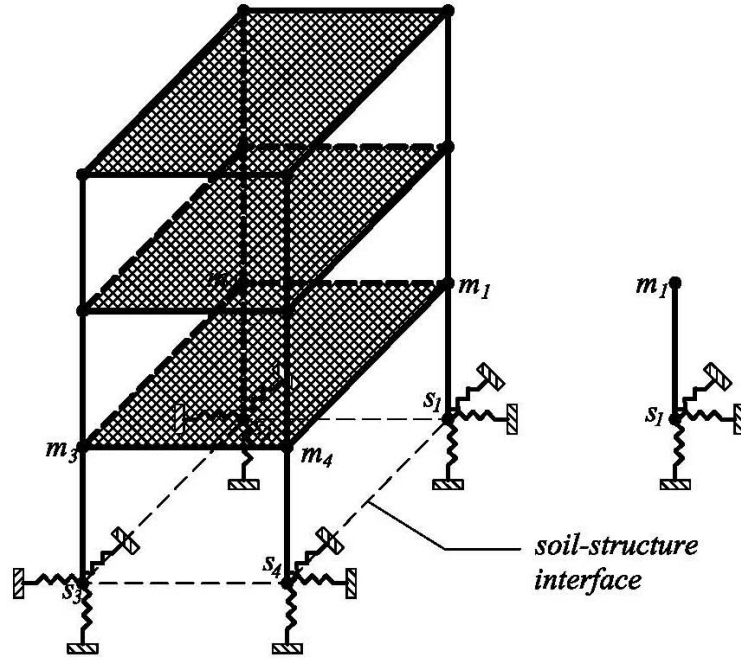


Figure 31. Numerical soil – structure model, consisting of one-dimensional and two-dimensional spectral elements

When the structure is subjected to traffic-induced vibrations or seismic loads, the vector of structural nodes \mathbf{P}_s defined in Eq. (239) will be zero, while the vector of the interaction nodes is $\mathbf{P}_i = \mathbf{K}_0^F \mathbf{u}'_i$, where consequently, the condensed force vector \mathbf{P}_c is:

$$\mathbf{P}_c = -\mathbf{K}_{ms} \mathbf{K}_{ss}^{-1} \mathbf{K}_0^F \mathbf{u}'_i. \quad (247)$$

5. Applications

Using the numerical model developed in the previous section the dynamic response analysis of 3D frame structures subjected to traffic-induced ground excitation has been carried out. Three frame structures of different height and number of stories are given in Figure 32, while the geometrical properties of structural members are presented in Table 13. The frames are founded on rigid and massless square footings with a length of 1 m.

The footings rest on elastic homogeneous half space. Material properties of the half space are:

- Mass density: 1900 kg/m^3 ,
- Poisson's ratio: 0.3,
- Shear wave velocity: varies from 200 m/s (soft soil) to 1000 m/s (stiff soil).

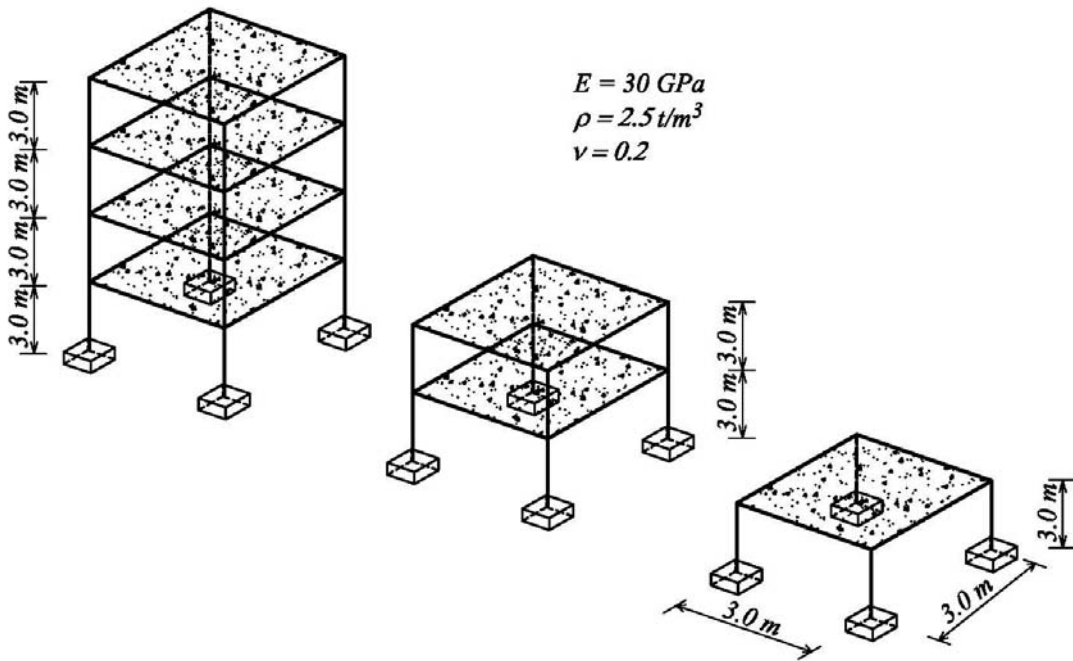


Figure 32. Layout and geometry of frame structures

Table 13. Geometrical properties of investigated frames

Frame	Columns	Beams	Floor slabs
One storey	30x30 cm	15x25 cm	15 cm
Two storey	30x30 cm (1-2 floor)		15 cm
Four storey	50x50 cm (1 st floor) 40x40 cm (2 nd floor) 30x30 cm (3-4 floor)		15 cm

5.1 Effects of soil stiffness and foundation size on natural frequencies

Natural frequencies of investigated frames have been calculated for different soil stiffness: $v_s = 200, 400, 1000 \text{ m/s}$ and presented in Figure 33 -Figure 35. As expected, the natural frequencies increase as the soil stiffness increases. In addition, natural frequency bias from the fixed base values decrease as the number of stories increase. The results also indicate that natural frequencies of the vertical vibration modes are more affected by the change of soil stiffness, since structure/soil stiffness ratio in the vertical direction is larger than the corresponding structure/soil stiffness ratio in the horizontal direction.

In order to increase the horizontal stiffness of the one storey frame, 50/50 cm columns were adopted. The corresponding natural frequencies of the short stiff structure have been presented in Figure 36. In this case the natural frequencies of the soil-structure system are significantly affected by the soil stiffness. Consequently, taking into account soil-structure interaction can have a very significant effect on the dynamic response of stiff structures founded on soft soils.

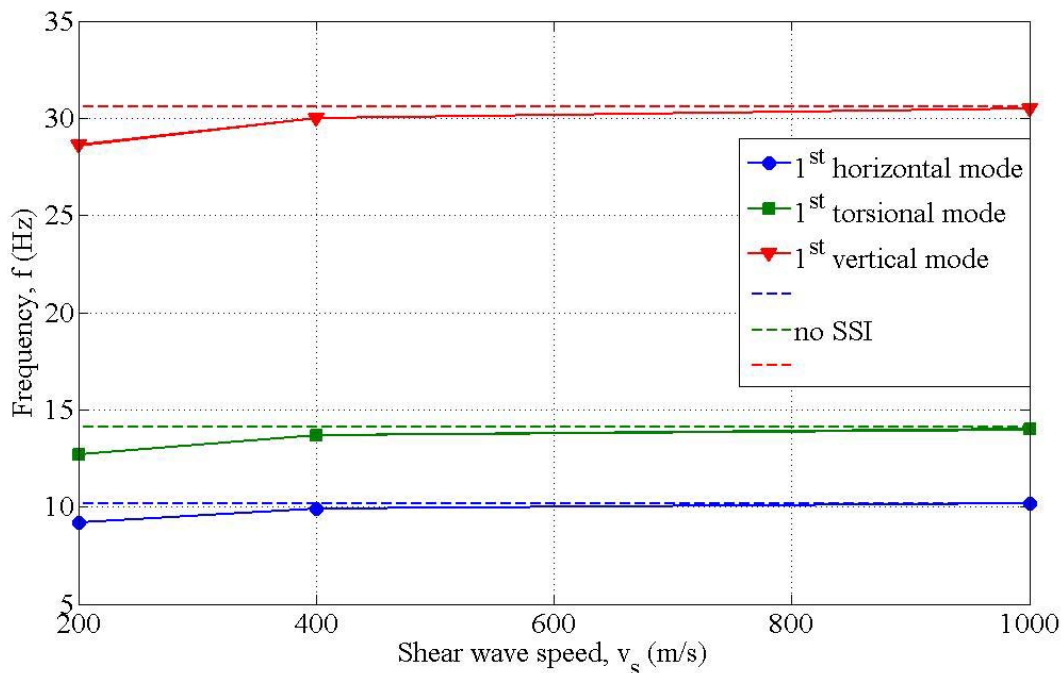


Figure 33. Natural frequencies of one storey frame

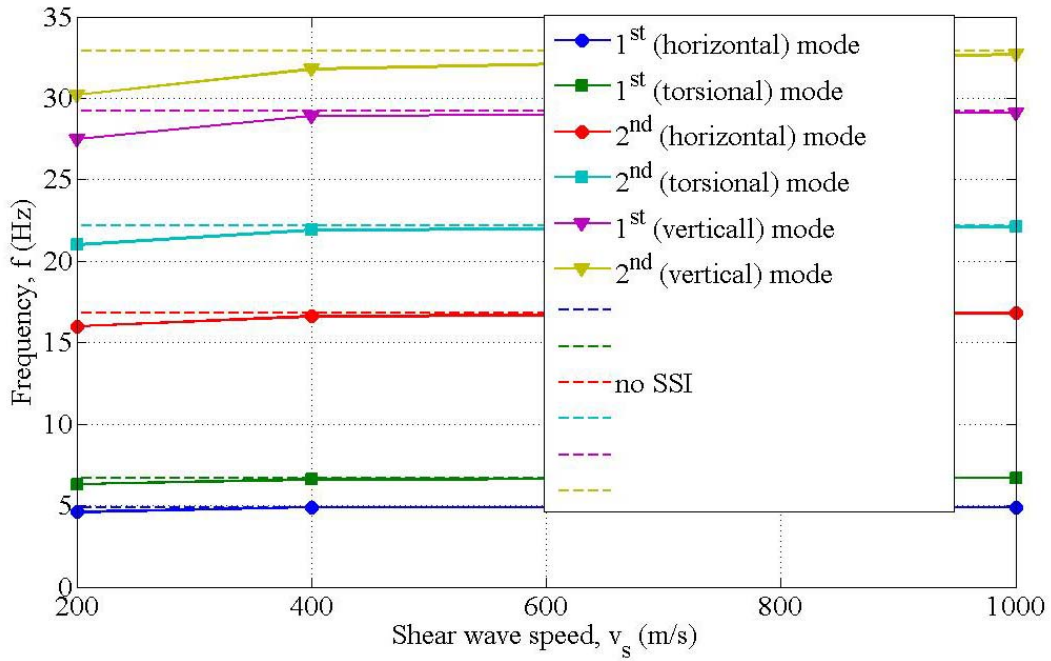


Figure 34. Natural frequencies of the two storey frame

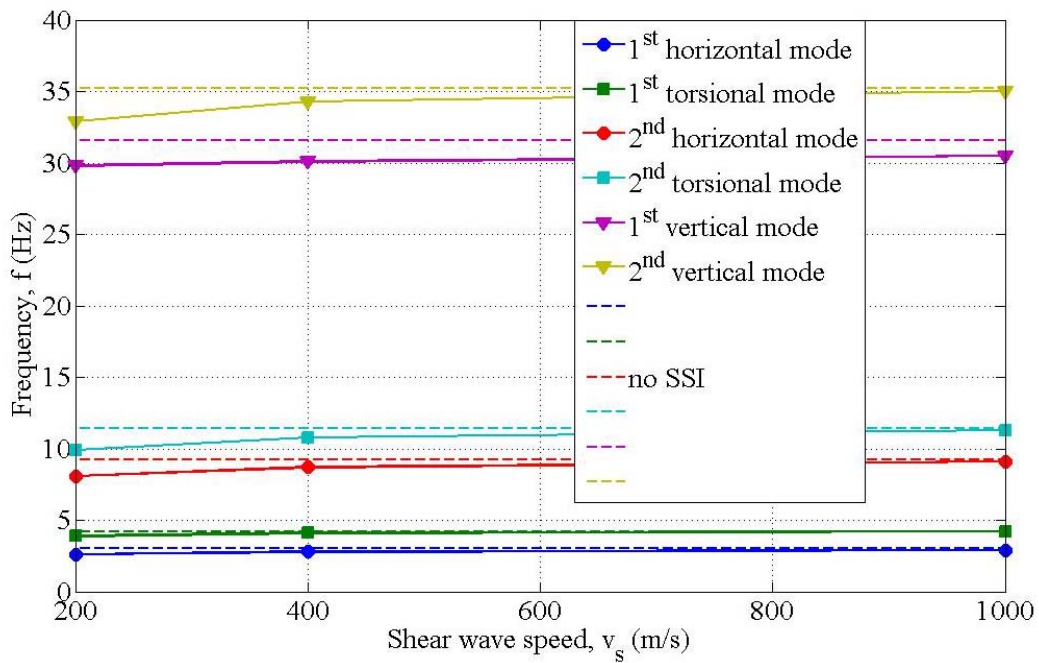


Figure 35. Natural frequencies of four storey frame

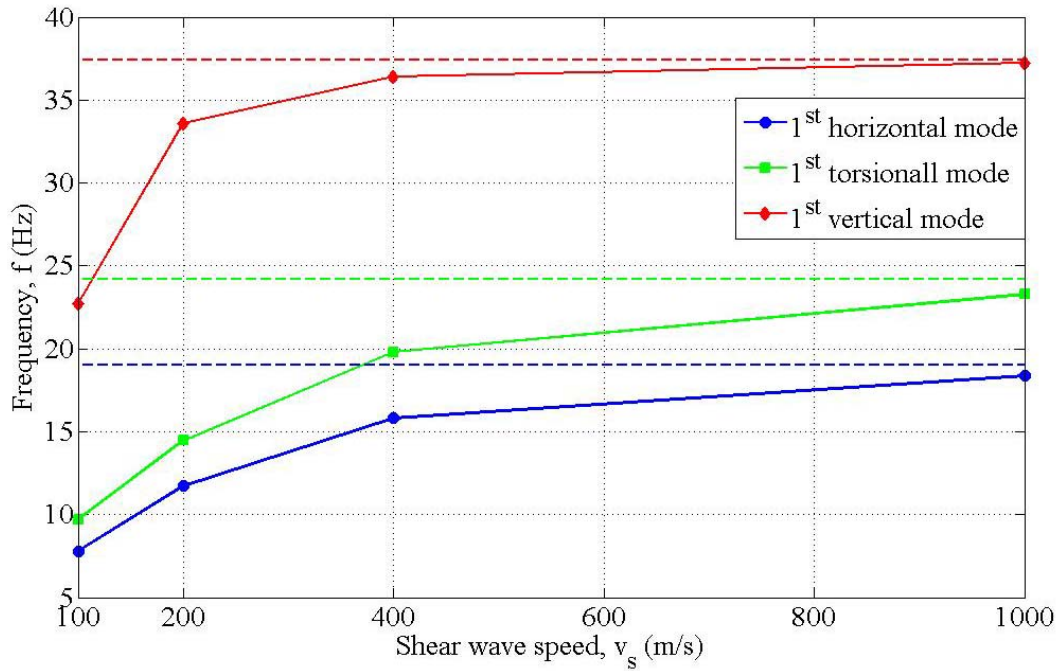


Figure 36. Natural frequencies of one storey frame (columns 50/50 cm)

Effects of the foundation size – B (B is half width of the square foundation) on natural frequencies of one storey frame have been presented in Figure 37. Natural frequencies increase as the foundation size increases. Also, the effect of the foundation size becomes insignificant as the soil stiffness increases.

5.2 Effects of soil stiffness on structural response

3D frame structures presented in Figure 32 have been subjected to traffic-induced ground vibrations measured in Belgrade in 2006, along the future metro line, (Petronijevic and Nefovska-Danilovic 2006). Some of the results have been presented and discussed.

5.2.1 Input ground excitation

The ground velocities were measured simultaneously in three orthogonal directions, relative to the road surface: vertical direction - W, horizontal direction parallel to the road - U and horizontal direction perpendicular to the road – V. The measurements showed that the highest vibration levels were generated by a tram and a heavy truck crossing 3 cm thick rubber speed bump in the King Alexander's Boulevard. Therefore, the ground vibrations induced by these two vibration sources were used as input ground motion in vibration simulation of the frame structures.

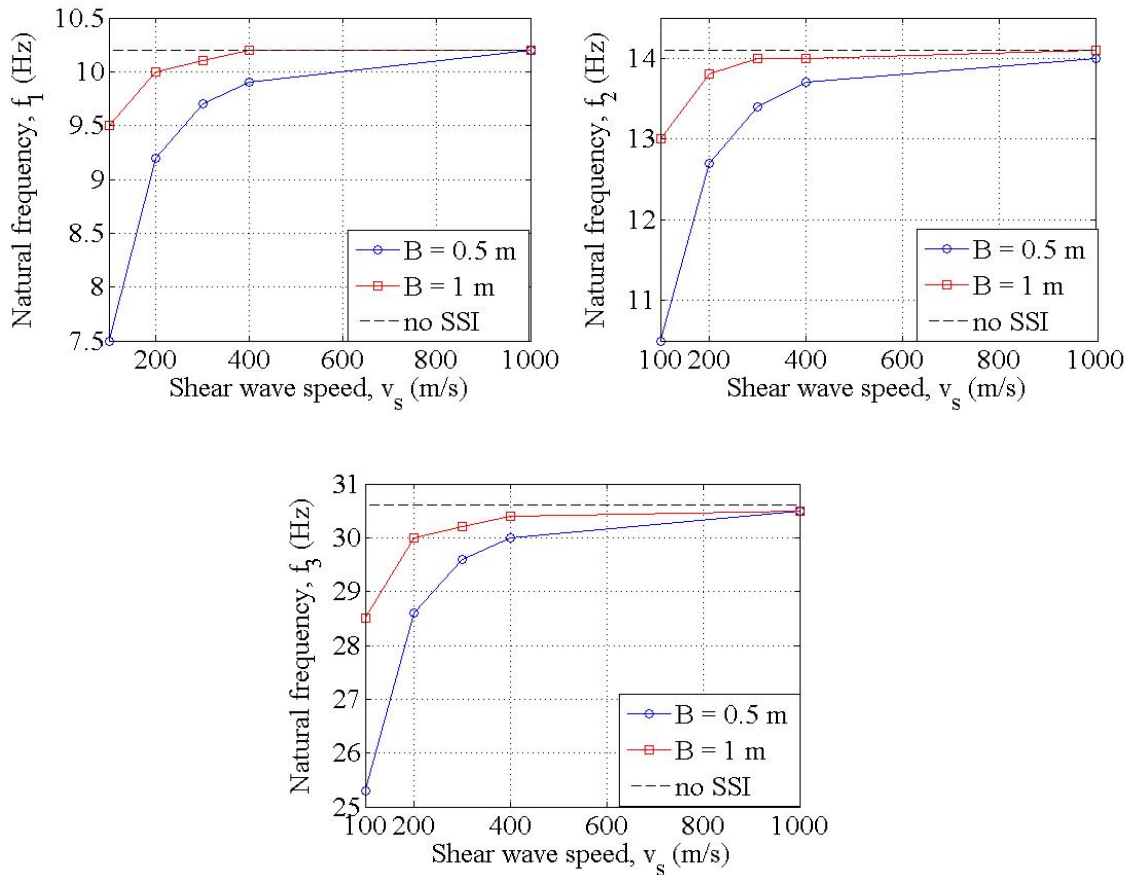


Figure 37. Effects of foundation size on first three natural frequencies of one storey frame

Velocity time histories and power spectra for horizontal and vertical ground vibrations at the measurement point located approximately 11 m from the road/track on the ground surface are presented in Figure 38 -Figure 43. In the case of tram traffic, the predominant frequency range was between 18 and 22 Hz for horizontal vibrations and between 18 and 27 Hz for vertical vibrations. For vibrations induced by the heavy truck crossing rubber speed bump the predominant frequency range was between 3 and 27 Hz for horizontal vibrations and between 2 and 6 Hz for vertical vibrations. Higher vibration levels were obtained for vertical vibrations. Time histories of ground displacements and corresponding power spectra, obtained from integrating ground velocities are presented in Figure 44 -Figure 49. These ground displacement time histories were used as inputs to excite the frame structures. The corresponding predominant frequency range for tram traffic was between 19 and 23 Hz for horizontal vibrations and between 13 and 27 Hz for vertical vibrations, whereas for road traffic

induced by the heavy truck crossing a rubber speed bump, the predominant frequency range was between 2 and 5 Hz for both horizontal and vertical vibrations.

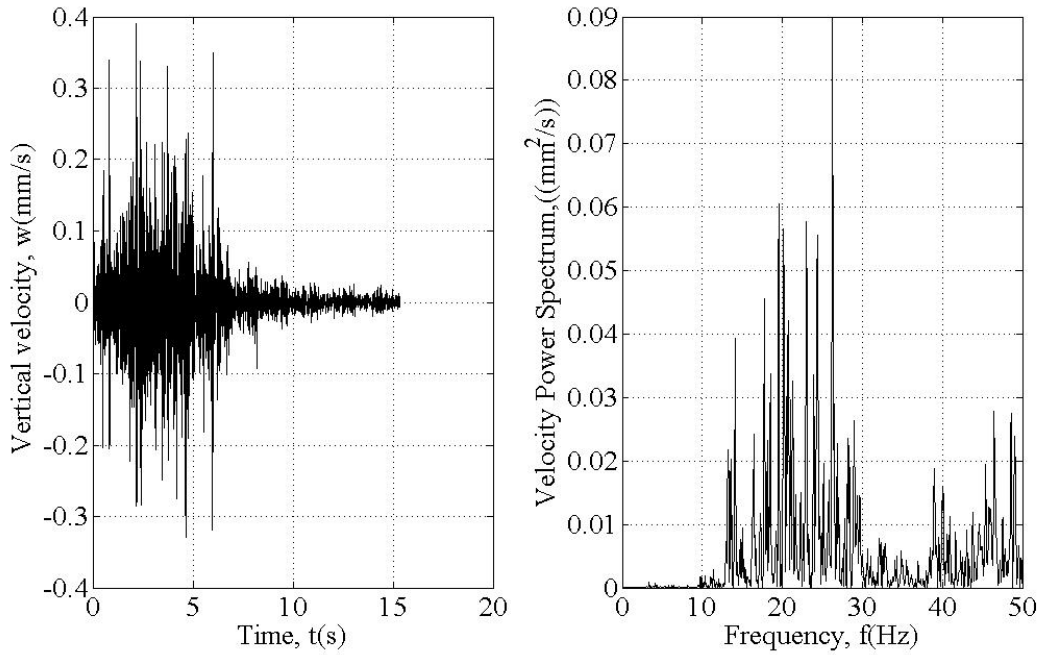


Figure 38. Time history and Power spectrum of vertical ground velocity from a tram ($v=20$ km/h)

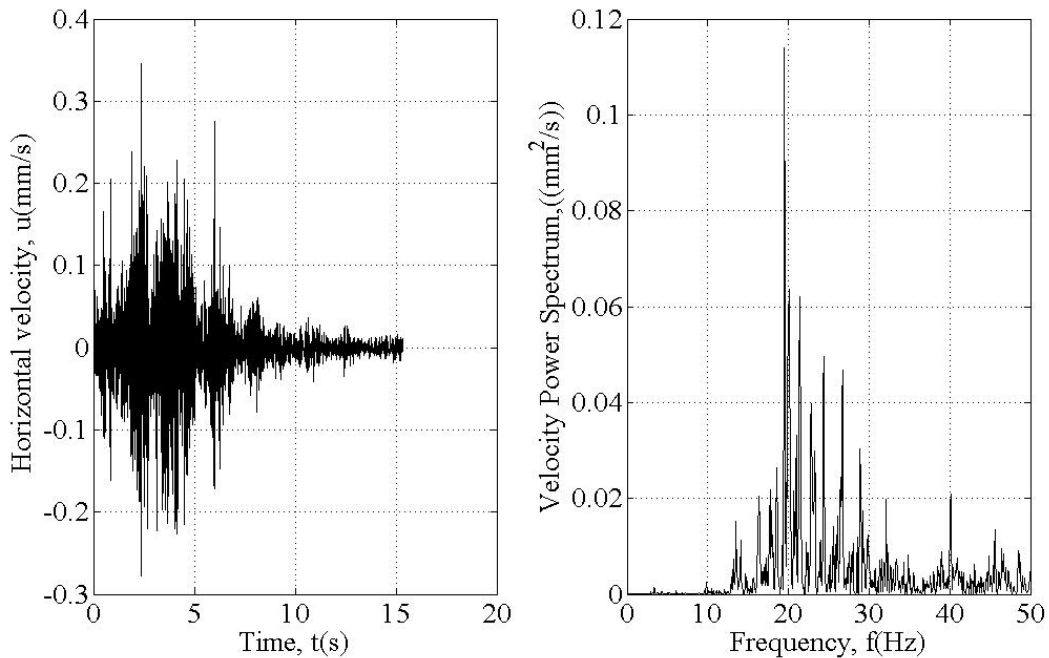


Figure 39. Time history and Power spectrum of horizontal ground velocity – U from a tram ($v=20$ km/h)

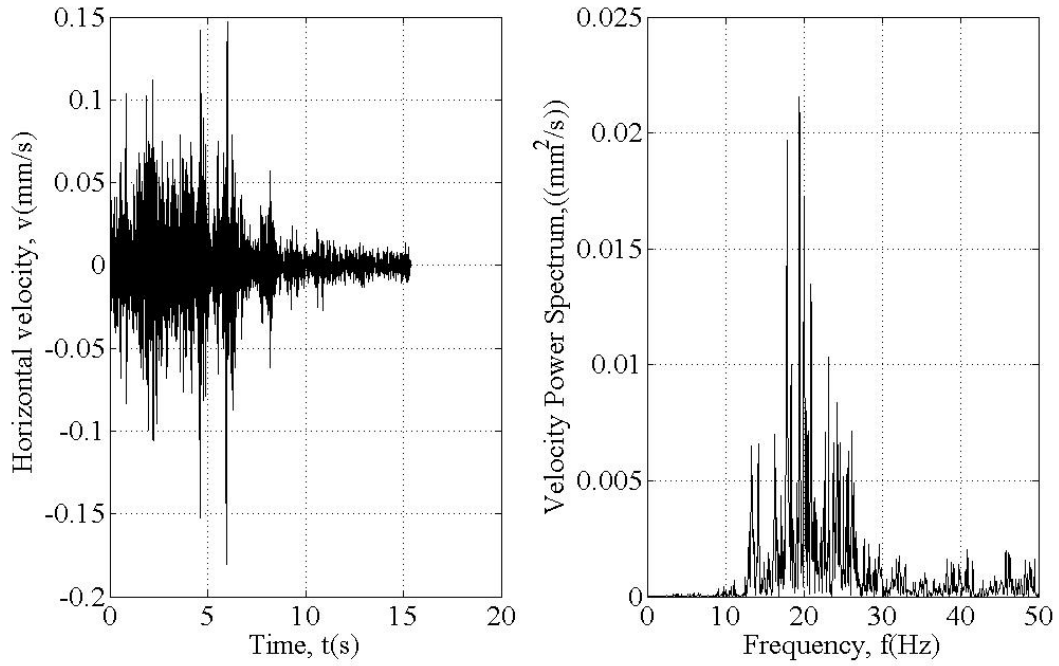


Figure 40. Time history and Power spectrum of horizontal ground velocity – V from a tram ($v=20$ km/h)

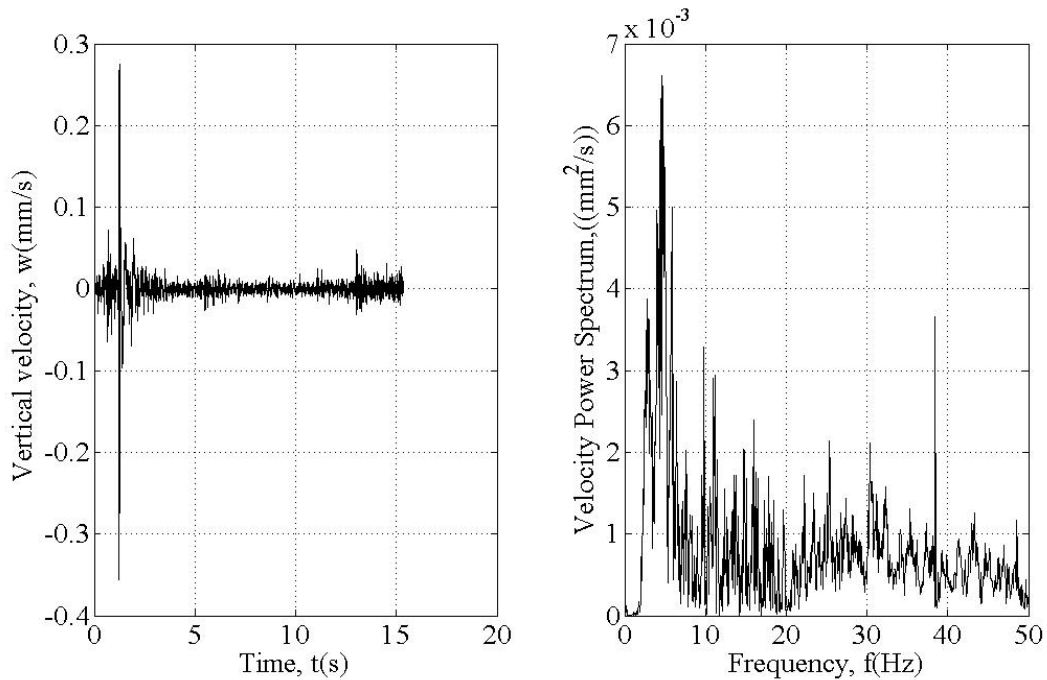


Figure 41. Time history and Power spectrum of vertical ground velocity from a truck (crossing rubber speed bump, $v=50$ km/h)

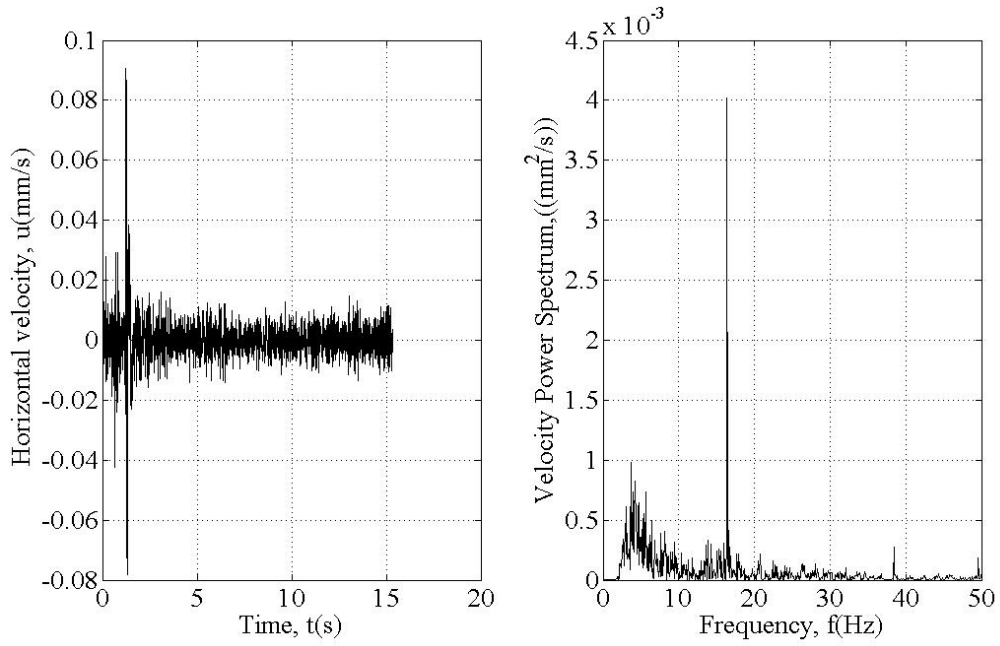


Figure 42. Time history and Power spectrum of horizontal ground velocity – U from a truck (crossing rubber speed bump, $v=50$ km/h, distance to road 11 m)

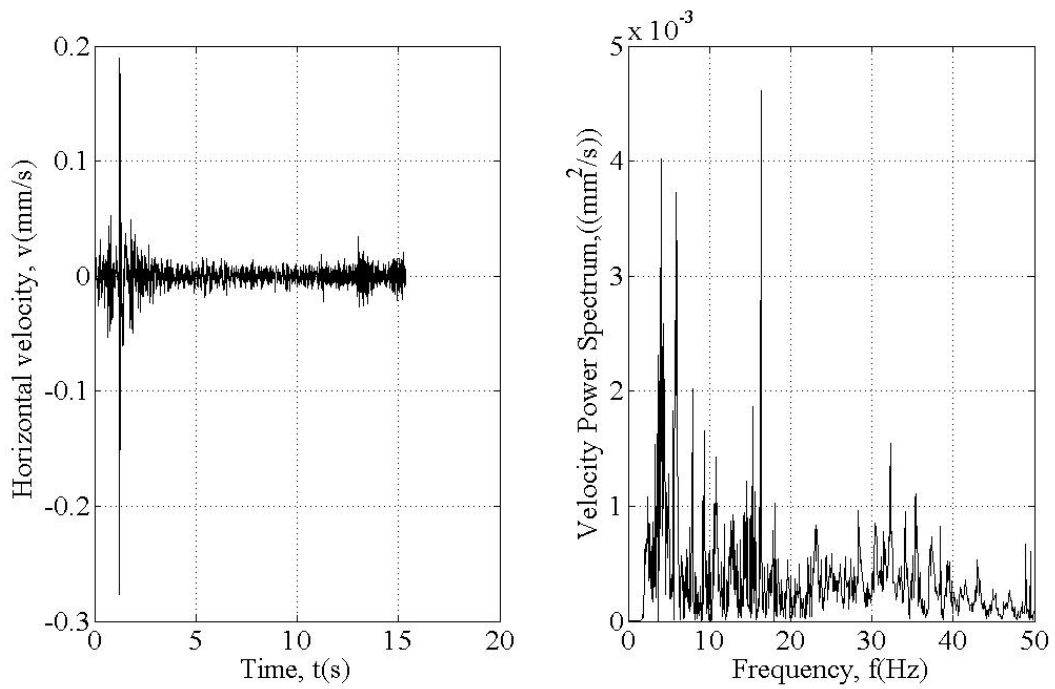


Figure 43. Time history and Power spectrum of horizontal ground velocity – V from a truck (crossing rubber speed bump, $v=50$ km/h)

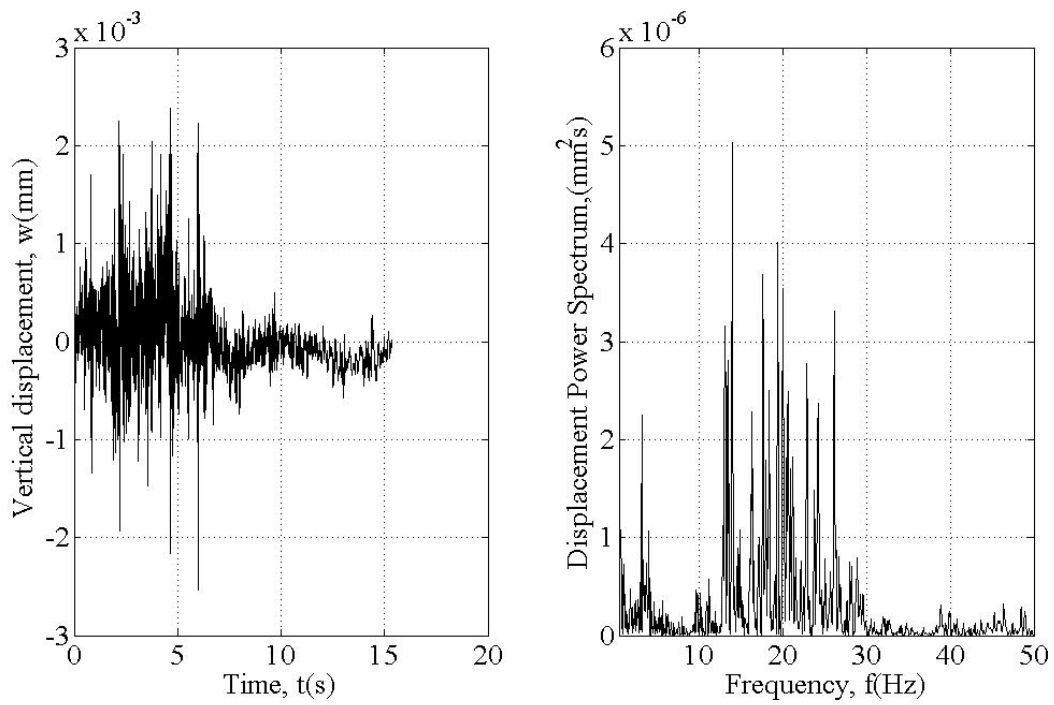


Figure 44. Time history and Power spectrum of vertical ground displacement from a tram ($v=20$ km/h)

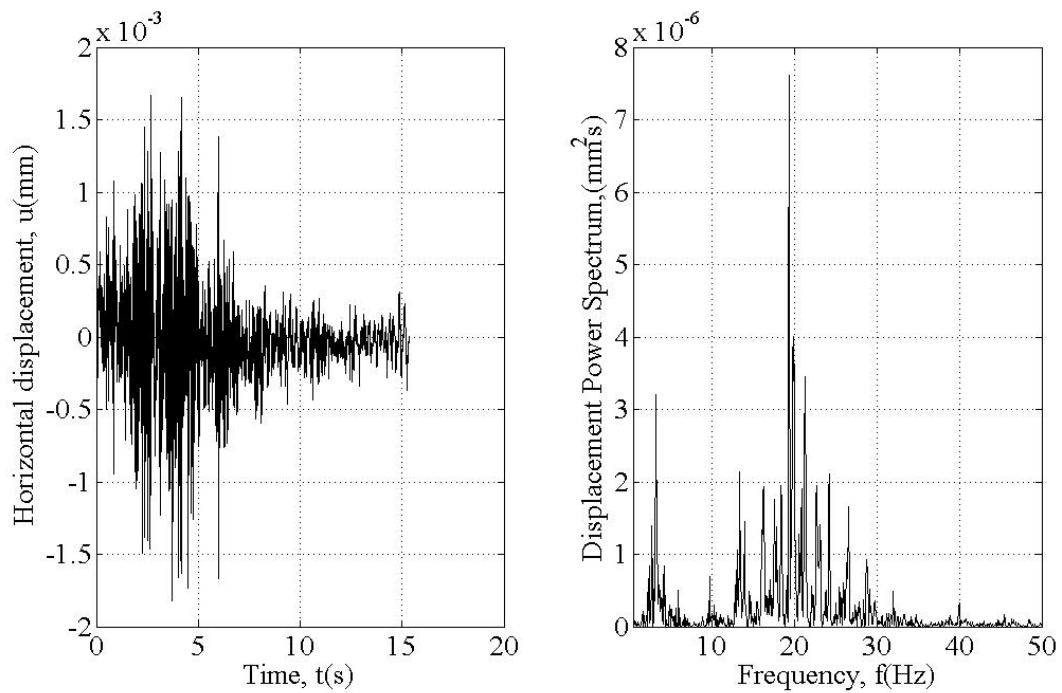


Figure 45. Time history and Power spectrum of horizontal ground displacement - U from a tram ($v=20$ km/h)

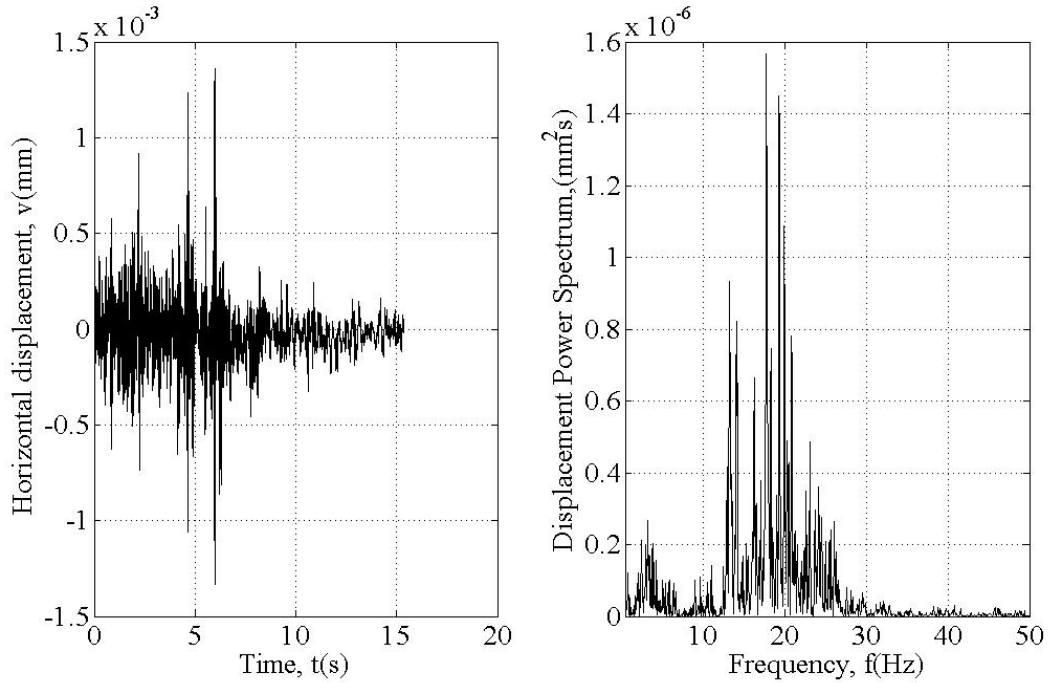


Figure 46. Time history and Power spectrum of horizontal ground displacement - V from a tram ($v=20$ km/h)

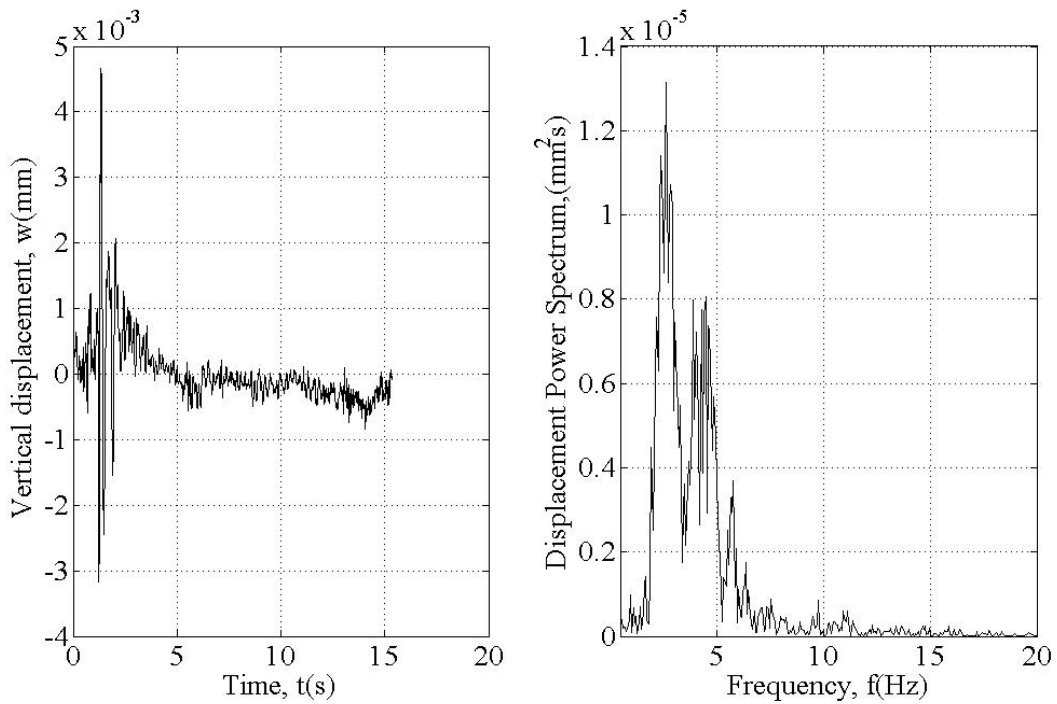


Figure 47. Time history and Power spectrum of vertical ground displacement from a truck (crossing rubber speed bump, $v=50$ km/h)

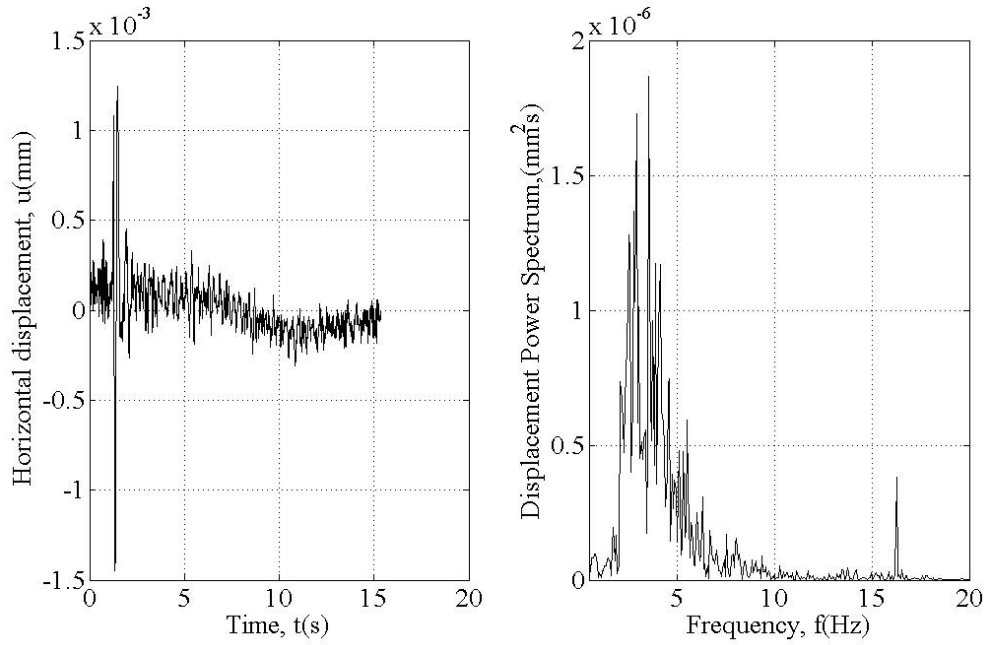


Figure 48. Time history and Power spectrum of horizontal – U ground displacement from a truck (crossing rubber speed bump, $v=50$ km/h)

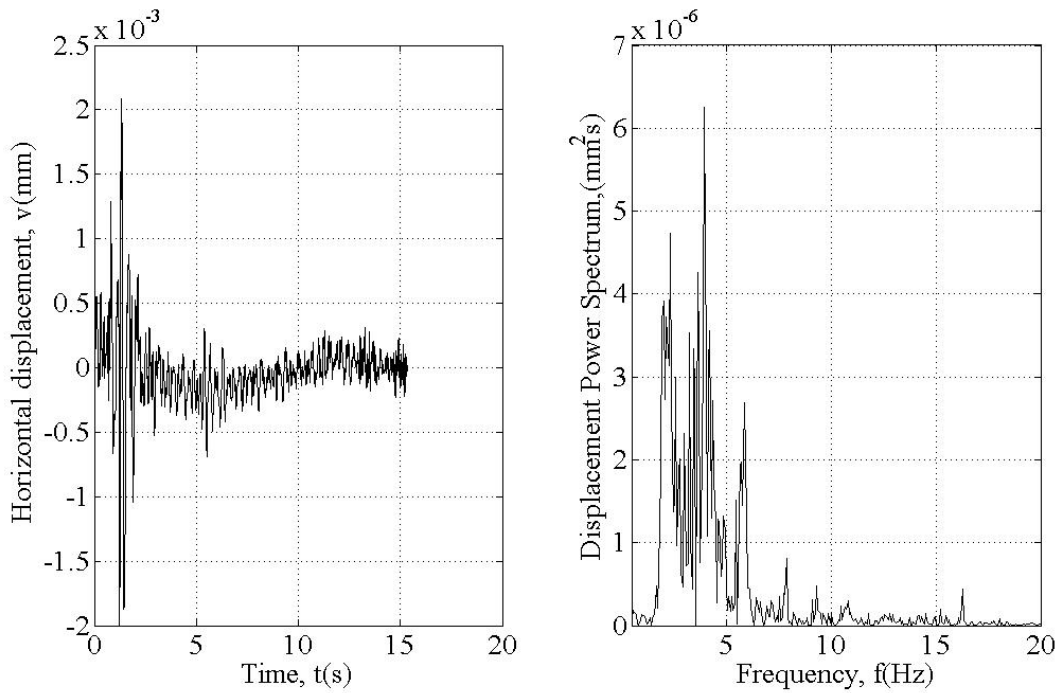


Figure 49. Time history and Power spectrum of horizontal ground displacement – V from a truck (crossing rubber speed bump)

5.2.2 Dynamic response to traffic-induced ground vibration

The dynamic responses of the investigated frames subjected to the measured ground vibrations have been calculated for the fixed base model, and for the model which accounted for the SSI assuming that the frame structures were founded on soft soil ($v_s = 200$ m/s) and stiff soil ($v_s = 1000$ m/s).

Displacement envelopes are presented in Figure 50 - Figure 58, whereas the displacement response spectra in the midpoint of the top floor slab are given in Figure 59 -Figure 66. Peak structural and foundation displacement response values as well as the amplification factors (a.f.) are summarized in Table 14 -Table 15. Time history of the foundation and structural displacements at the top node of the column and mid - point of the plate of the one-storey frame are presented in Figure 67 -Figure 70.

In almost all cases an increase in soil stiffness resulted in a decrease in the foundation displacements. Unlike the foundation response, the maximum structural displacements were increased with increasing the soil stiffness, Figure 59 -Figure 64. From Figure 59 - Figure 66 it can be concluded that the dynamic responses of the frames were influenced by lower vibration modes.

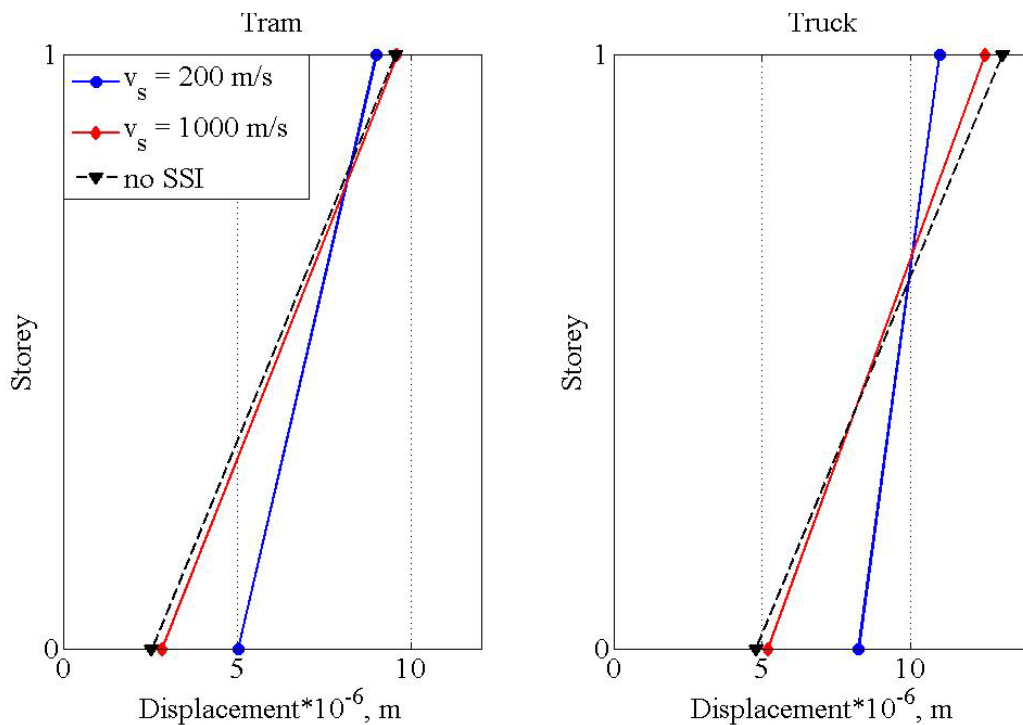


Figure 50. Vertical displacement envelopes of one-storey frame

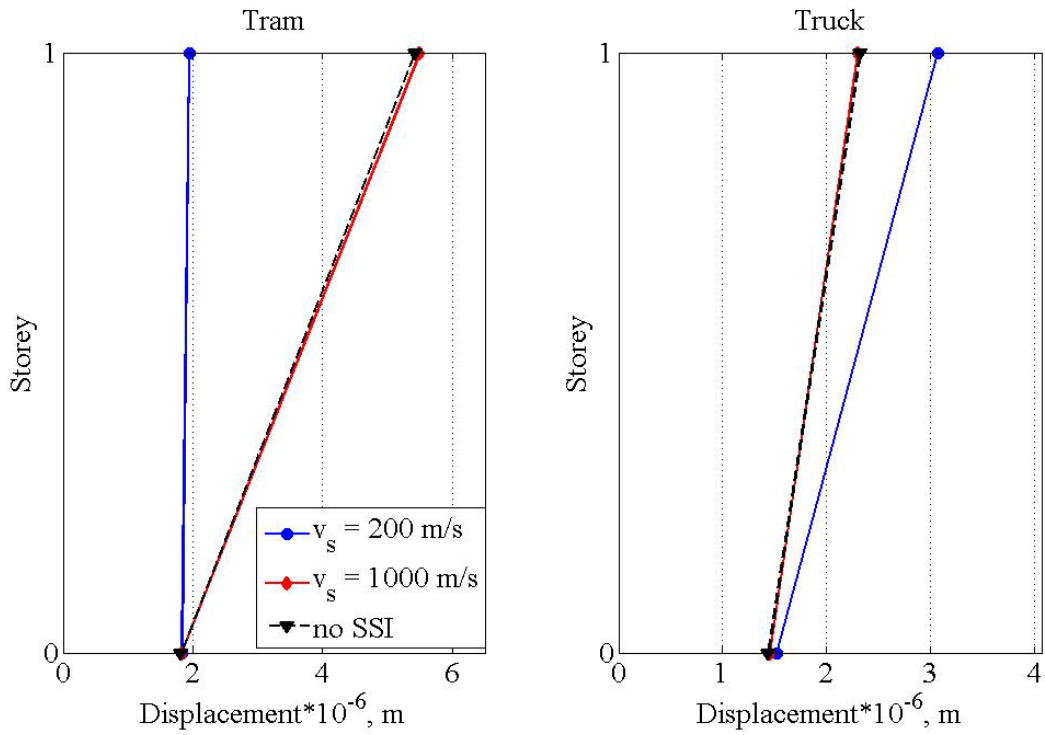


Figure 51. Horizontal displacement – U envelopes of one-storey frame

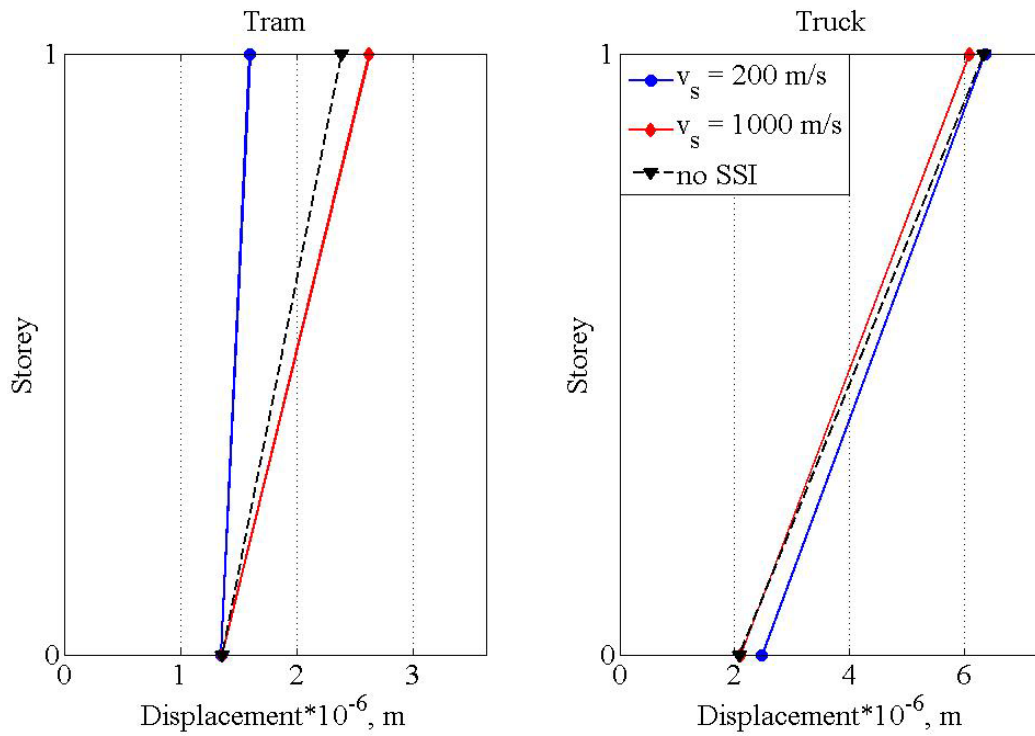


Figure 52. Horizontal displacement – V envelopes of one-storey frame

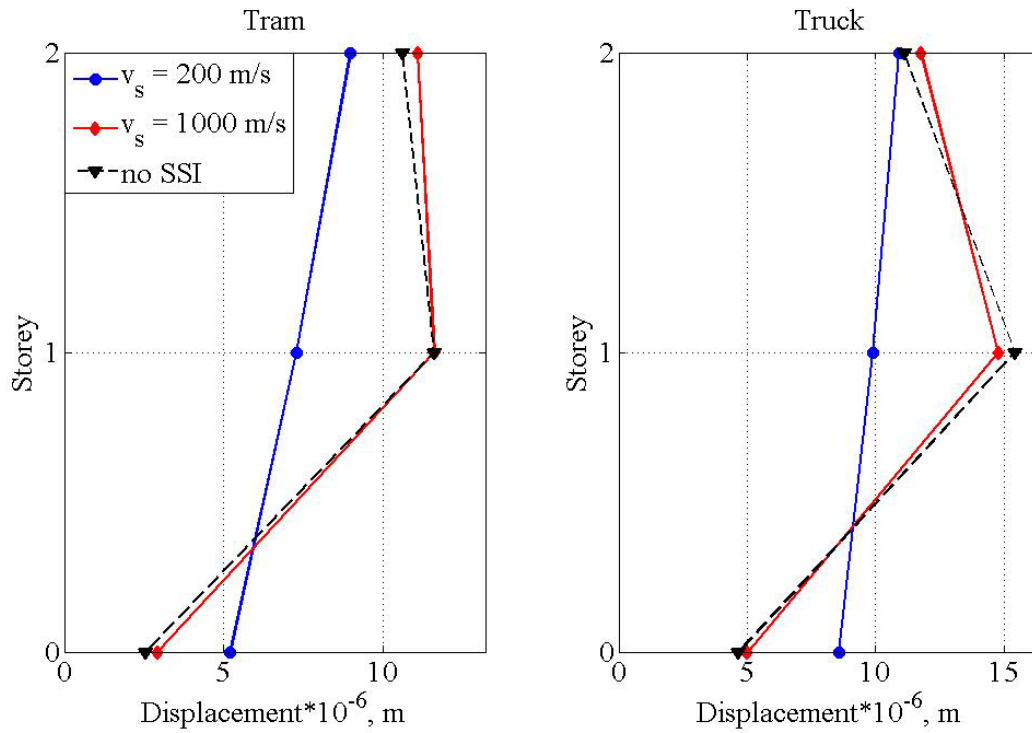


Figure 53. Vertical displacement envelopes of two-storey frame

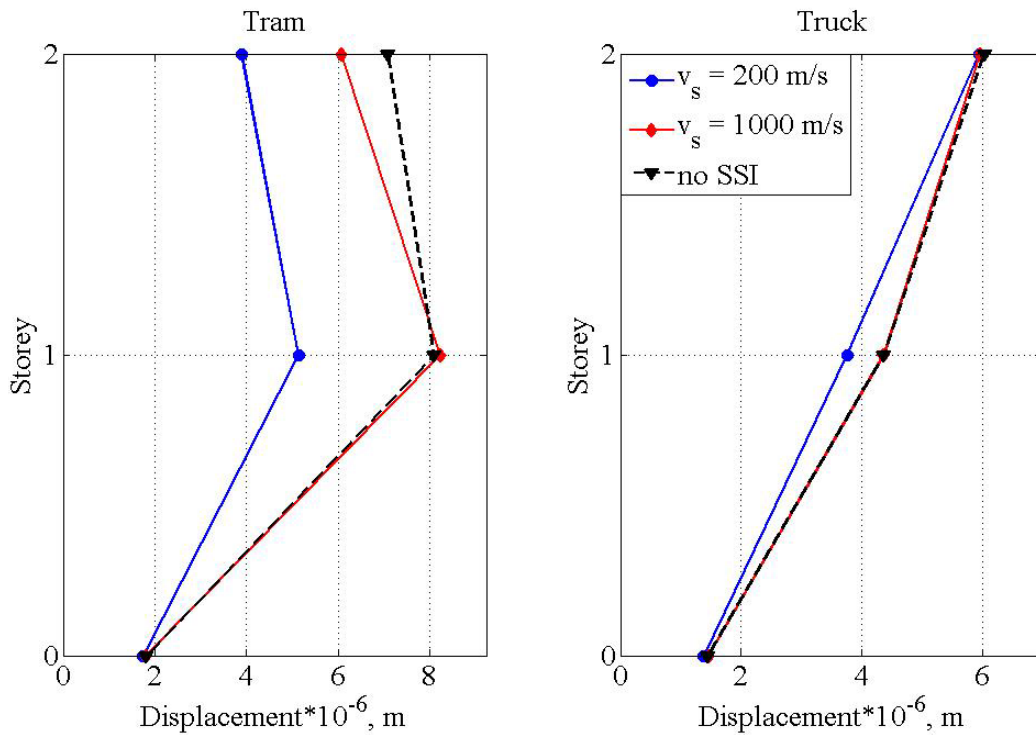


Figure 54. Horizontal displacement – U envelopes of two-storey frame

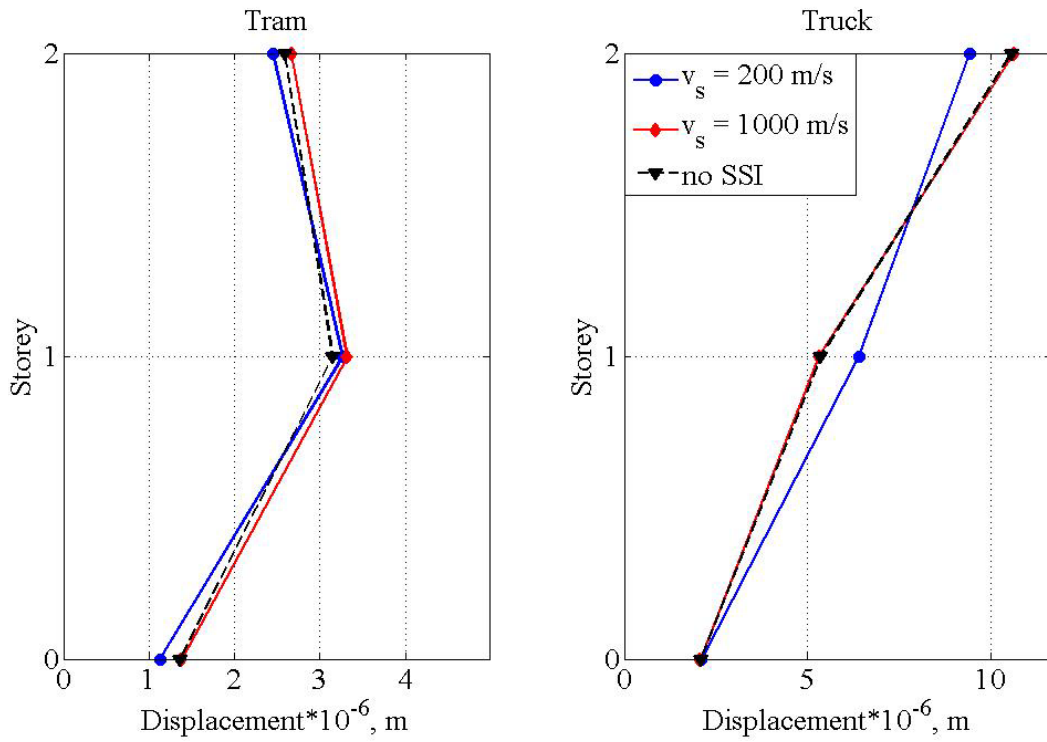


Figure 55. Horizontal displacement – V envelopes of two-storey frame

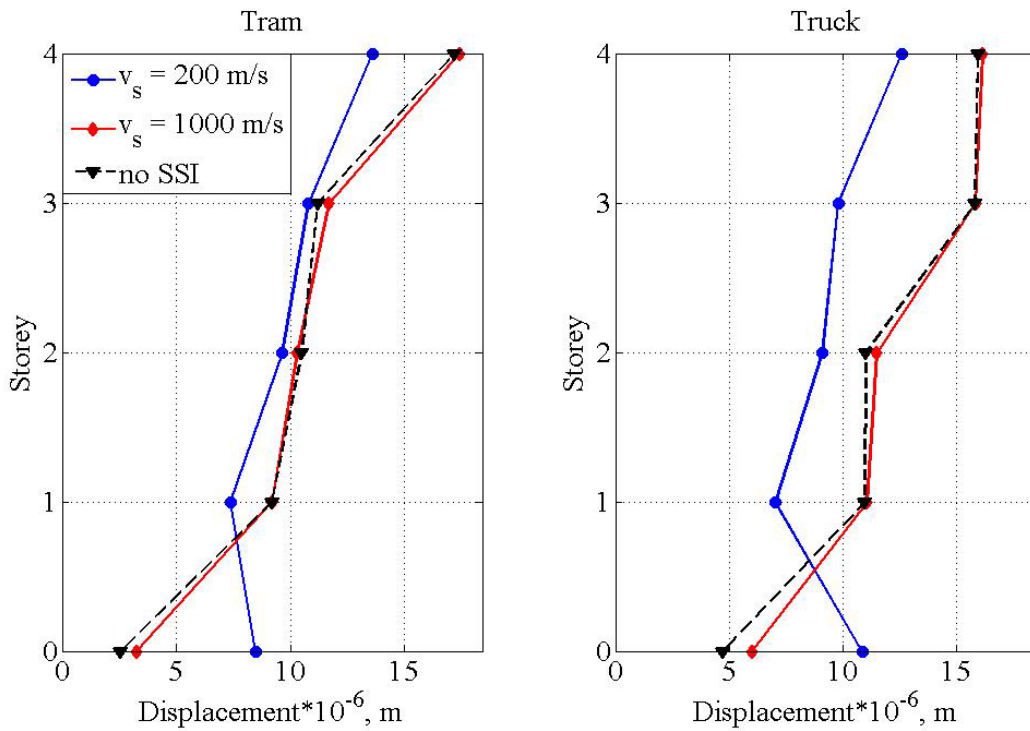


Figure 56. Vertical displacement envelopes of four-storey frame

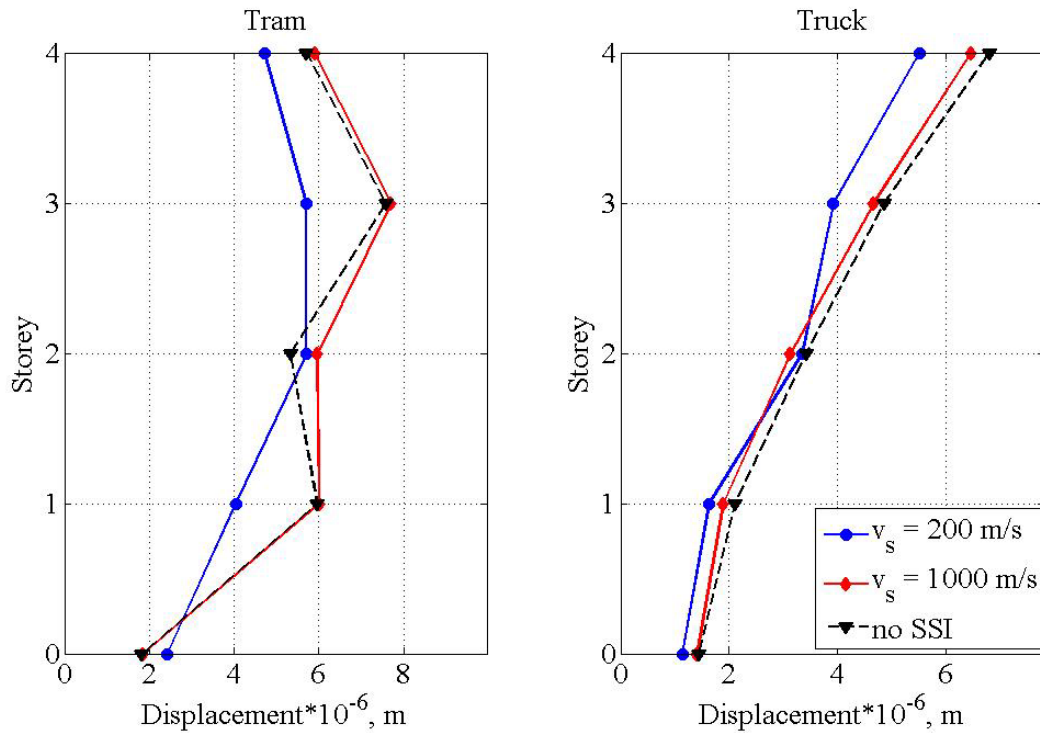


Figure 57. Horizontal displacement – U envelopes of four-storey frame

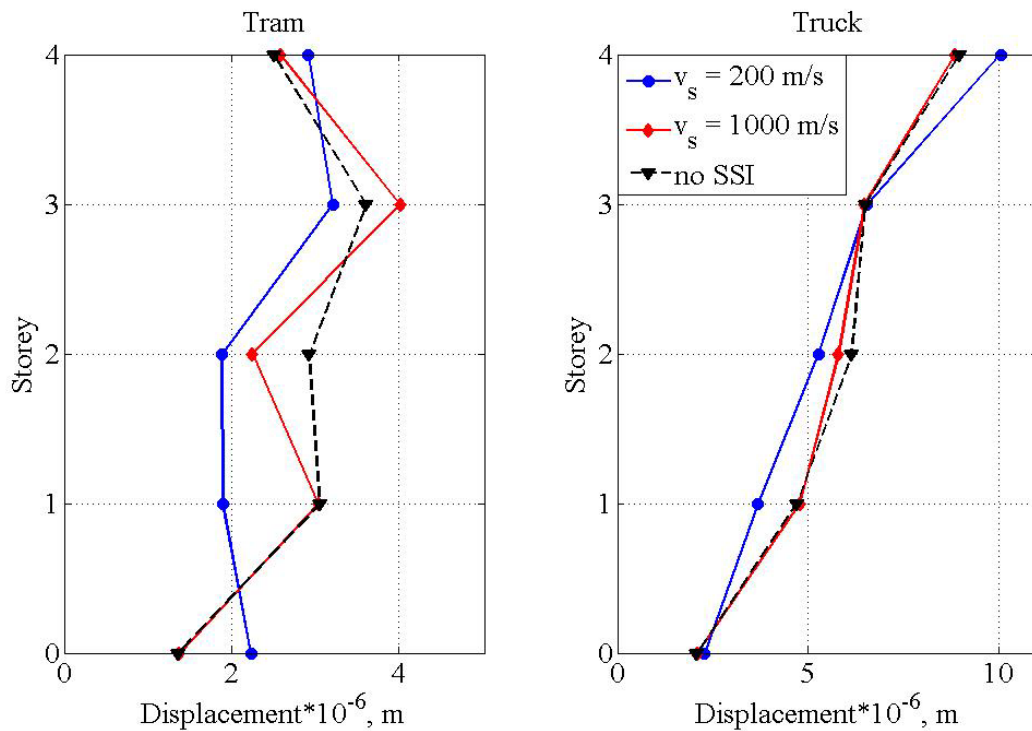


Figure 58. Horizontal displacement – V envelopes of four-storey frame

Tram traffic induced larger a.f. of vertical vibrations than truck traffic for all investigated frames for both soft and stiff soil, since the fundamental natural frequencies

of investigated frames were close to the predominant frequency range for tram traffic (13-27 Hz). Additionally, vertical vibrations for both tram and truck traffic were amplified as the number of stories increased. As waves propagate from the foundation through the column, vertical displacements have been reduced and then amplified from the top point of the column to the plate mid – point, Figure 67-Figure 68.

Very large amplification factors of horizontal vibrations induced by tram traffic were obtained for the short stiff frame structure founded on stiff soil, as the fundamental natural frequency of the horizontal mode of vibration (19 Hz) was very close to the predominant frequency of horizontal vibration induced by tram traffic (19.3 Hz), Table 14. In addition, two - storey frame had the largest amplification factors for tram traffic, since its vibration was influenced by the second horizontal mode (approx. 16 Hz), which fall into the predominant frequency range for tram traffic. In case of truck traffic, four - storey frame exhibited the largest amplification factors for horizontal vibrations.

Time history of horizontal displacement of the foundation, column top point and plate mid – point for one – storey frame are given in Figure 69 - Figure 70, for tram and truck traffic, respectively. In this case horizontal displacements were amplified from the foundation to the column top point. Horizontal displacement at the column top point and plate mid – point were almost identical, due to the large stiffness of the plate in horizontal direction.

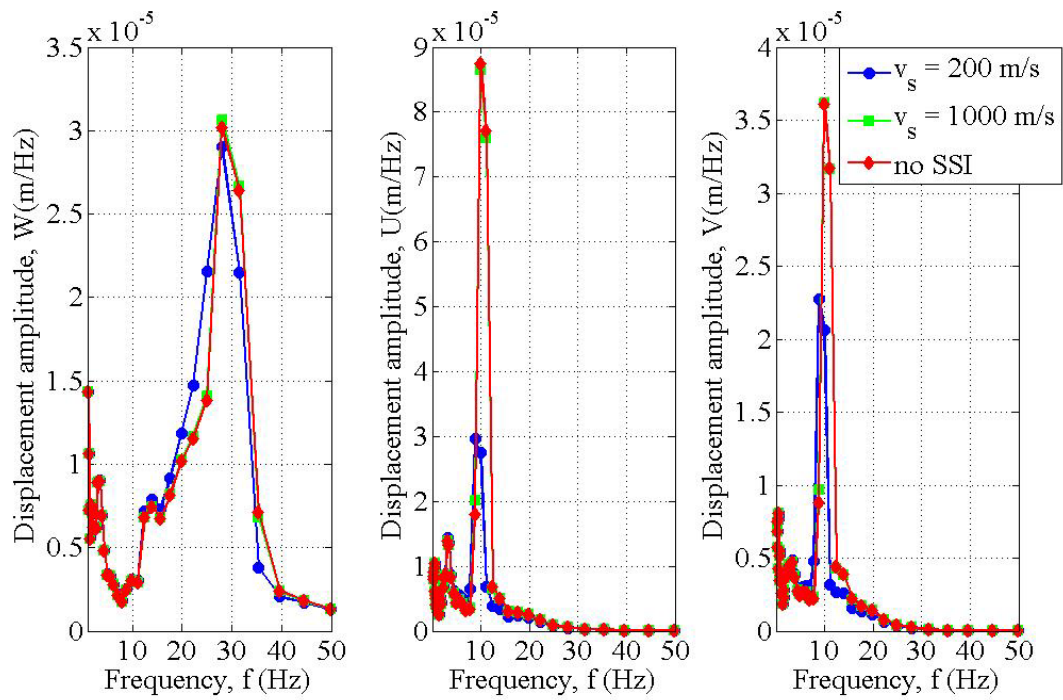


Figure 59. Top floor displacement response spectra of one storey frame, tram traffic

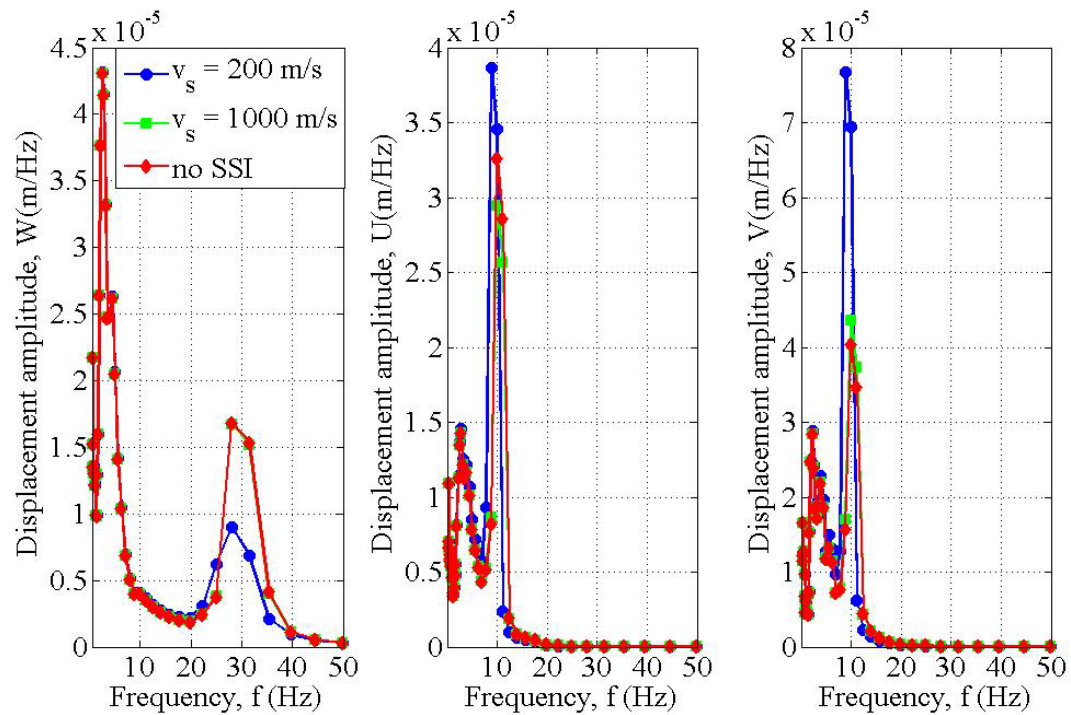


Figure 60. Top floor displacement response spectra of one storey frame, truck traffic

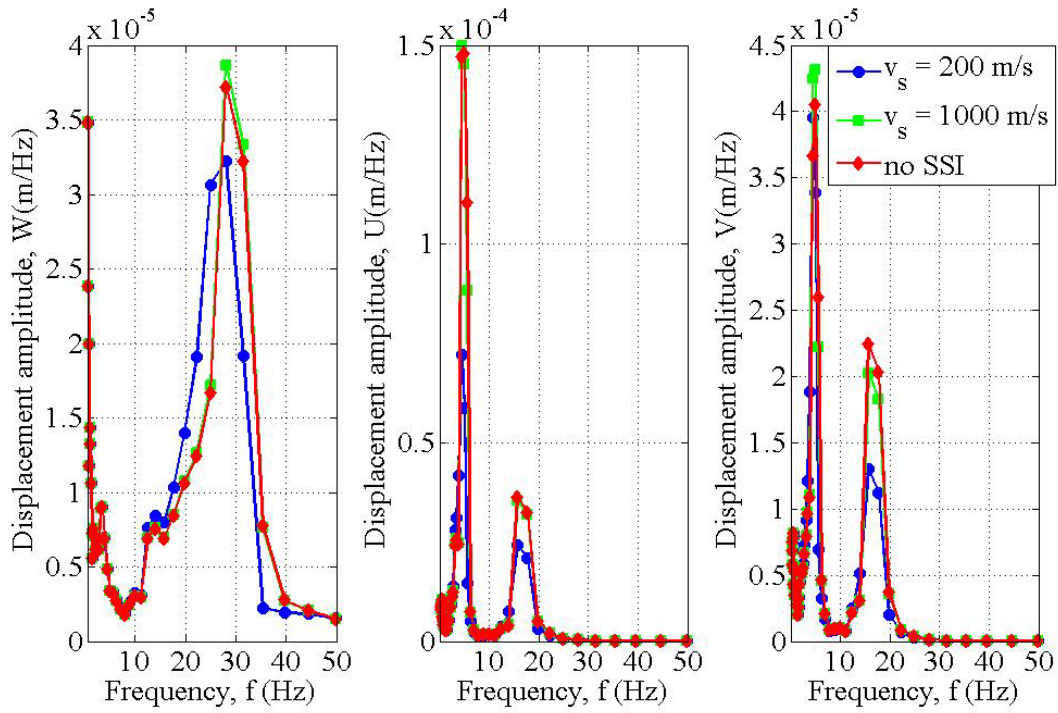


Figure 61. Top floor displacement response spectra of two storey frame, tram traffic

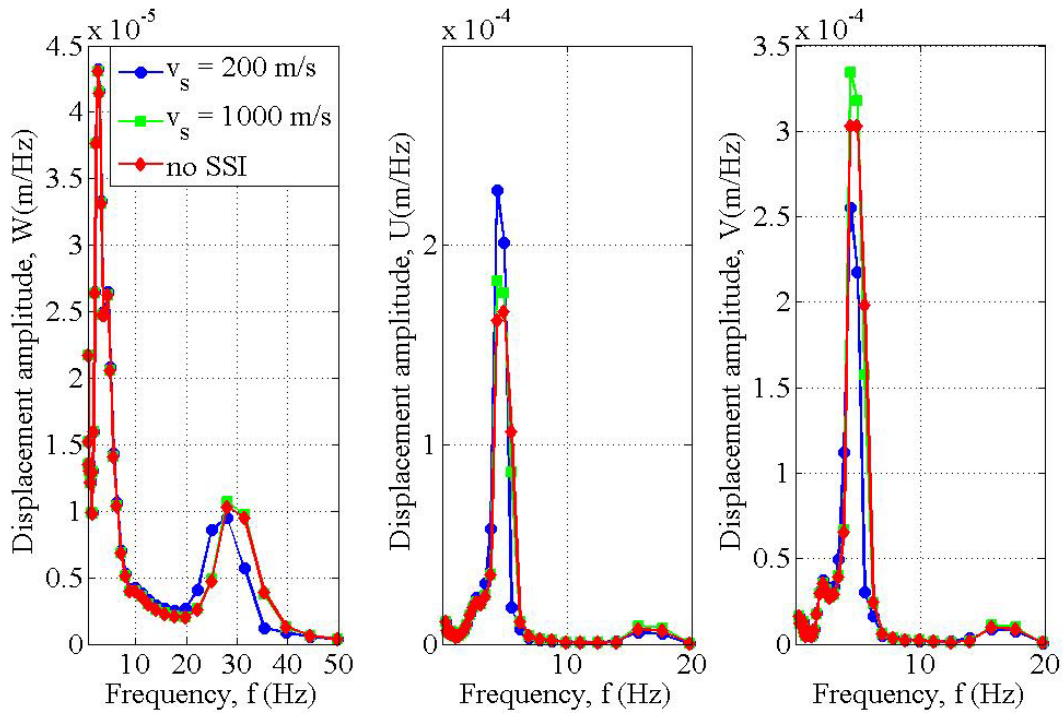


Figure 62. Top floor displacement response spectra of two storey frame, truck traffic

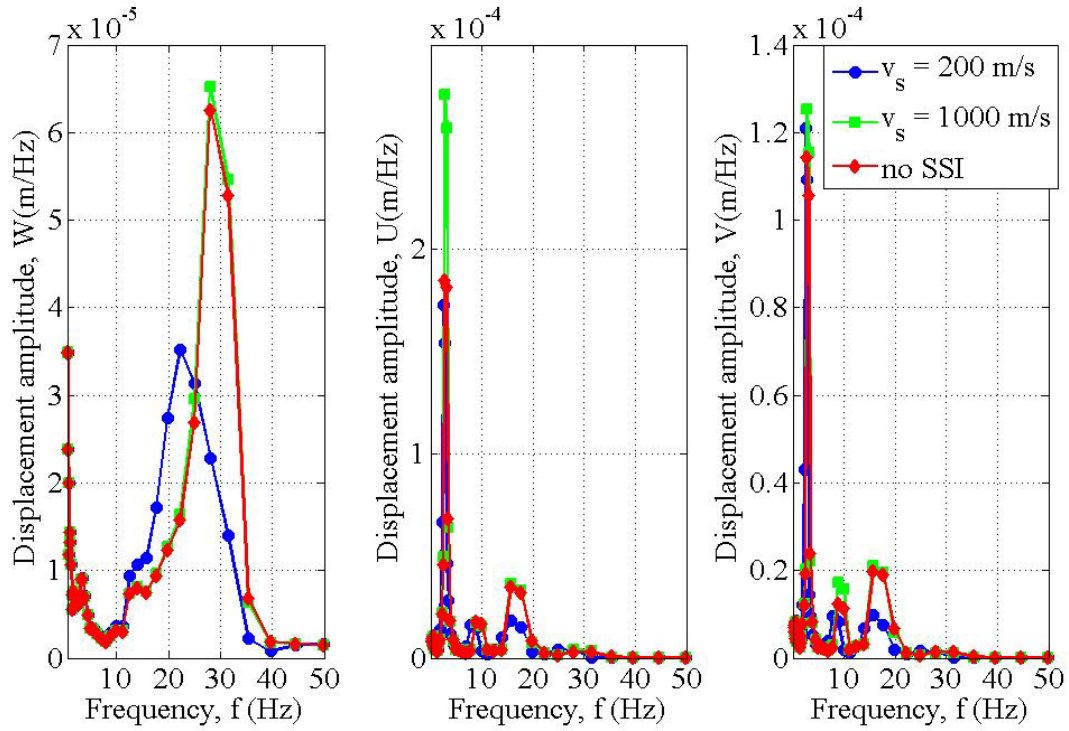


Figure 63. Top floor displacement response spectra of four storey frame, tram traffic

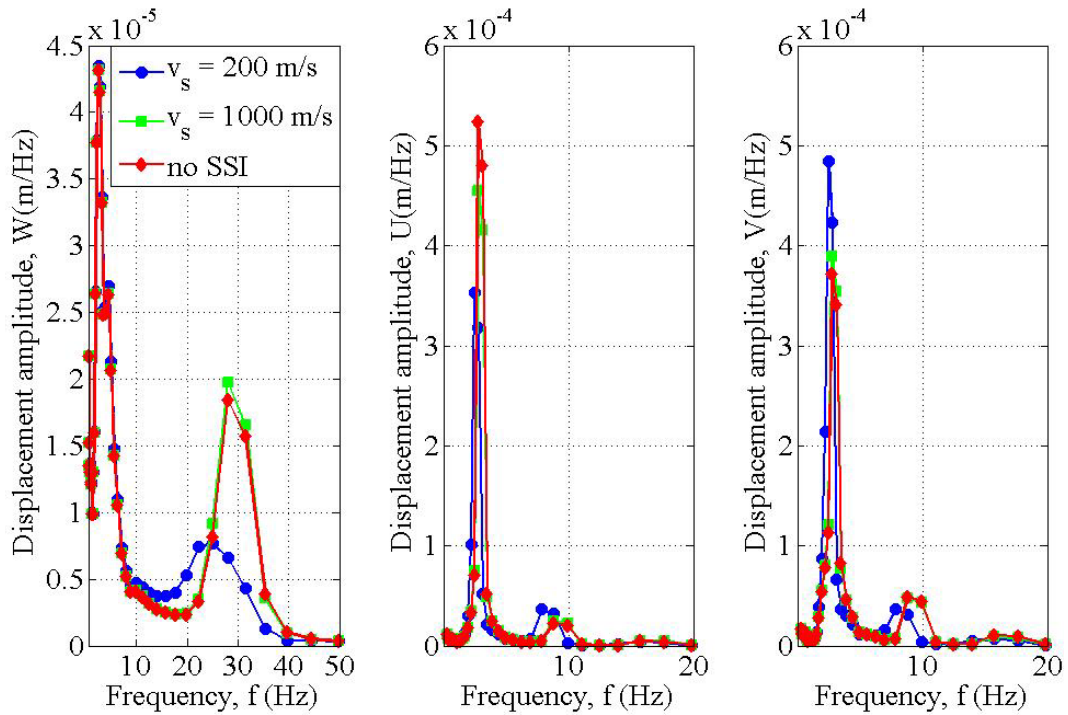


Figure 64. Top floor displacement response spectra of four storey frame, truck traffic

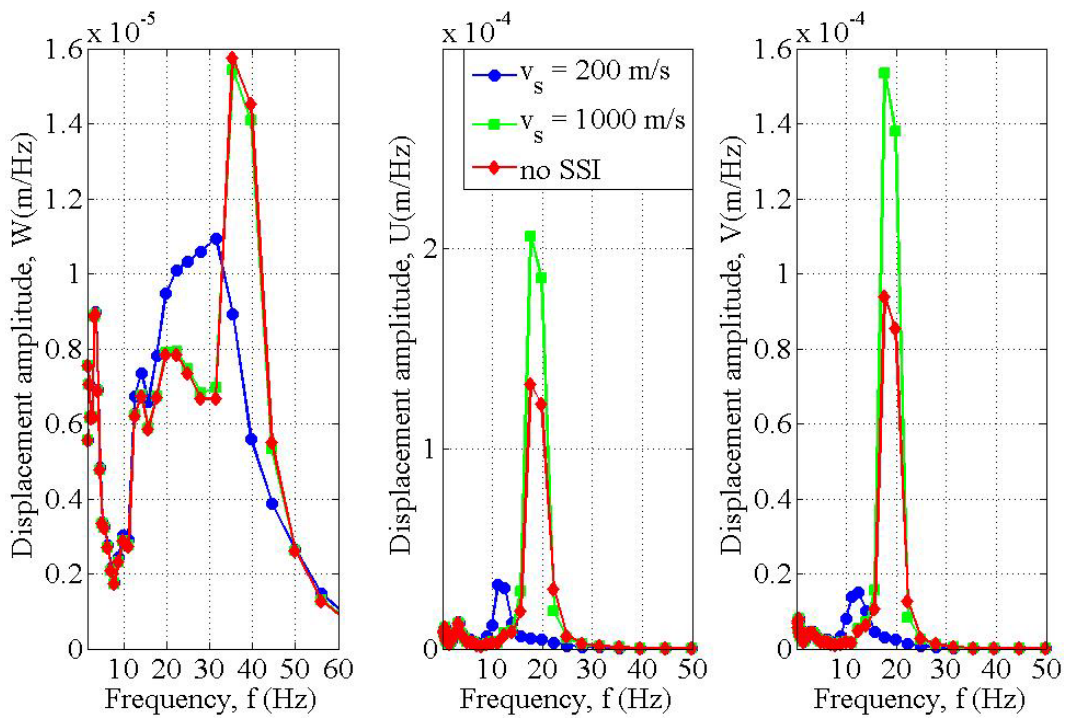


Figure 65. Top floor displacement response spectra of short stiff frame, tram traffic

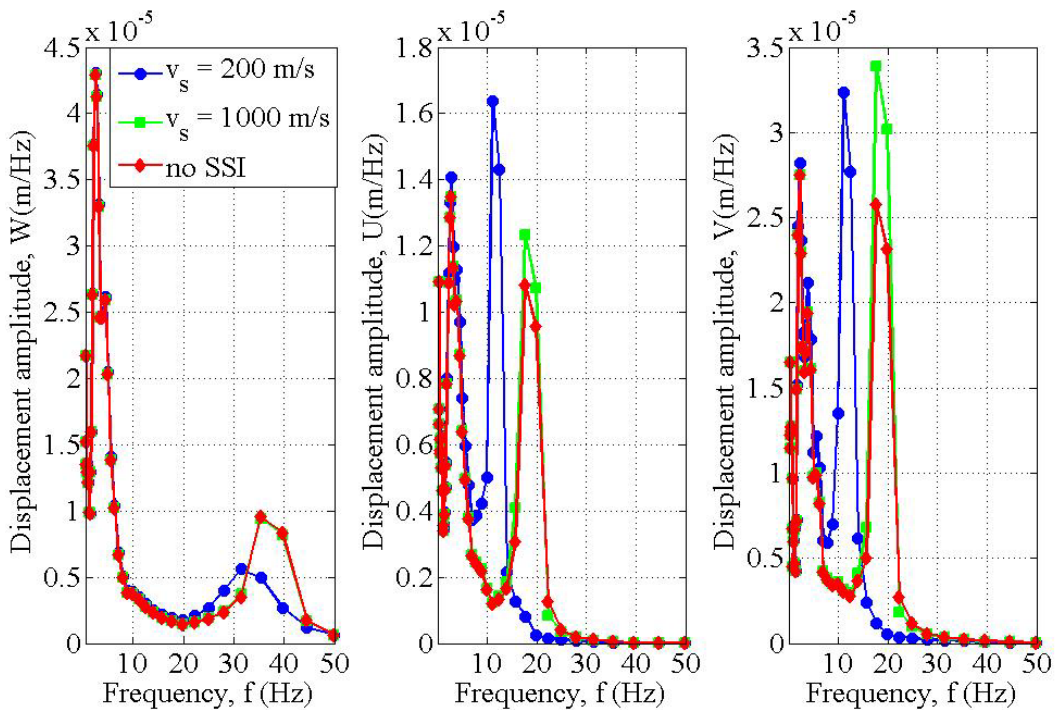


Figure 66. Top floor displacement response spectra of short stiff frame, truck traffic

Table 14. Peak displacement response values of investigated frames induced by tram traffic

Response parameter	One storey frame (columns 30/30 cm)			One storey frame (columns 50/50 cm)			Two storey frame			Four storey frame			
	Soil stiffness			Soil stiffness			Soil stiffness			Soil stiffness			
	Soft	Stiff	Fixed base	Soft	Stiff	Fixed base	Soft	Stiff	Fixed base	Soft	Stiff	Fixed base	
Foundation displacement ($\cdot 10^{-6}$ m)	w	5.0	2.8		5.6	3.6		5.2	2.9		8.5	3.2	
	a.f.	2.0	1.1	/	2.2	1.4	/	2.1	1.2	/	3.4	1.3	/
	u	1.8	1.8		2.5	1.8		1.7	1.8		2.4	1.9	
	a.f.	1.0	1.0	/	1.4	1.0	/	0.96	1.0	/	1.3	1.0	/
	v	1.4	1.4		2.2	1.3		1.1	1.4		2.2	1.4	
	a.f.	1.0	1.0	/	1.7	0.9	/	0.8	1.0	/	1.6	1.0	/
Structural displacement ($\cdot 10^{-6}$ m)	w	9.0	9.6	9.6	8.5	8.8	8.9	9.0	11.6	11.6	13.6	17.4	17.2
	a.f.	3.6	3.8	3.8	3.4	3.5	3.5	3.6	4.6	4.6	5.4	6.9	6.8
	u	2.0	5.5	5.4	3.7	29.7	22.4	5.1	8.2	8.1	5.7	7.7	7.6
	a.f.	1.1	3.0	3.0	2.0	16.3	12.3	2.8	4.5	4.5	3.1	4.2	4.2
	v	1.6	2.6	2.4	2.6	15.4	11.7	3.3	3.3	3.2	3.2	4.0	3.6
	a.f.	1.2	1.9	1.8	1.9	11.3	8.6	1.8	1.8	1.7	2.4	3.0	2.7

Table 15. Peak displacement response values of investigated frames induced by truck traffic

Response parameter	One storey frame (columns 30/30 cm)			One storey frame (columns 50/50 cm)			Two storey frame			Four storey frame			
	Soil stiffness			Soil stiffness			Soil stiffness			Soil stiffness			
	Soft	Stiff	Fixed base	Soft	Stiff	Fixed base	Soft	Stiff	Fixed base	Soft	Stiff	Fixed base	
Foundation displacement ($\cdot 10^{-6}$ m)	w	8.2	5.2		9.1	6.1		9.0	5.0		10.8	6.0	
	a.f.	1.8	1.1	/	3.6	2.4	/	1.8	1.1	/	2.3	1.3	/
	u	1.5	1.5		1.3	1.4		1.4	1.5		1.1	1.4	
	a.f.	1.1	1.1	/	0.9	1.0	/	1.0	1.1	/	0.8	1.0	/
	v	2.5	2.1		3.3	2.1		2.1	2.1		2.3	2.1	
	a.f.	1.2	1.0	/	1.6	1.0	/	1.0	1.0	/	1.1	1.0	/
Structural displacement ($\cdot 10^{-6}$ m)	w	11	12.5	13.1	10.4	11.5	11.4	10.9	14.8	15.4	12.6	16.2	16.0
	a.f.	2.4	2.7	2.8	4.1	4.5	4.5	2.4	3.2	3.3	2.7	3.5	3.4
	u	3.1	2.3	2.3	2.3	3.0	2.9	5.9	6.0	6.0	5.5	6.5	6.8
	a.f.	2.1	1.6	1.6	1.3	2.1	2.0	4.1	4.2	4.2	3.8	4.5	4.7
	v	6.4	6.1	6.4	3.6	6.0	4.6	9.4	10.6	10.6	10.1	8.8	9.0
	a.f.	3.1	2.9	3.1	1.7	2.9	2.2	4.5	5.1	5.1	4.8	4.2	4.3

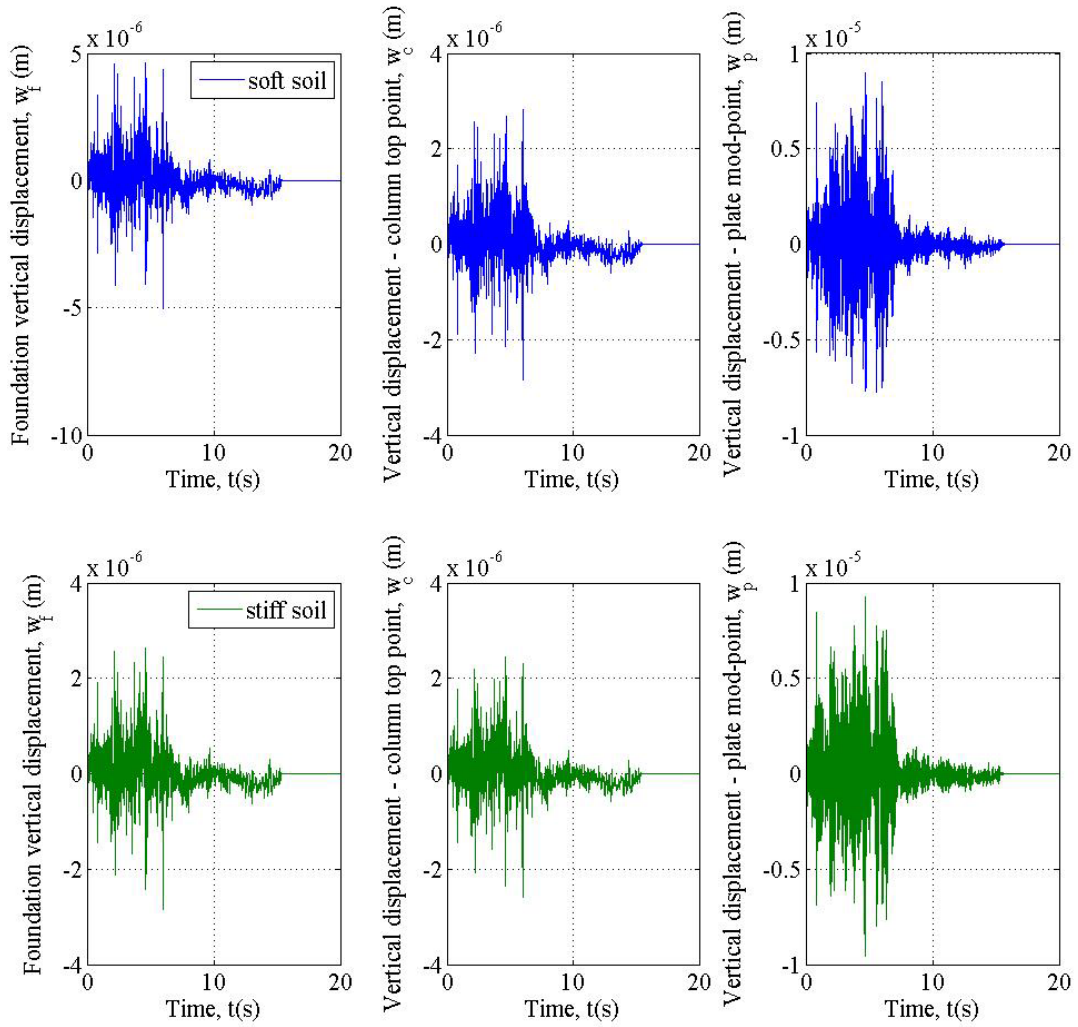


Figure 67. Time history of vertical displacement of one storey frame, tram traffic

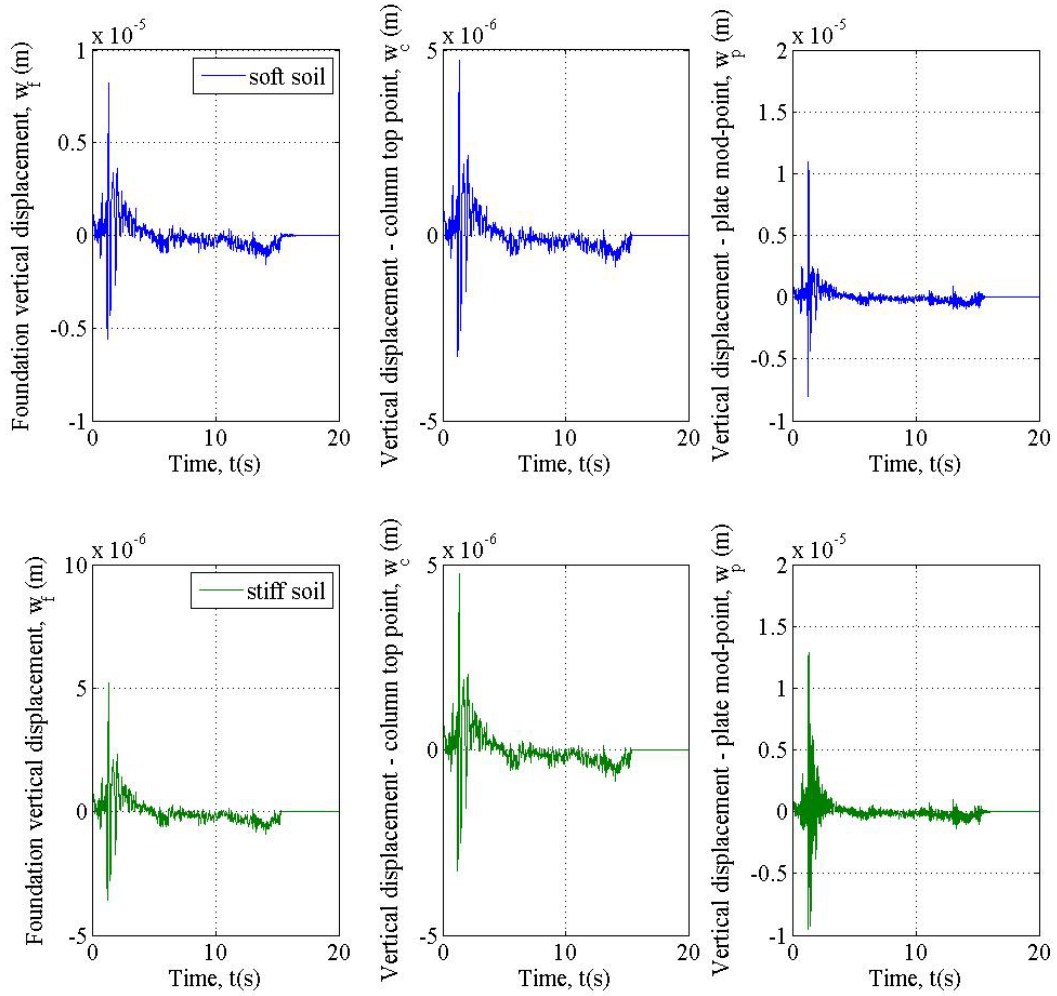


Figure 68. Time history of vertical displacement of one storey frame, truck traffic

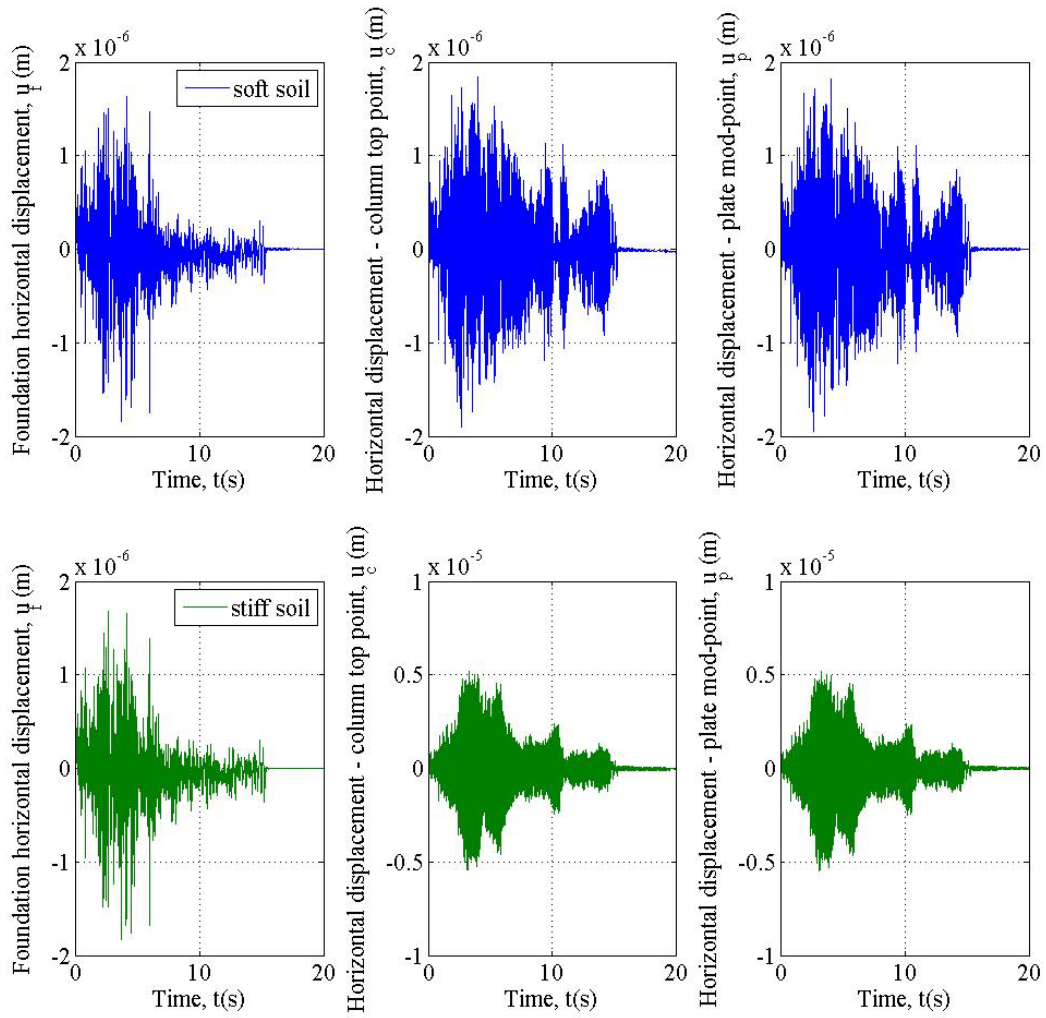


Figure 69. Time history of horizontal displacement - U of one storey frame, tram traffic

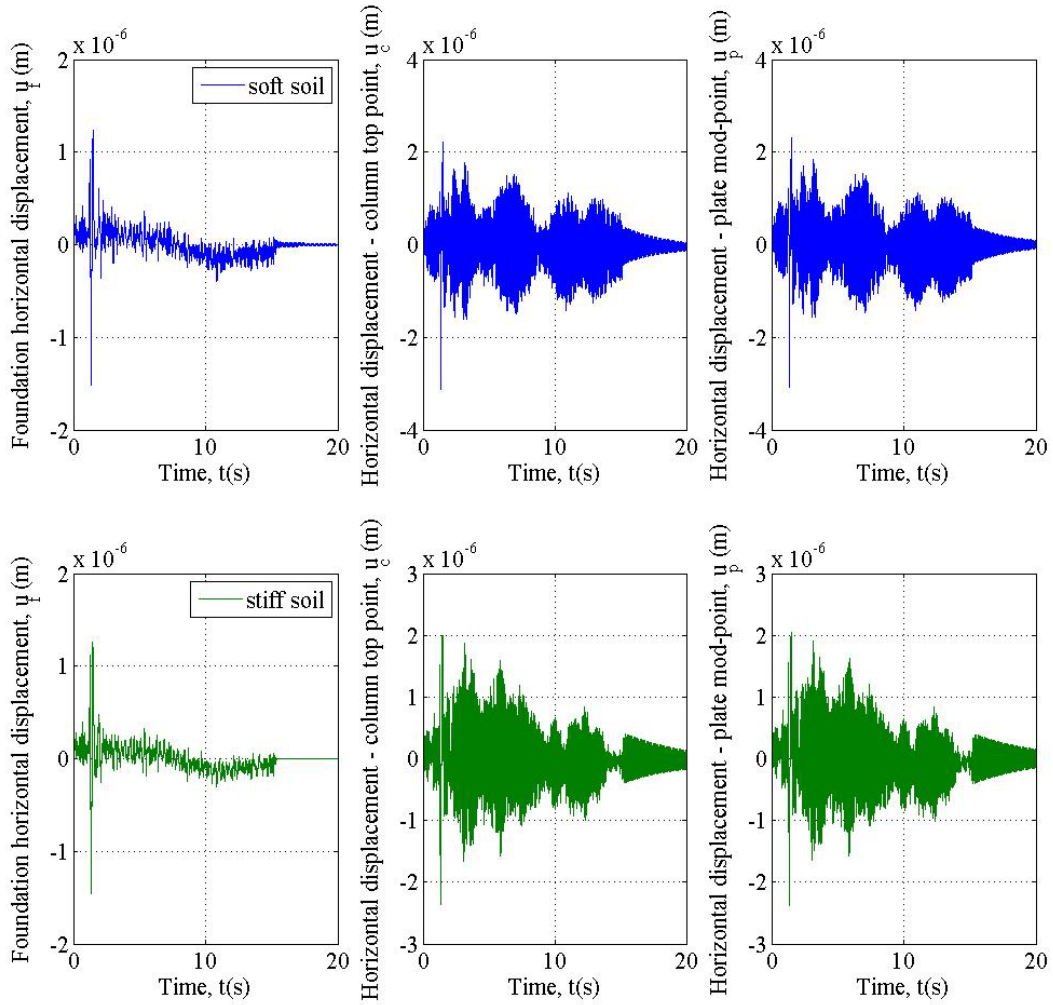


Figure 70. Time history of horizontal displacement - U of one storey frame, truck traffic

In order to assess the human perception to vibrations, the calculated vibration levels were compared with the allowable vibration levels according to British Standard BS: 6472 (1992). Peak particle velocities (PPV) were calculated for different soil stiffness and presented in Figure 71 -Figure 73. The calculated horizontal vibrations did not exceed the acceptable limits in terms of PPV, according to BS: 6472. The exception was the short stiff frame structure, where PPV were 2-4 times larger than the acceptable horizontal vibration limit. Unlike the horizontal vibrations, vertical PPV significantly exceeded the acceptable vertical vibration limits. Consequently, the vertical vibrations could be annoying to building occupants.

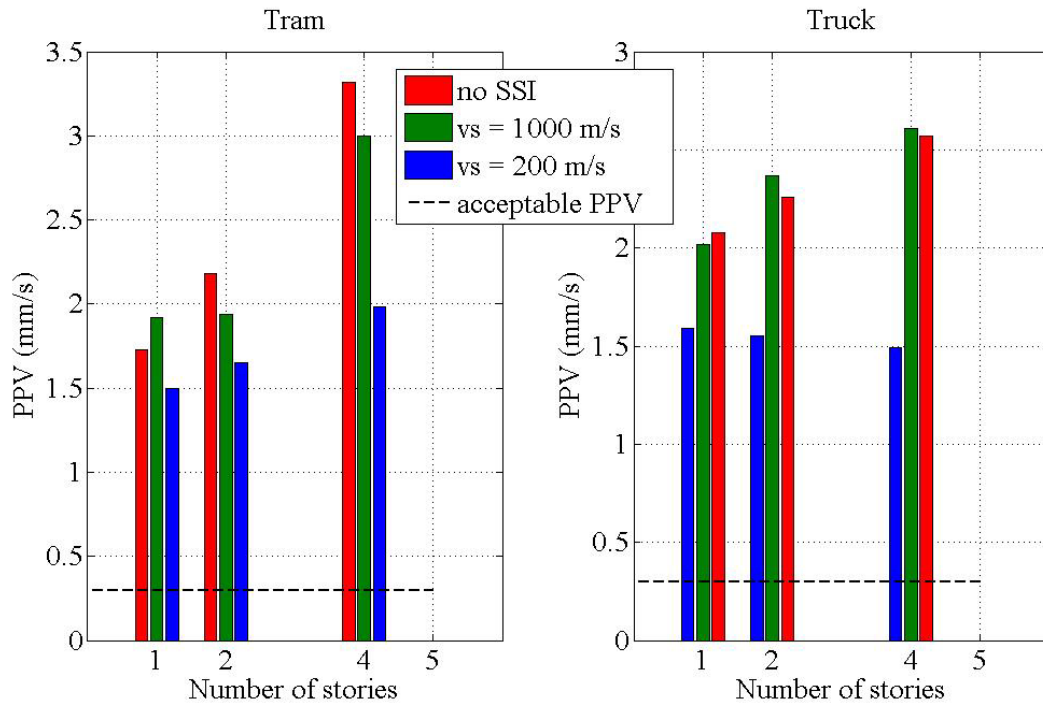


Figure 71. Peak particle velocities for vertical traffic-induced vibrations

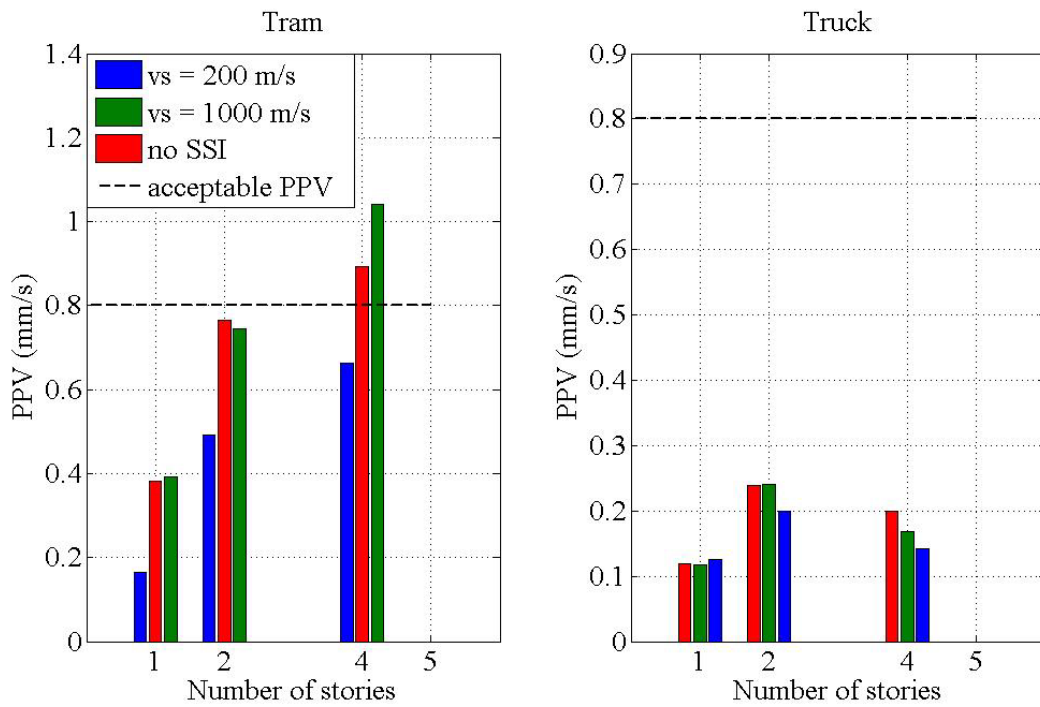


Figure 72. Peak particle velocities for horizontal - U traffic-induced vibrations

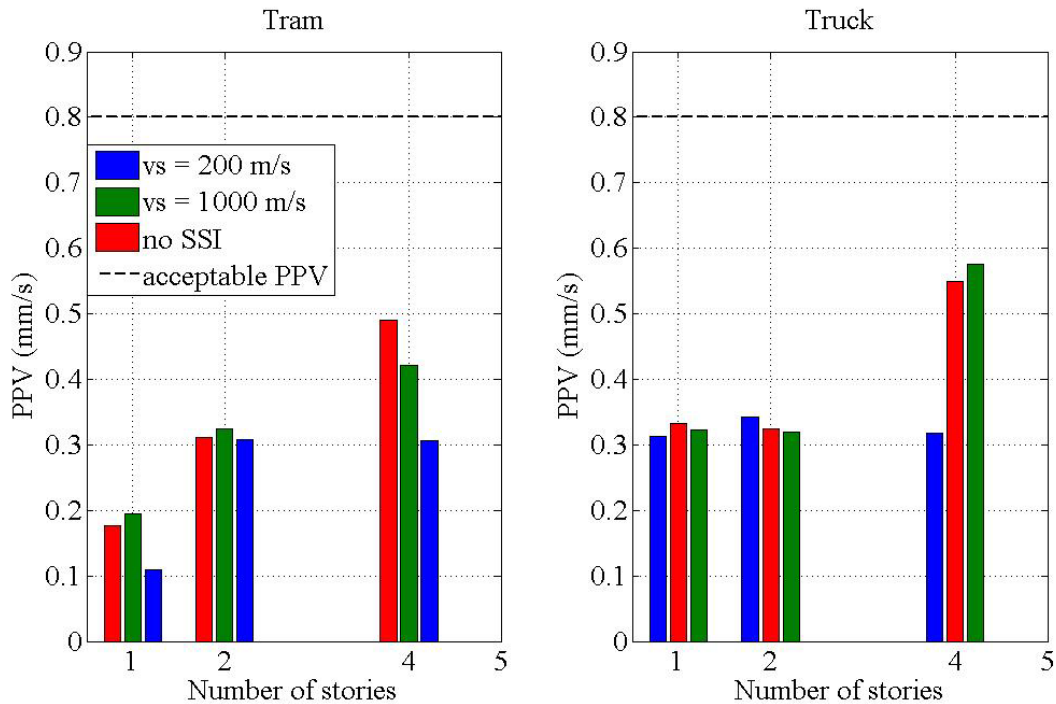


Figure 73. Peak particle velocities for horizontal – V traffic-induced vibrations

6. Conclusions and recommendations for further research

A 3D numerical model has been developed for the dynamic response analysis of soil-structure system. The key feature of the model is the development of both in-plane and transverse dynamic stiffness matrices of plate element with arbitrary boundary conditions as well as the coupling one-dimensional and two-dimensional spectral elements. In addition, the structural model has been coupled with the soil region, which has been modeled using the ITM.

The dynamic stiffness matrices for two-dimensional plate elements have been developed using the Projection method proposed by Kevorkian et al. and Gorman's superposition method. The basic idea was to express the plate displacements as infinite series, truncated to a point M . In order to avoid the spatial dependence of the plate displacements along the boundary, the projections of the boundary displacements have been adopted as the basic unknowns. Consequently, the basic relations between the projected displacement vector and the force vector were the same as for the one-dimensional spectral elements.

A method for coupling the one-dimensional and two-dimensional spectral elements has been presented. Assuming that there were no relative displacements at the junction nodes of the spectral elements and using the equilibrium equations along the plate boundary, the dynamic stiffness matrix of the coupled system has been obtained.

The spectral element model has been coupled with the soil region using the substructure approach. It was assumed that the structure was founded on rigid massless footings. The dynamic stiffness matrix of the soil-foundation interface was superimposed to the structure using the dynamic condensation of the column – soil springs system.

Based on the theoretical considerations a computer program for the dynamic response analysis of 3D frame structures including SSI has been developed using Matlab. The efficiency and accuracy of the proposed model has been demonstrated on several numerical examples. The application of the proposed numerical model has been presented on the example of 3 different types of frame structures surface-founded on homogeneous half space of variable stiffness. Using the proposed numerical model soil-structure systems subjected to ground vibrations induced by traffic, blast or earthquakes could be efficiently analyzed. The results indicated that soil-structure interaction could alter the dynamic properties of the system as well as the dynamic response, especially for short stiff structures.

The most important advantage of the SEM is its high precision. The results showed that for very small number of terms ($M = 3 - 5$) in the general solution of the displacement field of plate element, high degree of accuracy has been achieved. In the case when the structure consisted of columns and plates, more terms in the general solution were required ($M = 10 - 15$). The structural discretization, the number of unknowns and the calculation time were significantly decreased in comparison with the FEM. In addition, the continuous mass distribution, the usage of arbitrarily and even infinitely large elements without loss of accuracy and simple assemblage procedure like in the FEM makes the SEM a very efficient method for solving various types of dynamic SSI problems, especially when high frequency components are of interest.

On the one hand, future research could be directed toward the further development of plate spectral elements using more advanced plate theories like Midlin's theory. In addition, the numerical model could be extended in order to analyze 3D plate

assemblies consisting of plates of finite size joined along common edges and fluid-structure interaction of such systems. This could allow the practical application of the model to analyze not only vibrations but also the re-radiated noise generated by traffic. On the other hand, more advanced models for calculation of the dynamic stiffness matrix of the soil-foundation interface would improve the existing model which is capable to account for SSI of rigid surface-founded footings only.

Appendix

A.1. Fourier Transformations

The continuous function $f(x,y,z,t)$ defined in the space – time domain is transformed into the wave number - frequency domain as:

$$\hat{f}(k_x, k_y, z, \omega) = \int_{-\infty}^{+\infty} \int_{-\infty}^{+\infty} \int_{-\infty}^{+\infty} f(x, y, z, t) e^{-ik_x x} e^{-ik_y y} e^{-i\omega t} dx dy dt.$$

The inverse transformation from the wave number – frequency domain to the space – time domain is given as:

$$f(x, y, z, t) = \frac{1}{(2\pi)^3} \int_{-\infty}^{+\infty} \int_{-\infty}^{+\infty} \int_{-\infty}^{+\infty} \hat{f}(k_x, k_y, z, \omega) e^{ik_x x} e^{ik_y y} e^{i\omega t} dk_x dk_y d\omega.$$

If $f(x,y,z,t)$ is a discrete function, the discrete Fourier transform is defined as:

$$\hat{f}(k_{x_m}, k_{y_n}, z, \omega_p) = \Delta x \Delta y \Delta t \sum_{j=0}^{M-1} \sum_{k=0}^{N-1} \sum_{l=0}^{P-1} f(x_j, y_k, z, t_l) e^{-i2\pi m j / M} e^{-i2\pi n k / N} e^{-i2\pi p l / P},$$

while the inverse discrete Fourier transform is defined as:

$$f(x_j, y_k, z, t_l) = \frac{1}{X} \cdot \frac{1}{Y} \cdot \frac{1}{T} \sum_{m=0}^{M-1} \sum_{n=0}^{N-1} \sum_{p=0}^{P-1} \hat{f}(k_{x_m}, k_{y_n}, z, \omega_p) e^{i2\pi m j / M} e^{i2\pi n k / N} e^{i2\pi p l / P},$$

where $\Delta x = X/M$, $\Delta y = Y/N$, $\Delta t = T/P$, M , N , P are the number of segments of the function $f(x,y,z,t)$ with respect to x , y and t , respectively.

A.2. Fourier series

A Fourier series representation of periodic function $f(x)$ with period $L = 2a$ is defined as:

$$F = f_o + \sum_{m=1}^M f_{S_m} \cos \frac{2m\pi x}{L} + \sum_{m=1}^M f_{A_m} \sin \frac{(2m-1)\pi x}{L}$$
$$f_o = \frac{2}{L} \int_{-a}^a f(x) dx$$
$$f_{S_m} = \frac{2}{L} \int_{-a}^a f(x) \cos \frac{2m\pi x}{L} dx$$
$$f_{A_m} = \frac{2}{L} \int_{-a}^a f(x) \sin \frac{(2m-1)\pi x}{L} dx$$

If $f(x) = \delta(x - x_o)$, the Fourier coefficients are given as:

$$f_o = \frac{1}{L} \delta(x - x_o)$$
$$f_{S_m} = \frac{2}{L} \delta(x - x_o) \cos \frac{2m\pi x_o}{L}$$
$$f_{A_m} = \frac{2}{L} \delta(x - x_o) \sin \frac{(2m-1)\pi x_o}{L}$$

List of Figures

Figure 1. A bar spectral element.....	6
Figure 2. A beam spectral element.....	9
Figure 3. Torsional bar element.....	12
Figure 4. 3D frame element.....	13
Figure 5. Layout of beam geometry	15
Figure 6. Time history and spectrum of input force.....	16
Figure 7. Time history and frequency response spectrum of cantilever beam obtained using SEM	17
Figure 8. Comparison of vibration responses obtained using SEM and FEM	17
Figure 9. Layout and geometry of 3D frame structure.....	18
Figure 10. Internal forces of plate element undergoing transverse vibration.....	23
Figure 11. Infinitesimal element of plate	23
Figure 12. Geometry of the rectangular plate element	27
Figure 13. Mode shapes of simply supported square plate	38
Figure 14. Mode shapes of completely free square plate	40
Figure 15. Internal forces of plate element undergoing in-plane vibration.....	41
Figure 16. Mode shapes of completely free square plate	60
Figure 17. Rectangular plate with edge beams.....	62
Figure 18. Plate and beam forces.....	63
Figure 19. Resultant forces acting on the plate boundary	63
Figure 20. Column supported plate: a) Geometry, b) Resultant forces.....	65
Figure 21. First four transverse mode shapes of completely free square plate with edge beams.....	72
Figure 22. First four in-plane mode shapes of completely free plate with edge beams .	74
Figure 23. Mode shapes of column supported square plate	75
Figure 24. First antisymmetric dimensionless frequency vs. beam stiffness-to-plate stiffness ratio: a) $G_b I_t = 0$, b) $G_b I_t = E_b I_b$	77
Figure 25. Displacements and stresses at the boundaries of: a) layer element, b) half-space element.....	80
Figure 26. Horizontally layered soil over: a) bedrock, b) half-space	82
Figure 27. Soil-structure system.....	83

Figure 28. Rigid surface foundation – degrees of freedom	84
Figure 29. Interaction surface between the foundation and soil.....	86
Figure 30. Numerical soil - structure model.....	87
Figure 31. Numerical soil – structure model, consisting of one-dimensional and two-dimensional spectral elements	88
Figure 32. Layout and geometry of frame structures	89
Figure 33. Natural frequencies of one storey frame	90
Figure 34. Natural frequencies of the two storey frame	91
Figure 35. Natural frequencies of four storey frame	91
Figure 36. Natural frequencies of one storey frame (columns 50/50 cm).....	92
Figure 37. Effects of foundation size on first three natural frequencies of one storey frame.....	93
Figure 38. Time history and Power spectrum of vertical ground velocity from a tram (v=20 km/h).....	94
Figure 39. Time history and Power spectrum of horizontal ground velocity – U from a tram (v=20 km/h).....	94
Figure 40. Time history and Power spectrum of horizontal ground velocity – V from a tram (v=20 km/h).....	95
Figure 41. Time history and Power spectrum of vertical ground velocity from a truck (crossing rubber speed bump, v=50 km/h)	95
Figure 42. Time history and Power spectrum of horizontal ground velocity – U from a truck (crossing rubber speed bump, v=50 km/h, distance to road 11 m)	96
Figure 43. Time history and Power spectrum of horizontal ground velocity – V from a truck (crossing rubber speed bump, v=50 km/h).....	96
Figure 44. Time history and Power spectrum of vertical ground displacement from a tram (v=20 km/h).....	97
Figure 45. Time history and Power spectrum of horizontal ground displacement - U from a tram (v=20 km/h)	97
Figure 46. Time history and Power spectrum of horizontal ground displacement - V from a tram (v=20 km/h)	98
Figure 47. Time history and Power spectrum of vertical ground displacement from a truck (crossing rubber speed bump, v=50 km/h).....	98

Figure 48. Time history and Power spectrum of horizontal – U ground displacement from a truck (crossing rubber speed bump, $v=50$ km/h)	99
Figure 49. Time history and Power spectrum of horizontal ground displacement – V from a truck (crossing rubber speed bump).....	99
Figure 50. Vertical displacement envelopes of one-storey frame	100
Figure 51. Horizontal displacement – U envelopes of one-storey frame	101
Figure 52. Horizontal displacement – V envelopes of one-storey frame	101
Figure 53. Vertical displacement envelopes of two-storey frame	102
Figure 54. Horizontal displacement – U envelopes of two-storey frame.....	102
Figure 55. Horizontal displacement – V envelopes of two-storey frame.....	103
Figure 56. Vertical displacement envelopes of four-storey frame	103
Figure 57. Horizontal displacement – U envelopes of four-storey frame	104
Figure 58. Horizontal displacement – V envelopes of four-storey frame	104
Figure 59. Top floor displacement one third octave band response spectra of one storey frame, tram traffic.....	106
Figure 60. Top floor displacement one third octave band response spectra of one storey frame, truck traffic.....	106
Figure 61. Top floor displacement one third octave band response spectra of two storey frame, tram traffic.....	107
Figure 62. Top floor displacement one third octave band response spectra of two storey frame, truck traffic.....	107
Figure 63. Top floor displacement one third octave band response spectra of four storey frame, tram traffic.....	108
Figure 64. Top floor displacement one third octave band response spectra of four storey frame, truck traffic.....	108
Figure 65. Top floor displacement one third octave band response spectra of short stiff frame, tram traffic.....	109
Figure 66. Top floor one third octave band displacement response spectra of short stiff frame, truck traffic.....	109
Figure 67. Time history of vertical displacement of one storey frame, tram traffic	112
Figure 68. Time history of vertical displacement of one storey frame, truck traffic....	113

Figure 69. Time history of horizontal displacement - U of one storey frame, tram traffic	114
Figure 70. Time history of horizontal displacement - U of one storey frame, truck traffic	115
Figure 71. Peak particle velocities for vertical traffic-induced vibrations	116
Figure 72. Peak particle velocities for horizontal - U traffic-induced vibrations.....	116
Figure 73. Peak particle velocities for horizontal – V traffic-induced vibrations.....	117

References

- Alford, R M, K R Kelly, / D M Boore. „Accuracy of finite difference modeling of the acoustic wave equation.“ *Geophysics*, 1974: 834-842.
- Anderson, M S, F. W. Williams, / C. J. Wright. „Buckling and Vibration of Any Prismatic Assembly of Shear and Compression :oaded Anisotropic plates with an Arbitrary supporting Structure.“ *International Journal of Mechanical Sciences* 25 (1983): 585-596.
- Banerjee, J R. „Dynamic stiffness formulation for structural elements: A general approach.“ *Computers and Structures* 63, br. 1 (1997): 101-103.
- Banerjee, J R, / F W Williams. „Coupled bending-torsional dynamic stiffness matrix for Timoshenko beam elements.“ *Computers and Structures* 42, br. 3 (1992): 301-310.
- Bardell, N. S., R. S. Langley, / J. M. Dunsdon. „On the Free In-Plane Vibration of Isotropic Rectangular Plates.“ *Journal of Sound and Vibration* 191, br. 3 (1996): 459-467.
- Bathe, K J, / E Wilson. *Numerical method in finite element analysis*. Prentice-Hall, 1976.
- Bercin, A. N. „Eigenfrequencies of Rectangular Plate Assemblies.“ *Computers and Structures* 65 (1997): 703-711.
- Bercin, A. N., / R. S. Langley. „Application of the Dynamic Stiffness Technique to the In-Plane Vibrations of Plate Structures.“ *Computers and Structures* 59 (1996): 869-875.

Boscolo, M., / J. R. Banerjee. „Dynamic Stiffness Elements and Their Applications for Plates using First Order Shear Deformation Theory.“ *Computers and Structures* 89 (2011): 395-410.

Boscolo, M., and J. R. Banerjee. "Dynamic stiffness method for exact inplane free vibration analysis of plates and plate assemblies." *Journal of Sound and Vibration* 330, 2011: 2928-2936.

Bracewell, R. N. *The Fourier transform and its applications*. McGraw-Hill, Third edition, 2000.

BS. *Guide to evaluation of human exposure to vibration in buildings (1-80 Hz):BS6472*:. London: British standard institution, 1992.

Campos, N B F, / J R F Arruda. „On the modeling of beam reinforced thin plates using the spectral element method.“ *Shock and Vibration* 15 (2008): 425-434.

Casimir, J. B., S. Kevorkian, / T. Vinh. „The Dynamic Stiffness Matrix of Two-Dimensional elements: Application to Kirchhoff's Plate continuous Elements.“ *Journal of Sound and Vibration* 287 (2005): 571-589.

Danial, A. N., J. F. Doyle, / S. A. Rizzi. „Dynamic Analysis of Folded Plate Structures.“ *Journal of Vibration and Acoustics* 118 (1996): 591-598.

Doyle, J F. *Wave propagation in structures*. New York: Springer-Verlag, 1997.

Gorman, D. J. „Free In-Plane Vibration Analysis of Rectangular Plates by the Method of Superposition.“ *Journal of Sound and Vibration* 272 (2004): 831-851.

Gorman, D. J. „Free Vibration Analysis of the Completely Free Rectangular Plate by the Method of Superposition.“ *Journal of Sound and Vibration* 57 (1978): 432-447.

Grundmann, H, / E. Trommer. „Transform Methods-What Can They Contribute to (Computational) Dynamics.“ *Computers and Structures* 79 (2001): 2091-2101.

Howson, W. P., / A. Zare. „Exact Dynamic Stiffness Matrix for Flexural Vibration of Three-Layered Sandwich Beams.“ *Journal of Sound and Vibration* 282 (2005): 753-767.

Kausel, E., J. M. Roesset, / G. Waas. „Dynamic analysis of footing on layered media.“ *Journal of Engineering Mechanics* 101 (1975): 679-693.

Kevorkian, S., / M. Pascal. „An Accurate Method for Free Vibration Analysis of Structures with Application to Plates.“ *Journal of Sound and Vibration* 246, br. 5 (2001): 795-814.

Kulla, P. H. „High Precision Finite Elements.“ *Finite Elements in Analysis and Design* 26 (1997): 97-114.

Lee, U. „Vibration Analysis of One-Dimensional Structures Using the Spectral Transfer Matrix Method.“ *Engineering Structures* 22 (2000): 681-690.

Lee, U., / J. Kim. „Dynamics of Elastic-Piezoelectric Two-Layer Beams Using Spectral Element Method.“ *International Journal of Solids and Structures* 37 (2000): 4403-4417.

Lee, U., / J. Lee. „Dynamic Continuum Modeling of Truss-Type Space Structures Using Spectral Element Method.“ *Journal of Spacecrafts and Rockets* 33 (1996): 404-409.

Lee, U., / J. Lee. „Spectral-Element Method for Levy-Type Plates Subject to Dynamic Loads.“ *Journal of Engineering and Mechanics* 125 (1999): 243-247.

Lee, U., J. Kim, / A. Y.T. Leung. „The Spectral Element Method in Structural Dynamics.“ *The Shock and Vibration Digest* 32 (2000): 451-465.

Leissa, A. W. „The Free Vibration of Rectangular Plates.“ *Journal of Sound and Vibration* 31 (1973): 257-293.

Lysmer, J, F Ostadan, M Tabatabaie, F Tajiran, / S Vahdani. *SASSI 2000, Theoretical Manual*. University of Berkeley, 1999.

Lysmer, J. *Analytical Procedures in Soil Dynamics*. Report No EERC-78/29, University of California, Berkeley, 1978.

Lysmer, J., / G. Waas. „Shear Waves in Planar Infinite Structures.“ *Journal of Engineering Mechanics Division* 98 (1972): 85-105.

Matlab, MathWorks Inc. „The Language of Technical Computing. MATLAB 2011b.“ 2011.

Nefovska-Danilović, M, M Petronijević, / M Radišić. „Analysis of traffic induced building vibrations using spectral element method.“ *Third Serbian Congress of Theoretical and Applied Mechanics*. Vlasina lake, 2011.

- Petronijević, M, / M Nefovska-Danilović. *Geodinamička analiza osetljivosti objekata na dejstvo postojećih vibracija prema postojećim standardima i procena njihove osetljivosti na dejstvo lakog metroa*. Beograd: Geozavod, Gradjevinski fakultet, 2006.
- Petronijević, M, G Schmid, / I Kolekova. „Dynamic soil-structure interaction of frame structures with spectral elements-part I.“ *Drugi internacionalni naucno-strucni skup Gradjevinarstvo-nauka i praksa*. Žabljak: Crna Gora, 2008. 103-108.
- Petronijević, M. *Analiza dinamičkog sadejstva tla i objekta primenom metode konačnih elemenata, Doktorska disertacija*. Beograd: Gradjevinski fakultet, 1992.
- Radišić, M, M Nefovska-Danilović, / M Petronijević. „Vertical vibrations of 3D structure caused by moving load.“ *First international conference for PhD students in civil engineering*. Cluj, Romania, 2012. 177-183.
- Rafezy, B., / W. P. Howson. „Exact Dynamic Stiffness Matrix of a Three-Dimensional Shear Beam with Doubly Asymmetric Cross-Section.“ *Journal of Sound and Vibration* 289 (2006): 938-951.
- Rastandi, J I. *Modelization of Dynamic Soil-Structure Interaction Using Integral Transform-Finite Element Coupling*. TU Munchen, 2003.
- Roesset, J. M., / M. M. Ettouney. „Transmitting Boundaries: a Comparison.“ *International Journal of Analytical Methods in Geomechanics* 1 (1977).
- SAP2000. „SAP2000. Integrated finite element analysis and design of structures.“ Berkeley, California: Computers and Structures Inc., 1996.
- Schmid, G., / A. Tosecky. „Soil-Structure Interaction, Foundation Vibrations, Lectures for the Master Course Earthquake Engineering at IZIIS, University SS. Cyril and Methodius.“ Skopje, 2003.
- Waas, G. *Linear Two-Dimensional Analysis of Soil Dynamics Problems in Semi-Infinite Layered Media, Ph.D. Thesis*. UC Berkeley, 1972.
- Wang, T. M., / T. A. Kinsman. „Vibration of Frame Structures According to the Timoshenko Theory.“ *Journal of Sound and Vibration* 14 (1971): 215-227.

Williams, F. W., / D. Kennedy. „Exact Dynamic Member Stiffness for a Beam on an Elastic Foundation.“ *Earthquake Engineering and Structural Dynamics* 15 (1987): 133-136.

Wolf, J P. *Dynamic Soil-Structure Interaction* . New York: Prentice Hall, Inc., 1993.

Xing, Y. F., / B. Liu. „Exact Solutions for the Free In-Plane Vibrations of Rectangular Plates.“ *International Journal of Mechanical Sciences* 51 (2009): 246-255.

Биографија аутора

Марија Нефовска-Даниловић рођена је 09.10.1972. године у Скопју. Четврту београдску гимназију завршила је 1991. године, када уписује Грађевински факултет у Београду. Дипломирала је 1997. године са просечном оценом 8.68 и оценом 10 на дипломском раду под називом “Динамичка анализа цилиндричног резервоара применом методе коначних елемената”. Од октобра 1997. г. до маја 1998. била је запослена у Рачунском центру Грађевинског факултета у Београду. 1998. г. изабрана је у звање асистента приправника на Катедри за Техничку механику и теорију конструкција, где је учествовала у одржавању вежби из групе предмета Теорија конструкција. Магистарску тезу под називом “Еласто-пластична анализа челичних рамова са флексибилним везама” одбранила је 2003. године. 2004. године изабрана је у звање асистента на Катедри за Техничку механику и теорију конструкција, када уписује докторске студије у оквиру пројекта “SEEFORM” под покровитељством DAAD, на Грађевинском факултету у Скопју. Поред наставне активности, учествовала је у реализацији неколико научних пројеката под покровитељством Министарства за науку Републике Србије. Коаутор је 2 рада објављена у међународним часописима са SCI листе, 2 рада у домаћим часописима, као и бројних радова објављених у зборницима радова на домаћим и међународним конференцијама. Такође, учествовала је у изради стручних студија из области анализе дејства вибрација од саобраћаја на људе и објекте. Коаутор је збирке задатака из Статике конструкција 2. Удата је и има двоје деце.

Прилог 1.

Изјава о ауторству

Потписани-а Марија Нефовска-Даниловић

број уписа _____

Изјављујем

да је докторска дисертација под насловом

**ДИНАМИЧКА АНАЛИЗА СИСТЕМА ТЛО-КОНСТРУКЦИЈА ПРИМЕНОМ
СПЕКТРАЛНИХ ЕЛЕМЕНАТА**

- резултат сопственог истраживачког рада,
- да предложена дисертација у целини ни у деловима није била предложена за добијање било које дипломе према студијским програмима других високошколских установа,
- да су резултати коректно наведени и
- да нисам кршио/ла ауторска права и користио интелектуалну својину других лица.

Потпис докторанда



У Београду, децембар 2012.

Прилог 2.

Изјава о истоветности штампане и електронске верзије докторског рада

Име и презиме аутора: Марија Нефовска-Даниловић

Број уписа _____

Студијски програм: Грађевинарство

Наслов рада: **ДИНАМИЧКА АНАЛИЗА СИСТЕМА ТЛО-КОНСТРУКЦИЈА
ПРИМЕНОМ СПЕКТРАЛНИХ ЕЛЕМЕНАТА**

Ментор : проф. Др Мира Петронијевић, дипл. грађ. инж.

Потписани : Марија Нефовска-Даниловић

изјављујем да је штампана верзија мог докторског рада истоветна електронској верзији коју сам предао/ла за објављивање на порталу **Дигиталног репозиторијума Универзитета у Београду.**

Дозвољавам да се објаве моји лични подаци везани за добијање академског звања доктора наука, као што су име и презиме, година и место рођења и датум одбране рада.

Ови лични подаци могу се објавити на мрежним страницама дигиталне библиотеке, у електронском каталогу и у публикацијама Универзитета у Београду.

Потпис докторанда



У Београду, децембар 2012.

Прилог 3.

Изјава о коришћењу

Овлашћујем Универзитетску библиотеку „Светозар Марковић“ да у Дигитални репозиторијум Универзитета у Београду унесе моју докторску дисертацију под насловом:

ДИНАМИЧКА АНАЛИЗА СИСТЕМА ТЛО-КОНСТРУКЦИЈА ПРИМЕНОМ СПЕКТРАЛНИХ ЕЛЕМЕНАТА

која је моје ауторско дело.

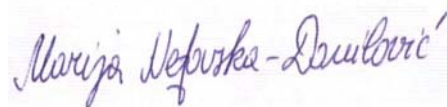
Дисертацију са свим прилозима предао/ла сам у електронском формату погодном за трајно архивирање.

Моју докторску дисертацију похрањену у Дигитални репозиторијум Универзитета у Београду могу да користе сви који поштују одредбе садржане у одабраном типу лиценце Креативне заједнице (Creative Commons) за коју сам се одлучио/ла.

1. Ауторство
2. Ауторство - некомерцијално
3. Ауторство – некомерцијално – без прераде
4. Ауторство – некомерцијално – делити под истим условима
5. Ауторство – без прераде
6. Ауторство – делити под истим условима

(Молимо да заокружите само једну од шест понуђених лиценци, кратак опис лиценци дат је на полеђини листа).

Потпис докторанда



У Београду, децембар 2012 .